การสังเคราะห์พอลิอิมีดที่มีหน่วยเททระเฟนิลพอร์ไฟริน

นางสาววัชรา อนันต์นฤการ

วิทยานิพนธ์นี้เป็นส่วนหนึ่งของการศึกษาตามหลักสูตรปริญญาวิทยาศาสตรดุษฎีบัณฑิต
สาขาวิชาปิโตรเคมี
คณะวิทยาศาสตร์ จุฬาลงกรณ์มหาวิทยาลัย
ปีการศึกษา 2548
ISBN 974-14-1798-5

SYNTHESIS OF POLYIMIDES CONTAINING TETRAPHENYLPORPHYRIN MOIETIES

Miss Watchara Anannarukan

A Dissertation Submitted in Partial Fulfillment of the Requirements
for the Degree of Doctor of Philosophy Program in Petrochemistry
Program of Petrochemistry
Faculty of Science
Chulalongkorn University
Academic Year 2005

ISBN 974-14-1798-5

Thesis Title	Synthesis of Polyimides Containing Tetraphenylporphyrin Moieties
By	Miss Watchara Anannarukan
Field of Study	Petrochemistry
Thesis Advisor	Associate Professor Supawan Tantayanon, Ph.D.
Thesis Co-advisor	Professor Frank W. Harris, Ph.D.

Accepted by the Faculty of Science, Chulalongkorn University in Partial Fulfillment of the Requirements for the Doctor's Degree

.....Dean of the Faculty of Science
(Professor Piamsak Menasveta, Ph.D.)

Thesis Committee

.....Chairman
(Professor Pattarapan Prasassarakich, Ph.D.)

.....Thesis Advisor
(Associate Professor Supawan Tantayanon, Ph.D.)

.....Thesis Co-advisor
(Professor Frank W. Harris, Ph.D.)

.....Member
(Associate Professor Nuanphun Chantarasiri, Ph.D.)

.....Member
(Assistant Professor Warinthorn Chavasiri, Ph.D.)

.....Member
(Associate Professor Pranee Phinyocheep, Ph.D.)

วัชรา อนันต์นฤการ: การสังเคราะห์พอลิอิมีดที่มีหน่วยเททระเฟนิลพอร์ไฟริน (SYNTHESIS OF POLYIMIDES CONTAINING TETRAPHENYL-PORPHYRIN MOIETIES) อาจารย์ที่ปรึกษา: รศ.ดร. ศุภวรรณ ตันตยานนท์, อาจารย์ที่ปรึกษาร่วม: Professor Dr. Frank W. Harris, 122 หน้า ISBN 974-14-1798-5.

ได้สังเคราะห์ 5,15-บิส(4-แอมิโนเฟนิล)-10,20-ไดเฟนิลพอร์ไฟริน (ทรานส์-ดีเอทีพีพี) ด้วยปฏิกิริยาควบแน่นของ เมโซ-(4-ไนโทรเฟนิล)ไดพิโรมีเทนและเบนซาลดีไฮด์ เมื่อทำปฏิกิริยาต่อไปกับซิงค์แอซีทิลแอซีโทเนตไฮเดรต ได้ซิงค์ 5,15-บิส(4-แอมิโนเฟนิล)-10,20-ไดเฟนิลพอร์ไฟริน (ทรานส์-ซิงค์ดีเอทีพีพี) การพิสูจน์เอกลักษณ์ของสารประกอบที่สังเคราะห์ได้ทั้งสองชนิดและสารมัธยันต์ทำโดยใช้สเปกโทรสโกปิกเทคนิค ได้เตรียมพอลิอิมีดที่ละลายได้ 4 กลุ่ม จาก ทรานส์-ดีเอทีพีพี ทรานส์-ซิงค์ดีเอทีพีพี 2,2′-บิส(ไทรฟลูออโรเมทิล)-4,4′-ไดแอมิโนไบเฟนิล (พี เอฟเอ็มบี) 4,4′-เฮกซะฟลูออโรไอโซโพรพิลิดีนไดพทาลิกแอนไฮไดรด์ (6 เอฟดีเอ) และ 3,6-บิส (3-ไทรฟลูออโรเมทิลเฟนิล)พิโรเมลลิทิกไดแอนไฮไดรด์ (3 เอฟพีเอ็มดีเอ) ที่อัตราส่วนต่างๆ ได้ยืนยันโครงสร้างของพอลิอิมีดเหล่านี้ด้วยเทคนิคเอฟทีไออาร์ และ โปรตอน-เอ็นเอ็มอาร์ และได้หาปริมาณของพอร์ไฟรินในพอลิอิมีดด้วยเทคนิคยูวี-วิซิเบิลสเปกโทรสโกปี พบว่าพอลิอิมีดที่มีทรานส์-ดีเอทีพีพี หรือ ทรานส์-ซิงค์ดีเอทีพีพี มีความหนืดสูงกว่าพอลิอิมีดที่ไม่มีพอร์ไฟริน นอกจากนี้พอลิอิมีดที่มีทรานส์-ซิงค์ดีเอทีพีพี มีความหนืดต่ำกว่าและอุณหภูมิเปลี่ยนสถานะคล้ายแก้วสูงกว่าพอลิอิมีดที่มีทรานส์-ดีเอทีพีพี ที่ปริมาณพอร์ไฟรินเท่ากัน และพอลิอิมีดที่มีพอร์ไฟรินมีอุณหภูมิเปลี่ยนสถานะคล้ายแก้วสูงกว่าพอลิอิมีดที่ไม่มีพอร์ไฟริน พอลิอิมีดเหล่านี้มีความเสถียรทางความร้อนที่ดีซึ่งวิเคราะห์ด้วยวิธีเทอร์โมกราวิเมทริก สเทดิสเทตฟลูออเรสเซนต์สเปกโทรสโกปีของพอลิอิมีดเหล่านี้ได้ถูกศึกษา การทดลองทางเคมีไฟฟ้าและไทม์ดอรีเลเทตชิงเกิลโฟตอนเคาทิงของพอลิอิมีดที่เป็นตัวแทน แสดงให้เห็นว่าพอลิอิมีดเหล่านี้สามารถใช้งานทางโฟโทนิกได้

สาขาวิชา ปิโตรเคมี ลายมือชื่อนิสิต วัชรา อนันต์นฤการ

ปีการศึกษา 2548 ลายมือชื่ออาจารย์ที่ปรึกษา

ลายมือชื่ออาจารย์ที่ปรึกษาร่วม Frank W. Harris

4373870023 : MAJOR PETROCHEMISTRY
KEYWORD: SOLUBLE POLYIMIDES / DIAMINOTETRAPHENYLPORPHYRIN / PHOTOINDUCED ELECTRON TRANSFER
WATCHARA ANANNARUKAN: SYNTHESIS OF POLYIMIDES CONTAINING TETRAPHENYLPORPHYRIN MOIETIES. THESIS ADVISOR: ASSOCIATE PROFESSOR SUPAWAN TANTAYANON, Ph.D., THESIS CO-ADVISOR: PROFESSOR FRANK W. HARRIS, Ph.D., 122 pp. ISBN 974-14-1798-5.

5,15-*Bis*(4-aminophenyl)-10,20-diphenylporphyrin (*trans*-DATPP) was synthesized via the condensation of *meso*-(4-nitrophenyl)dipyrromethane and benzaldehyde. The further reaction with zinc acetylacetonate hydrate afforded zinc 5,15-*bis*(4-aminophenyl)-10,20-diphenylporphyrin (*trans*-ZnDATPP). The identification of both synthesized compounds and their intermediates was performed by spectroscopic technique. Four series of soluble polyimides based on *trans*-DATPP or *trans*-ZnDATPP, 2,2′-*bis*(trifluoromethyl)-4,4′-diaminobiphenyl (PFMB), 4,4′-hexafluoroisopropylidene-diphthalic anhydride (6FDA) and 3,6-*bis*(3-trifluoromethylphenyl)pyrromellitic dianhydride (3FPMDA) at various ratios were then prepared. The structures of these polyimides were confirmed by FTIR and ^{1}H-NMR, and porphyrin content in polyimides was determined by UV-vis spectroscopy. It was found that most polyimides containing either *trans*-DATPP or *trans*-ZnDATPP had higher viscosity than the polyimide without porphyrin moiety. In addition, the polyimides containing *trans*-ZnDATPP showed lower viscosity and higher glass transition temperature (T_g) than the ones containing *trans*-DATPP at approximately the same porphyrin content and both had higher T_g than polyimide without porphyrin. These polyimides displayed good thermal stabilities when subjected to thermogravimetric analysis. All polyimides were soluble in polar aprotic solvents, THF, CH_2Cl_2 and acetone. Steady state fluorescence spectroscopy of these polyimides were investigated, electrochemical and Time-correlated single photon counting experiments of the representative polyimides indicated that these polyimides could be used in photonic applications.

Field of study Petrochemistry Student's signature Watchara Anannarukan
Academic year 2005 Advisor's signature
Co-advisor's signature Frank W. Harris

ACKNOWLEDGEMENTS

I would like to express my sincere thanks and grateful appreciation to Associate Professor Dr. Supawan Tantayanon, my advisor who has been giving all her support and guidance throughout the research work. Although this thesis had obstacles, finally it could be completed by her advice and her willpower. I am sincerely grateful to Professor Dr. Frank W. Harris, my co-advisor for his suggestions, guidance, encouragement and supporting during my research. In addition, my appreciation also extends to all thesis committee, Professor Dr. Pattarapan Prasassarakich, Associate Professor Dr. Nuanphun Chantarasiri, Assistant Professor Dr. Warinthorn Chavasiri and Associate Professor Dr. Pranee Phinyocheep, for their comments regarding this thesis

I am grateful to a research funding from The Thailand Research Fund (TRF), The Royal Golden Jubilee Scholarship, Grant no. PHD/0029/2544. I am also grateful to The Maurice Morton Institute of Polymer Science, The University of Akron for research facilities.

I would like to thank Dr. David A. Modarelli for his guidance and encouragement during my research. Special thanks are extended to Mr. Elvin A. Alemán on his assistance for fluorescence lifetime measurement. I would like also to thank Department of Chemistry and Department of Chemical Technology, Chulalongkorn University.

Many thanks go to group members in Dr. Harris's group and especial to Dr. Dong Zhang, for advice and friendships over the years. I would like also to thank Mr.

Jon R. Page, Ms. Deborah Citraro for their friendship and help over the past year. In addition, I would like to thank all my friends, my group members and members of Organic Synthesis Research Unit, for their contributed suggestions and support during my research.

Special thanks are extended to Tulyapitak's family for advice, encouragement and friendship over the past year.

Finally, I would like to express my gratitude to my family for their love, encouragement, understanding and support throughout my life.

CONTENTS

Page

Page

CHAPTER IV RESULTS AND DISCUSSION

Page

Page

LIST OF TABLES

LIST OF FIGURES

Figure Page

LIST OF SCHEMES

Scheme Page

Scheme Page

LIST OF ABBREVIATION

$BF_3.OEt_2$	: Borontrifluoride etherate
DDQ	: 2,3-Dichloro-5,6-dicyanobenzoquinone
DMAc	: Dimethylacetamide
DMF	: *N*,*N*′-Dimethylformamide
DMSO	: Dimethylsulfoxide
6FDA	: 4,4′-Hexafluoroisopropylidenediphathalic dianhydride
3FPMDA	: 3,6-*Bis*(3-trifluoromethylphenyl)pyrromellitic dianhydride
NMP	: *N*-methyl-2-pyrrolidone
PFMB	: 2,2′-*Bis*(trifluoromethyl)-4,4′-diaminobiphenyl
TFA	: Trifluoroacetic acid
TGA	: Thermogravimetric analysis
TMA	: Thermomechanical analysis
TPP	: Tetraphenylporphyrin
Trans-DATPP	: 5,15-*Bis*(4-aminophenyl)-10,20-diphenylporphyrin
Trans-ZnDATPP	: Zinc 5,15-*bis*(4-aminophenyl)-10,20-diphenylporphyrin
ZnTPP	: Zinc tetraphenylporphyrin
η_{sp}	: Specific viscosity
$[\eta]$	: Intrinsic viscosity

CHAPTER I

INTRODUCTION

1.1 Introduction

Aromatic polyimides are known for their excellent mechanical and electrical properties [1] as well as their outstanding thermal stability [2,3]. They also display high softening temperatures and excellent chemical resistance. This combination of properties makes them essentially impossible to fabricate. However, aromatic polyimides are generally insoluble in common organic solvents. Thus, they must be processed in the form of their soluble poly(amic acid) (PAA) precursors, which are then chemically or thermally imidized in place. However, there are several drawbacks to the PAA approach. For example, water released during imidization can create weakening voids in thick parts of material. Even with thin films, the thermal imidization process must be carefully controlled in order to minimize depolymerization and maximize the degree of imidization [4]. Therefore a considerable amount of research aimed at the development of aromatic polyimides has been carried out [1-3].

Porphyrins are well known as sensitizers in the photosynthesis of plants, and are frequently used in assemblies related to artificial solar energy conversion [5]. Various types of polymer containing porphyrins can therefore be used as

photoresponsive materials [6], photorefractive materials [7], and molecular wires [8]. Recently, much attention has been paid to polyimide containing porphyrins, since they can be used potentially as photoconductive materials and charge transporting materials [9-12]. Although a few studies on photoinduced electron transfer in polyimides containing porphyrin had been reported [13-15], those polyimides were prepared *via* the imidization of PAA films which had several disadvantages as mentioned earlier.

Accordingly, this research has been designed to synthesize polyimides containing porphyrin which can be soluble in common organic solvents. Such purpose has been achieved by using 4,4′-hexafluoroisopropylidenediphathalic dianhydride (6FDA), 2,2′-*bis*(trifluoromethyl)-4,4′-diaminobiphenyl (PFMB) in condensation polymerization following the method of Harris and his coworker [1-3]. The syntheses include polyimides containing porphyrin with and without zinc incorporation. Then physical and optical properties have been compared. In particular, the optical study in solution can be evaluated to gain more and better information than the porphyrin-containing polyimide films prepared *via* imidization of PAA films as previously reported by other research groups.

1.2 Objective

The aim of this research is to synthesize organo-soluble polyimides containing tetraphenylporphyrin moieties and study both physical and optical properties of these polyimides.

1.3 Scope of the research

1. Synthesis of 5,15-*bis*(4-aminophenyl)-10,20-diphenylporphyrin from *meso*-(4-nitrophenyl)dipyrromethane

2. Synthesis of zinc 5,15-*bis*(4-aminophenyl)-10,20-diphenylporphyrin from 5,15-*bis*(4-aminophenyl)-10,20-diphenylporphyrin

3. Synthesis of 1,4-*bis*(3-trifluoromethyl)pyrromellitic dianhydride and 2,2′-*bis*(trifluoromethyl)-4,4′-diaminobiphenyl

4. Copolymerization of polyimides at various ratios of monomer

5. Investigation of both physical and optical properties of the polyimides

CHAPTER II

THEORETICAL BACKGROUND

2.1 Polyimide

Polyimides (PIs) are a class of representative high-performance polymers possessing the cyclic imide and aromatic groups in the main chains. The most familiar polyimide is widely known as Kapton H® (Scheme 2.1), developed by Du Pont in the 1960s. After marketing of this polyimide, many other polyimides with some modified properties were commercially developed. High molecular weight aromatic polyimides can be synthesized in a two-step procedure, where a soluble poly(amic acid) was formed and then, in a second step, was converted into the desired polyimides. This two-step procedure prompted considerable research into polyimides due to the processibility of the poly(amic acid) precursor. A one-step method to prepare soluble aromatic polyimide was then reported. In this method diamines and dianhydrides are polymerized at elevated temperature to form the polyimides.

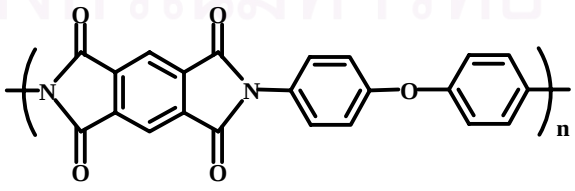

Scheme 2.1 A commercial polyimide, Kapton H®

2.1.1 Synthesis of polyimides [4]

2.1.1.1 Two-step method

In the general method of polyimide synthesis, a tetracarboxylic acid dianhydride is added to a solution of diamine in a polar aprotic solvent, such as *N*-methyl-2-pyrrolidone (NMP), dimethylacetamide (DMAc) and *m*-cresol [16-21]. The generated poly(amic acid) is then cyclodehydrated to the corresponding polyimide (Scheme 2.2).

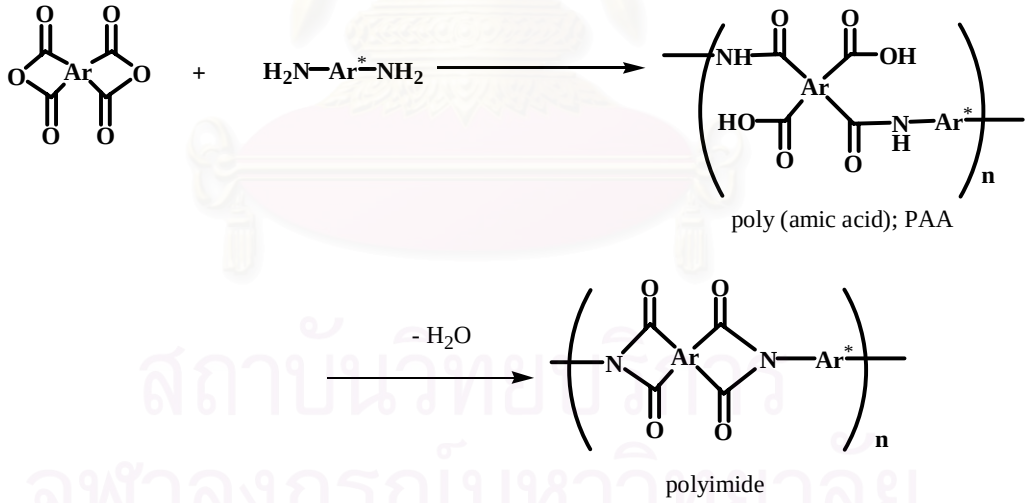

Scheme 2.2 Conventional polyimide synthesis

2.1.1.1.1 Poly(amic acid) formation

Since the polyimide is often insoluble and infusible, the polymer is usually processed in the form of the poly(amic acid). The poly(amic acid) precursor is formed *via* nucleophilic attack of the amine at an anhydride carbonyl carbon. The mechanism is illustrated in Scheme 2.3. Each of the steps is reversible.

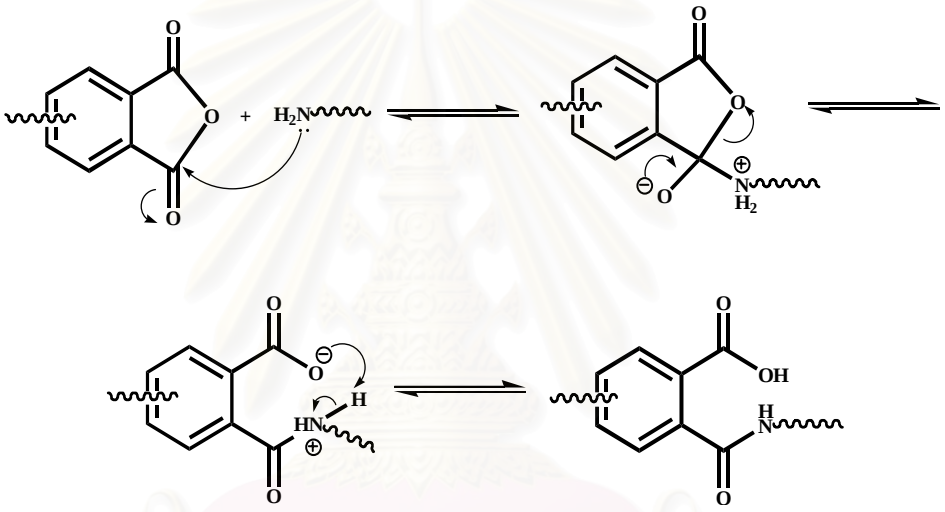

Scheme 2.3 Mechanism of nucleophilic attack in poly(amic acid) formation

Solvent, monomer concentration and temperature can be manipulated to shift the equilibrium towards the right to obtain high molecular weight poly(amic acid). For example, polar aprotic solvents form strongly hydrogen bonded complexes with the free carboxyl groups preventing the reverse reaction. An increase in monomer concentration also favors the formation of higher molecular weight products because the forward reaction is bimolecular, while the reverse is unimolecular. Since the forward reaction is exothermic, a decrease in reaction temperature increases the

molecular weight of the product. The cyclodehydration of poly(amic acid) could be carried out by two methods; extended heating at high temperature, *i.e.*, thermal imidization, or the treatment with a chemical dehydrating agent, *i.e.*, chemical imidization.

2.1.1.1.2 Thermal imidization

The most widely used second step in the two-step method of polyimide synthesis involves heating the poly(amic acid) in the solid state. This is usually preceded by a processing operation, whereby a poly(amic acid) solution is used to cast into the desired shape. The polymer in its different forms is dried and then subjected to specific heating cycles. One of the most popular heating cycles consists of one hour at 100 ^{o}C, followed by one hour at 200 ^{o}C followed by one hour at 300 ^{o}C. The imidization can occur *via* two different pathways as shown in Scheme 2.4. In the first path, the amine proton is lost after cyclization. In the second pathway, the proton is lost prior to or during ring closure. Ring closure is faster in the second pathway because the nucleophilicity of the conjugate base of the amide is much stronger than that of the amide. During the imidization process, some depolymerization of the poly(amic acid) occurs. However, above 180 ^{o}C the molecular weight again increases. The imidization process gives off water as a by product, which can cause voids. Due to these complications, it is scarcely able to obtain reproducible properties in fibers and films.

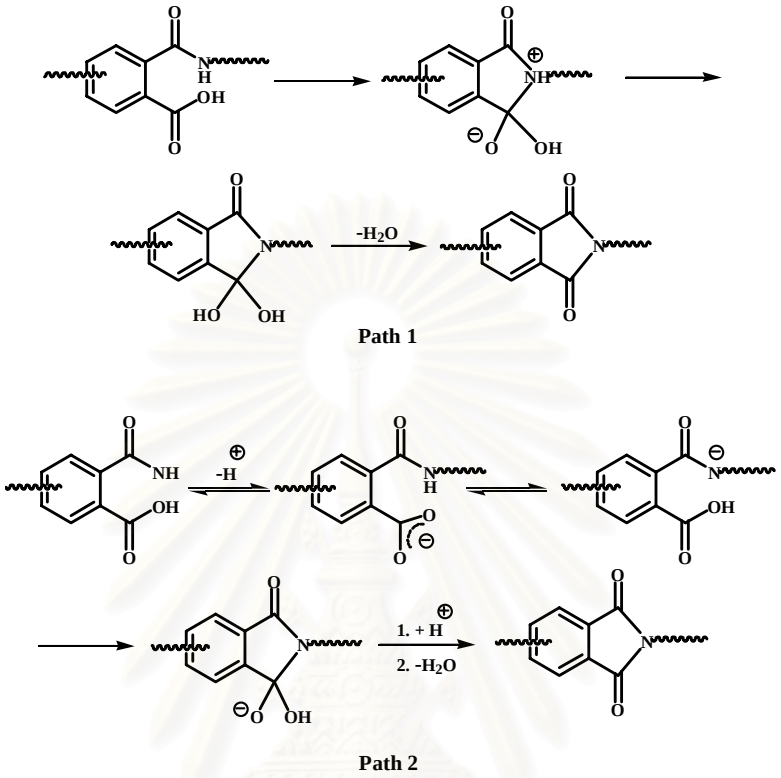

Scheme 2.4 The imidization pathways of polyimide

2.1.1.1.3 Chemical imidization

Poly(amic acid) can be converted to the corresponding polyimide at ambient temperature by treatment with mixture of aliphatic carboxylic acid dianhydrides and tertiary amines [22-24]. Acetic anhydride and pyridine are normally used. The mechanism for chemical imidization is shown in Scheme 2.5. During the reaction, the acid's hydroxyl group is converted to a better leaving group, *i.e.*, an acetate group, by the reagent mixture. The tertiary amine plays several

important roles in this conversion, which proceeds by nucleophilic substitution. It converts the carboxylic acid to a better nucleophile, *i.e.*, its ionic, conjugate base.

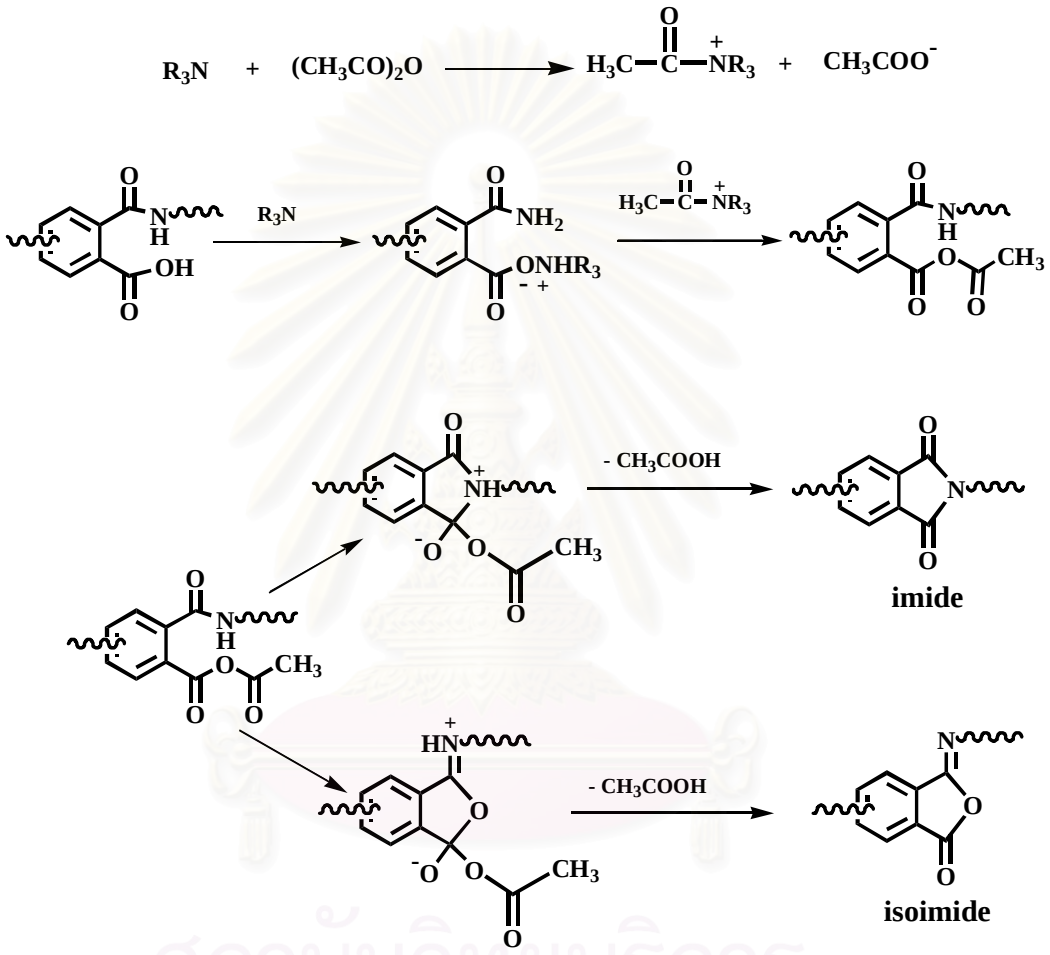

Scheme 2.5 Mechanism for chemical imidization

It also converts the aliphatic dianhydride to a salt form, which is more susceptible to nucleophilic attack. Ring closure proceeds *via* a second nucleophilic substitution reaction. Cyclization can occur by two different pathways: if nitrogen atom attacks, the product is the imide; if the oxygen atom attacks, the product is the isoimide. The

isoimide is the kinetically favored imide product, the isoimide subsequently rearranges to the imide. The rearrangement is catalyzed by the acetate ion present in the reaction medium, as illustrated in Scheme 2.6.

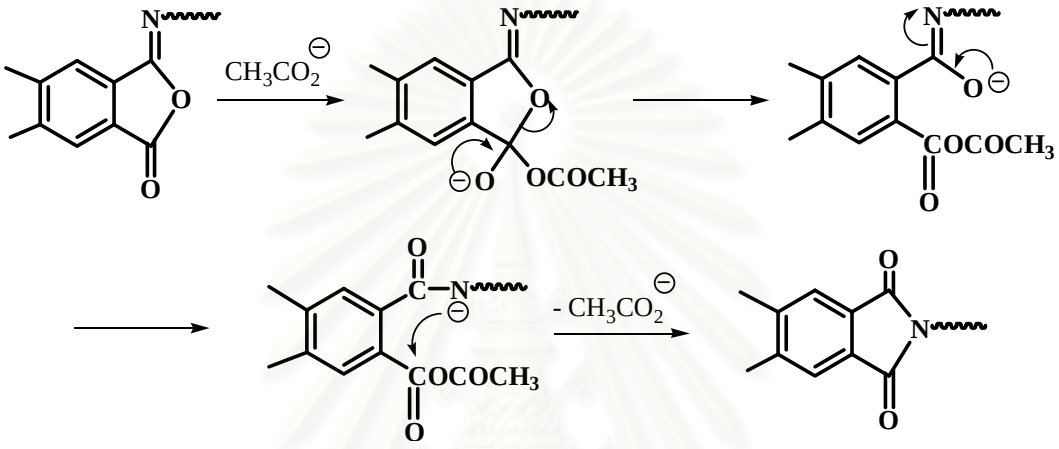

Scheme 2.6 Cyclization reaction in chemical imidization

2.1.1.2 One-step method

In the one-step method, the dianhydride and diamine are stirred in a high boiling organic solvent at 180-220 ^{o}C. In these conditions, chain growth and imidization occur without isolation of the poly(amic acid) intermediate (Scheme 2.7).

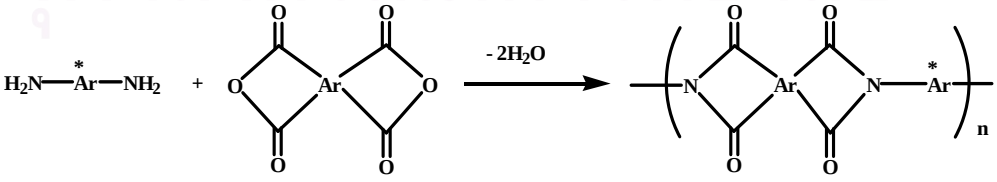

Scheme 2.7 One-step method for polyimide synthesis

This method is suitable for synthesizing polyimides that can be soluble in organic solvents. The water generated by imidization is usually allowed to distil from the reaction mixture to drive the imidization reaction to completion. With this method unreactive or sterically hindered monomers can be successfully polymerized due to the high temperature used. In this study, porphyrin-containing polyimides have been synthesized by using one-step method.

2.2 Porphyrin [25]

Porphyrins are aromatic tetrapyrrolic macrocycles consisting of four pyrrole units jointed by methane groups as shown in Scheme 2.8. The numbering is shown below, the "α" positions are those at carbons 1, 4, 6, 9, 11, 14, 16 and 19, the "β" positions are those at carbons 2, 3, 7, 8, 12, 13, 17 and 18. The positions 5, 10, 15 and 20 are referred to as the "*meso*"-positions.

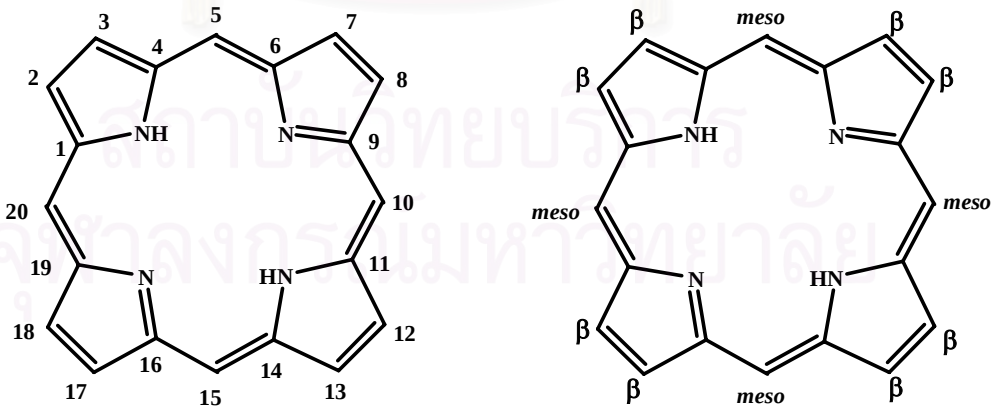

Scheme 2.8 Positioning in porphyrin

These compounds possess 22 π–electrons but only 18 of these are included in a cyclic delocalized conjugation pathway (Scheme 2.9). The vast majorities of porphyrins are planar and thus fulfill the requirements for aromaticity according to Hückel's rules (4n+2; n = 4). The large diamagnetic ring current observed in porphyrins is expressed by their ^{1}H-NMR spectra wherein the inner NH protons are highly shielded (δ= -1 to -5 ppm), and the *meso*-protons on the bridging carbons are strongly deshielded (δ = 8 to 10 ppm). The ring current that deshields proton from the external magnetic field on the outside of the macrocycles simultaneously shields protons on the insides of the macrocycle.

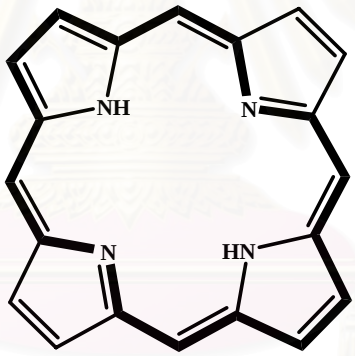

Scheme 2.9 The 18π-electron pathway

Porphyrins can complex with a variety of metals with the concomitant loss of the inner NH protons, these porphyrins called a metalloporphyrin. Some metalloporphyrins play essential roles in biological system. For example, the conversion of sunlight to chemical energy stored in the form of carbohydrates in green plants which is mediated by compounds as chlorophylls in which magnesium porphyrin is basic structural

component. Iron porhyrin appears in heme, associated with the proteins hemoglobin and myoglobin, which are responsible for the transport and storage of oxygen in the body tissues of warm-blood animals. The earlier work on porphyrin-containing polymers mainly involved the incorporation of porphyrins for the study of artificial solar energy conversion system [26, 27], and to study the catalytic effect [28-29] and electron transfer or photoinduced electron transfer of these polymers [30-33]. More recently, the interest in advanced electronic and photonic materials has been increased dramatically, and porphyrin and its derivatives are attracting more attention because of their unique structures and interesting electronic and optical materials applications. In addition, the wide choices of different metalloporphyrins offer a unique opportunity in material design because these compounds have also been found to exhibit high photoconductivity and large optical nonlinearity [34-37]. With the development of new synthetic methods, soluble and processable main-chain porphyrin-containing polymers have been synthesized. Through careful design, different functional groups have been attached to the porphyrin-containing polymers to yield materials exhibiting enhanced properties and better process ability.

2.3 Fundamental Concept of Electron Transfer

2.3.1 Photophysical processes

The principles of electron transfer are illustrated by a modified Jablonski diagram shown in Figure 2.1. The absorption of light by a molecule in its ground state (S_0) causes an electron to be promoted from the highest occupied molecular orbital

(HOMO) into the lowest unoccupied molecular orbital (LUMO), resulting in the formation of the lowest singlet excited state of the molecule (S_1). If the photon emission

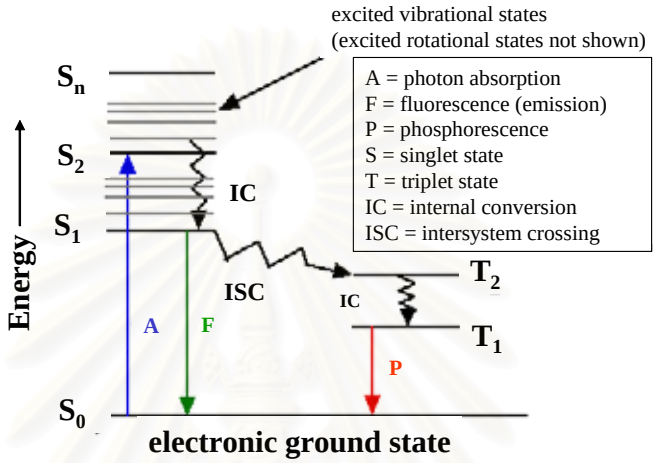

Figure 2.1 Jablonski diagram.

occurs between states of the same spin state (e.g. $S_1 \rightarrow S_0$), this is termed fluorescence. If the spin state of the initial and the final energy levels are different (e.g. $T_1 \rightarrow S_0$), the emission (loss of energy) is called phosphorescence. Since fluorescence is statistically much more likely than phosphorescence, the lifetimes of fluorescence states are very short and ones of phosphorescence are somewhat longer. Three non-radiative deactivation processes are also significant: internal conversion (IC), intersystem crossing (ISC) and vibrational relaxation. Internal conversion is the radiationless transition between energy states of the same spin state. Intersystem crossing is a radiationless transition between different spin states. The energy difference between the ground state (S_0) and, singlet state (S_1, S_2) and triplet state (T_1,

T_2) are progressively lower at higher vibrational state. Each process is characterized by the rate constant (k).

2.3.2 Quenching pathway

Electron transfer is classified as quenching pathway. Quenching is defined as the deactivation of an excited sensitizer by quencher. Quenching of the excited state by electron transfer occurs when an electron jumps from an occupied orbital on the donor (D) molecule to an unoccupied orbital of the acceptor (A) (Figure 2.2), with the net result being the formation of the radical ion pair.

Figure 2.2 Electron transfer from an electron donor (D) to an electron acceptor (A) forming a radical ion pair.

2.4 Photovoltaic (PV) Principle

Almost all organic solar cells have a planar-layered structure, where the organic light-absorbing layer is sandwiched between two different electrodes. One of the electrodes must be (semi-) transparent, often Indium–tin-oxide (ITO), but a thin metal layer can also be used. The other electrode is very often aluminium (calcium, magnesium, gold and others are also used). Basically, the underlying principle of a light-harvesting organic PV cell (sometimes referred to as photodetecting diodes) is the reverse of the principle in light emitting diodes (LEDs) (Figure 2.3) and the development of the two are somewhat related. In LEDs an electron is introduced at the cathode with the balanced introduction of a hole at the anode. At some point the electron and the hole meets, and upon recombination light is emitted. The reverse happens in a PV device.

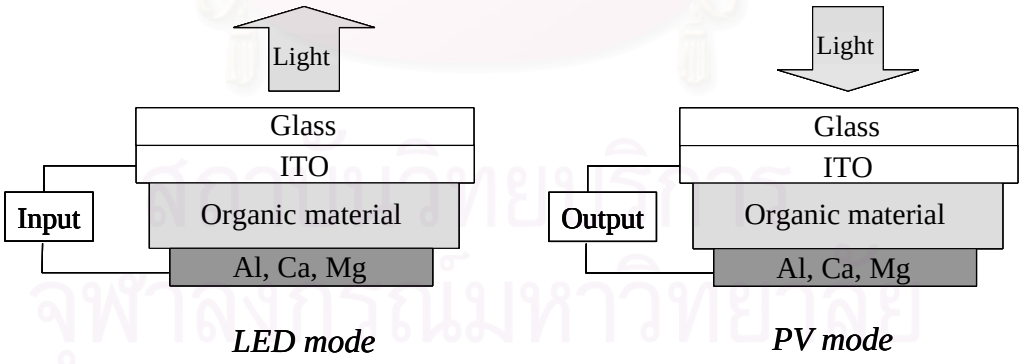

Figure 2.3 A PV device (right) is the reverse of a LED (left).

When light is absorbed an electron is promoted from the highest occupied molecular orbital (HOMO) to the lowest unoccupied molecular orbital (LUMO) forming an exciton (Figure 2.4). In a PV device this process must be followed by exciton dissociation. The electron must then reach one electrode while the hole must reach the other electrode. In order to achieve charge separation an electrical field is needed, which is provided by the asymmetrical ionization energy/workfunctions of the electrodes. This asymmetry is the reason why electron-flow is more favoured from the low-workfunction electrode to the high-workfunction electrode (forward bias), a phenomenon referred to as rectification. The light harvesting process along with the positioning of energy levels is depicted in Figure 2.4.

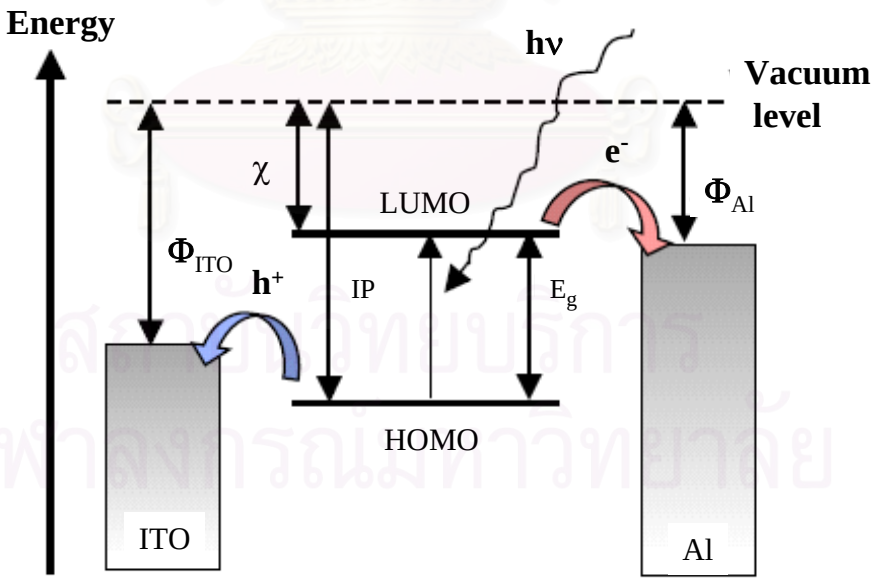

Figure 2.4 Energy levels and light harvesting. Φ: workfunction, χ: electron affinity, IP: ionization potential, E_g: optical band gap.

Since porphyrin is highly conjugated (highly electron density); this conforms to Hückel's 4n + 2 rule for aromaticity, the incorporation of porphyrin into polymer structure could be improved the ability of materials for function as the electron donor. In this study, porphyrin-containing polyimides were synthesized for using as the donor material which could be used in photonic application.

2.5 Literature Reviews

At present, polyimides extensively used in microelectronics, photonics, optics, and aerospace industries not only for their considerably excellent thermal stability but also for their good mechanical properties, low dielectric constant, low coefficient of thermal expansion, high chemical resistance, high transparency and high refractivity. Significant effort has been expanded to improve their properties further by chemical modification of the chain backbones and higher-order structure control, so at present polyimides having different chain structures are used, according to the particular application. The synthesis of polymer containing porphyrin moieties is an active area in polymer science. Polymer containing porphyrin can be used as photorefractive materials [39-40], and molecular wires [41-42]. Much attention has also been paid on the synthesis of polyimides containing porphyrin recently, since they can be used as photoconductive materials and charge transporting materials.

Imai, *et al.* [43] synthesized fluoro and nonfluoro polyimides. Polyimides with hexafluoroisopropylidene moieties either in the diamine or in the dianhydride component were soluble in polar solvent. The good solubility is governed by the

structure modification through the incorporation of the bulky hexafluoroisopropylidene group into the polyimide structure. The thermal behavior of the fluorine containing polyimides had a slightly higher thermal stability than the nonfluoro polyimides. Higher T_g values were recorded for the fluoro polyimides than those of the nonfluoro polyimides. Visually, the polyimides prepared from the fluorine-containing diamine were much less yellow compared to the nonfluoro polyimide films.

Cheng, *et al*. [1] had synthesized polyimide which contains 2,2′-*bis*(trifluoromethyl)-4,4′-diaminobiphenyl (Scheme 2.10). It has been observed that

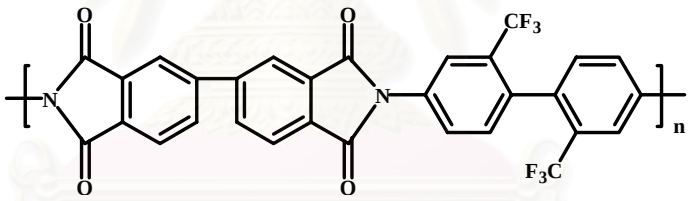

Scheme 2.10 The chemical structure of polyimide based on BPDA-PFMB

the polyimide films exhibit a high thermal and thermo-oxidative stability. The dielectric constant was measured; it was found that the polymers showed a low dielectric constant, which is vital for microelectronic use. High dimensional stability of polymers was observed with a coefficient of thermal expansion (CTE) of 6.98 × 10^{-6} $^{o}C^{-1}$ in a temperature region of 50-200 ^{o}C. This CTE of this polyimide films is in between the values of copper (16.6 × 10^{-6} $^{o}C^{-1}$) and silicon (3 × 10^{-6} $^{o}C^{-1}$), which are two important inorganic materials widely used for microelectronic applications.

Harris, *et al*. [2] synthesized polyimides which involved the polymerization of 2,2′-disubstituted-4,4′-diaminobiphenyl with aromatic dianhydride . The introduction of substituents in the 2 and 2′-positions of the dianhydride component results in dramatic changes in polymer properties. The T_gs and CTEs of the polymers are significantly increased. It was found that polyimide obtained from 2,2′-*bis*(trifluoromethyl)-4,4′-diaminobiphenyl, was soluble in acetone, THF, DMSO, DMAc and NMP. The polymers exhibited high T_g and high decomposition temperature (Scheme 2.11).

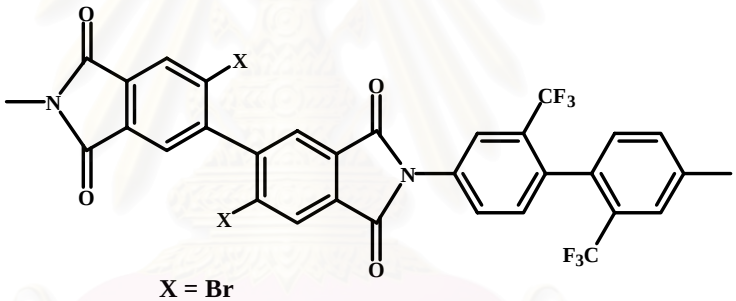

X = Br
X = C_6H_5

Scheme 2.11 Polyimide containing 2,2′-disubstituted dianhydride and 2,2′-disubstituted diaminobiphenyl

Tomikawa, *et al.* [44] had synthesized the new soluble polyimides which obtained from the substituted pyromellitic dianhydride and 2,2′-*bis*(trifluoromethyl)-4,4′-biphenyl (PFMB) (Scheme 2.12). These polyimides were soluble in *N*-methyl-2-pyrrolidone (NMP), dimethylacetamide (DMAc), *m*-cresol and other solvents. The color and viscosity of the polyimide solution have been changed after UV irradiation.

The new visible absorbance and the ESR signal were then observed. They are attributed to the anion radical of the diimide moiety in the polyimide.

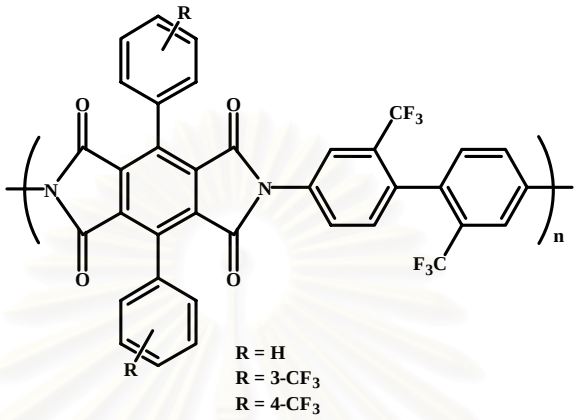

Scheme 2.12 Structure of soluble polyimide obtained from substituted pyromellitic dianhydride and 2,2′-*bis*(trifluoromethyl)-4,4′-diaminobiphenyl (PFMB)

Harris, *et al,* [45] synthesized polyimides from 2,2′-*bis*(trifluoromethyl)-4,4′,5,5′-biphenyltetracarboxylic dianhydride and various types of diamine. It was found that polymer that was prepared from this dianhydride and 2,2′-*bis*(trifluoromethyl)-4,4′-biphenyl (PFMB) (Scheme 2.13), was soluble in most solvents, *i.e.*, acetone, THF, DMF, DMSO, DMAc and NMP. It also gave the higher thermal stabilities than the polymers, which were prepared by this dianhydride and other diamines.

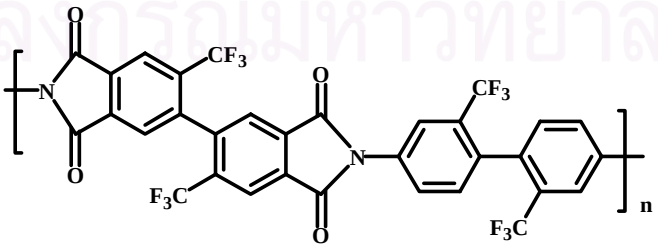

Scheme 2.13 Structure of polyimide prepared from 2,2′-*bis*(trifluoromethyl)-4,4′,5,5′-biphenyltetracarboxylic dianhydride

Fujihara, *et al.* [7] prepared and studied the photocurrent properties of tin dioxide electrode modified by polyimide Langmuir-Blodgett (LB) films containing tetraphenylporphyrin unit (TPP). Two kinds of electrodes were prepared, electrode I was prepared by the deposition of polyimide LB film containing TPP onto tin dioxide electrode. The electrode II was prepared by the deposition of monomeric TPP LB film onto tin dioxide electrode, which prepared form 1:1 mixture of monoamino-TPP and stearic acid. These electrodes were stable under the irradiation of monochromatic light of 430 nm, while the direct irradiation of the xenon lamp, electrode I kept the same level of the initial photocurrent for a long time, but electrode II decreased to 50% within one hour. The decrease of the photocurrent of electrode II was explained by the hydrophobicity of the surface of the LB film containing the long alkyl chain and by the diffusing effect of the reducing agent in the electrolyte solution.

Xu, *et al*. [10] had prepared the copolyimide films containing tetraphenylporphyrin (TPP) and carbazole (Cz) units. These copolyimides were fabricated into bilayer photoreceptors as a charge-generating layer to investigate their photoconductivity. It was found that the photoconductivity of the copolyimides increased with the incorporation of TPP into polymer chains (Scheme 2.14). The formation of charge transfer complex (CTCs) in these polyimides appeared to increase the photosensitivity of polymers.

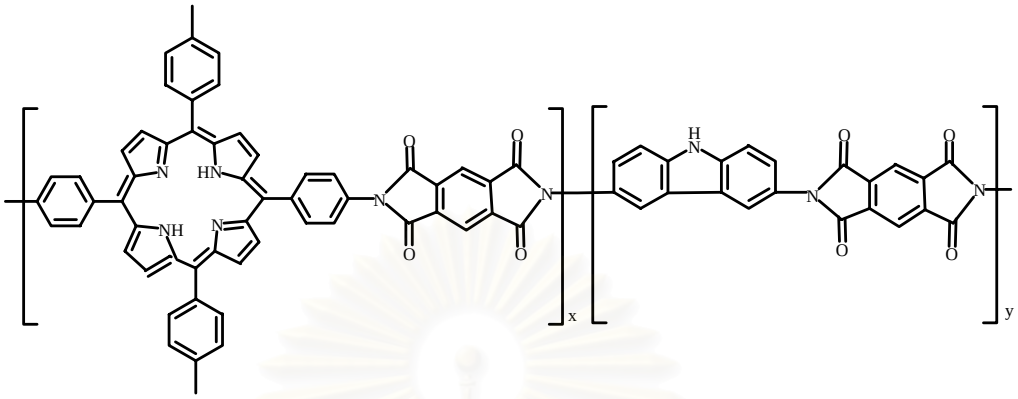

Scheme 2.14 Copolyimide films containing tetraphenylporphyrin (TPP) and carbazole (Cz) units.

Xu, *et al*. [11] synthesized a series of copolyimides based on pyrromellitic dianhydride (PMDA), oxydianiline (ODA) and tetra(4-aminophenyl)porphyrin (Scheme 2.15) and investigated the photoconductivity of these polymers. Copolyimide films, which act as charge-generating layers, were fabricated. It was found that the photosensitivity of the copolyimides increased with the amount of tetra(4-aminophenyl)porphyrin incorporated in the polymer chains.

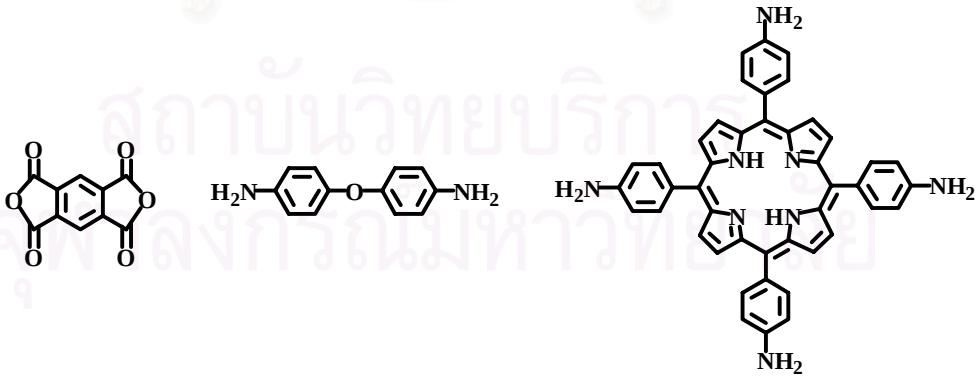

PMDA ODA tetra(4-aminophenyl)porphyrin

Scheme 2.15 Structures of pyrromellitic dianhydride (PMDA), oxydianiline (ODA) and tetra(4-aminophenyl)porphyrin

Zhu, *et al.* [12] had synthesized polyimide containing biphenylporphyrin (BPP) (Scheme 2.16) by two-step method. It was found that the photoconductive sensitivities of polyimide increased with increasing BPP content. These results were attributed to the formation of CTCs of BPP units and imide groups (BPP-imide) which could significantly improve the photosensitivity of polyimide systems.

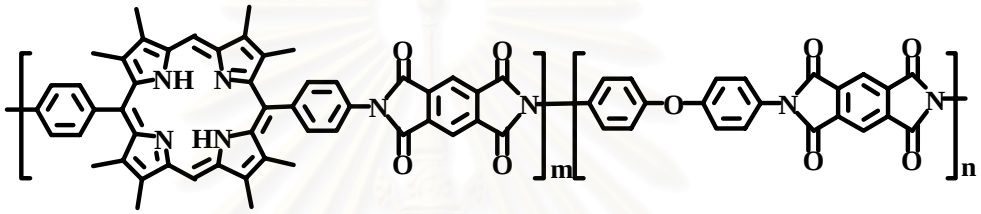

Scheme 2.16 Polyimide containing biphenylporphyrin (BPP)

Ito, *et al*. [14] prepared of ultrathin film polyimide containing porphyrin moieties. Photoinduced electron transfer between porphyrin moieties and pyromellitimide fragments has been investigated in multi-layered structures of ultrathin films prepared by LB techniques. The LB films were composed of three kinds of polyimides, which contained zinc tetraphenylporphyrin (ZnTPP) unit as electron donor (D-layer), no chromophoric group as a spacer (S-layer), and pyromellitimide fragments as electron acceptor (A-layer) (Scheme 2.l7). The fluorescence intensity of polyimide without spacer layer steeply decreased as the number of A-layers increased. On the other hand, the fluorescence intensity of polyimide film, which contained three kinds of polyimides, increased as the number of S-layers increased. Thus, the fluorescence quenching was due to the electron

transfer from the excited porphyrin moieties to the pyromellitimide and that the overall efficiencies were controlled by the separation distance or S-layers between the donor and acceptor layers.

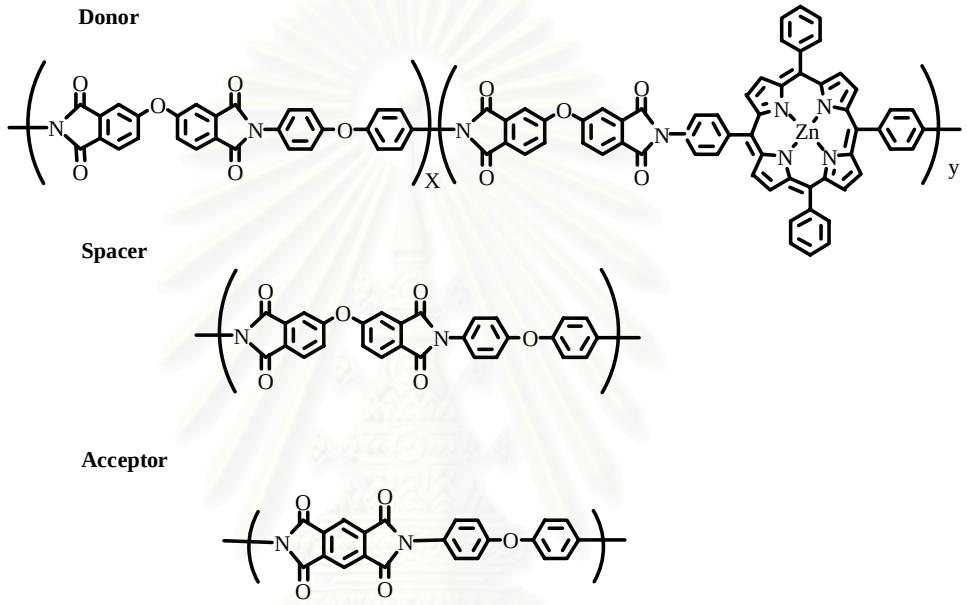

Scheme 2.17 Polyimide containing porphyrin moieties

CHAPTER III

EXPERIMENTAL

3.1 Instrumentation

Proton nuclear magnetic resonance (^{1}H-NMR) spectra were obtained with a Varian Gemimi 300 MHz NMR spectrometer. Chemical shift (δ) is in ppm using the residual proton signal in deuterated solvents as internal references. All melting points were determined on a Mel-Temp melting point apparatus and were uncorrected. ESI-QIT-MS was obtained with a Bruker Esquire-LC ion trap mass spectrometer. IR spectra were recorded on a Nicolet NEXUS 870 FT-IR spectrometer equipped with a Thunderdom ATR accessory. Absorption experiments were carried out on a Hitachi 3100 single monochromator UV-vis spectrophotometer. Steady state fluorescence measurements were run on a ISA Jobin Yvon-SPEX Fluorolog 3-22 fluorometer having dual input and output monochrometers. Fluorescence spectra were collected using argon-saturated solutions by exciting at the Soret band. Quantum yield measurements were made relative to TPP and ZnTPP.

Thermogravimetric analyses (TGA) were obtained in nitrogen and air with a TA Hi-Res TGA 2950 thermogravimetric analyzer using heating rate of 10 ^{o}C/min. Glass transition temperatures (T_gs) of polyimide films were determined with thermo-mechanical analysis (TMA) using a TA TMA 2940 thermomechanical analyzer with a tension mode, the films were subjected to three different stresses with heating rate

of 10 ^{o}C/min. The T_g was taken as the temperature at which the slope of a plot of film dimensional change versus temperature occurred. The T_gs obtained at each stress level were then extrapolated to zero stress. Intrinsic viscosities were determined with SCHOTT-Ostwald viscometer (2 mL). Flow times were recorded for *N*-methyl-2-pyrrolidone (NMP) with polymer concentrations of approximately 0.2-1.0 g/dL at 35 ± 0.1 ^{o}C.

3.2 Time-Correlated Single Photon Counting (TCSPC)

All solvents used for spectroscopic measurements were either Spectral or HPLC grade. Time-resolved fluorescence experiments were performed using the time-correlated single photon counting (TCSPC) technique. The instrument used in this work utilized the pulses from a Coherent cavity dumped 702 dye laser pumped by the 527 nm output of a Quantronix 4417 CW mode-locked Nd:YLF laser. The fluorescence signal was detected at 54.7^{o} with an emission polarizer and depolarizer, using a Hamamatsu R3809U-51 red-sensitive multichannel plate detector (MCP). Data collection and analysis was accomplished with an Edinburgh Instruments data collection system, with resolution estimated at ~ 7-9 ps. Fluorescence decays having multiple components were fit using the Marquardt algorithm. Most measurements were fit such that values of $\chi^2 < 1.20$ were obtained, although some fits were made to $\chi^2 < 1.40$ due to the complexity of the decays and the limitations of the data analysis software. Error limits in these measurements were typically ± 10%. All TCSPC experiments were run with argon-saturated CH_2Cl_2 and DMAc solutions with an optical density of 0.15 at the excitation wavelength of 573 nm. The decay profiles of

PI3 and WPI3 were monitored at 650 nm and the decay profiles of ZPI3 and WZPI3 at 610 nm. Electron-transfer rate constants were calculated using Equation 3.1 where

$$k_{ET} = \frac{1}{\tau_{PI}} - \frac{1}{\tau_{ref}} \qquad (3.1)$$

τ_{PI} represents the fluorescence lifetime of polyimides and includes contributions from each fluorescence lifetime, such that $\tau_{PI} = a_1(\tau_1) + a_2(\tau_2) + a_3(\tau_3)$, and a_1- a_3 represents the pre-exponential factors for each component as determined by the equation: $a_i = (a_i\tau_i/\Sigma\ a_i\tau_i)100$.

3.3 Electrochemistry

Cyclic voltammograms (CV) were recorded on a BAS-100 electrochemistry apparatus from Bioanalytical System, Inc. at 20 ^oC. A three-electrode configuration was used with a platinum working and auxiliary electrodes, and the standard calomel electrode as a reference (0.1 M supporting electrolyte, tetrabutylammonium perchlorate, TBAP).

3.4 Reagents and Solvents

3.4.1 Reagents

Ammonium hydroxide (EMD) was used as received.

Benzaldehyde (EMD) was distilled under reduced pressure prior to use.

Borontrifluoride etherate, $BF_3.OEt_2$ (Acros) was used as received.

Calcium hydride (Acros) was used as received.

Celite® (Aldrich) was used as received.

2,3-Dichloro-5,6-dicyanobenzoquinone, DDQ (Acros) was used as received.

4,4′-Hexafluoroisopropylidenediphthalic anhydride, 6FDA (Daikin) was sublimed before use.

Hydrochloric acid (Fisher) was used as received.

Isoquinoline (Aldrich) was distilled over zinc dust under reduced pressure.

Magnesium sulfate anhydrous (EMD) was used as received.

4-Nitrobenzaldehyde (Acros) was used as received.

Phosphorous pentoxide (Acros) was used as received.

Pyrrole (Acros) was distilled over calcium hydride under reduced pressure prior to use.

Sodium hydroxide (Fisher) was used as received.

Silica gel, 230-400 mesh, 60 Å (Merck) was used as received.

Sodium sulfate anhydrous (Fluka) was used as received.

Stannous chloride dihydrate (Aldrich) was used as received.

Tetrabutylammonium perchlorate, TBAP (Fluka) was used as received.

Trifluoroacetic acid, TFA (Acros) was used as received.

Zinc acetylacetonate hydrate (Alfa Aesar) was used as received.

3.4.2 Solvents

Chloroform (Fisher) was used as received.

Chloroform-d, $CDCl_3$ (Aldrich) was used as received.

Dichloromethane (EMD) was distilled over calcium hydride before use.

Dichloromethane, spectral grade (Acros) was used as received.

Dimethylacetamide, DMAc (Aldrich) was used as received.

Dimethylacetamide, HPLC grade (Acros) was used as received.

N, *N*′-Dimethylformamide, DMF (Aldrich) was used as received.

Dimethylsulfoxide, DMSO (EMD) was used as received.

Dimethylsulfoxide-d_6, DMSO-d_6 (Aldrich) was used as received.

Ethanol, absolute (Fisher) was used as received.

Ethylacetate (Fisher) was used as received.

Hexane (EMD) was used as received.

N-methyl-2-pyrrolidone, NMP (Aldrich) was distilled over calcium hydride under reduced pressure prior to use.

Triethylamine (Aldrich) was used as received.

3.5 Monomer Syntheses

3.5.1 Synthesis of *meso*-substituted phenyldipyrromethane

3.5.1.1 *Meso*-phenyldipyrromethane (1a)

A mixture of benzaldehyde (3.44 g, 32.3 mmol) and pyrrole (90 mL, 1.2958 mol) was degassed with N_2 for 15 min, then trifluoroacetic acid (0.25 mL, 3.2 mmol) was added. The solution was stirred for 30 min at room temperature, at which point no starting aldehyde was shown by TLC analysis. The mixture was diluted with

dichloromethane (450 mL), then washed with 0.1 M sodium hydroxide (2 × 100mL), washed with water and dried with anhydrous sodium sulfate. The solvent was removed under reduced pressure and then the unreacted pyrrole was removed by vacuum distillation at room temperature. The resulting brownish solid was dissolved in a minimal quantity of the eluent and was purified by flash chromatography (silica, 7 × 25 cm, CH_2Cl_2/hexane/triethylamine = 60/40/1) affords the white *meso*-phenyldi-pyrromethane (**1a**) (2.70 g, 37 %): m.p. 102-103 ^oC (Ref. 100-101^oC [46]); IR (KBr): 3343 (NH), 3137 (CH-aromatic) , 3090 (CH-heteroaromatic) cm^{-1}; ^1H-NMR ($CDCl_3$) δ: 7.90 (bs, 2H, NH), 7.35-7.18 (m, 5H, ArH), 6.70 (q, J = 2.4 Hz, 2H), 6.17 (q, J = 2.6 Hz, 2H), 5.92-5.89 (m, 2H), 5.47 (s, *meso*-H),

3.5.1.2 *Meso*-(4-nitrophenyl)dipyrromethane (1b)

A mixture of 4-nitrobenzaldehyde (0.511 g, 1 mmol) and pyrrole (2.8 mL, 40 mmol) was degassed with N_2 for 15 min, then trifluoroacetic acid (8 μL, 0.1 mmol) was added. The solution was stirred for 30 min at room temperature, at which point no starting aldehyde was shown by TLC analysis. The mixture was diluted with dichloromethane (50 mL), washed with 0.1 M sodium hydroxide (2 × 25mL), then washed with water and dried with anhydrous sodium sulfate. The solvent was removed under reduced pressure and then the unreacted pyrrole was removed by vacuum distillation at room temperature. The crude product was precipitated from CH_2Cl_2/hexane and the recrystallized from ethanol/water to afford the yellow solid of *meso*-(4-nitrophenyl)dipyrromethane (**1b**) (0.2 g, 75 %): m.p. 163-165 ^oC (Ref. 159-

160 ^{o}C [47]), IR (KBr): 3390 (NH), 3353 (NH), 1512 (C-NO_2), 1348 (NO_2), 857 (1,4-subst. benzene) cm^{-1}; ^{1}H-NMR ($CDCl_3$) δ: 8.17 (d, J = 8.6 Hz, 2H), 8.01 (bs, 2H), 7.37 (d, J = 8.8 Hz, 2H), 6.74-6.71 (m, 2H), 6.17 (q, J = 2.6 Hz, 2H), 5.86-5.83 (m, 2H), 5.57 (s, *meso*-H) ppm.

3.5.2 5,15-*Bis*(4-nitrophenyl)-10,20-diphenylporphyrin (2), [46]

A solution of *meso*-(4-nitrophenyl)dipyrromethane (1.068 g, 4 mmol) and benzaldehyde (0.4245 g, 4 mmol) in 400 mL CH_2Cl_2 was purged with N_2 for 15 min, then $BF_3.OEt_2$ (0.6 mL of 2.5 M stock solution in CH_2Cl_2) was added. The solution was stirred for 90 min at room temperature, then 2,3-dichloro-5,6-dicyanobenzoquinone (DDQ) (0.6810 g, 3 mmol) was added. The mixture was stirred at room temperature for an additional 90 min and the solvent was removed until the amount of solvent is maintained about 50 mL. It was then pre-adsorbed on silica gel. Flash chromatography (silica, CH_2Cl_2:hexane = 60:40) gave dinitro tetraphenylporphyrin (**2**) (0.1341 g, 4.76%): m.p.>300 ^{o}C, IR (KBr): 3315 (NH), 1517 (asym, C-NO_2), 1343 (sym, C-NO_2), 962 (NO_2), 847 (1,4 subst. benzene) cm^{-1}, ^{1}H-NMR ($CDCl_3$) δ: 8.90 (d, J = 8.8 Hz, 4H, β-H), 8.75 (d, J = 9.0 Hz, 4H, β-H), 8.65 (d, J = 8.4 Hz, 4H, nitrophenyl), 8.40 (d, J = 8.4 Hz, 4H, nitrophenyl), 8.21 (d, J = 7.4 Hz, 4H, *o*-phenyl), 7.78-7.75 (m, 6H, *p*-, *m*- phenyl), -2.81 (s, 2H, internal NH) ppm.

3.5.3 5,15-*Bis*(4-aminophenyl)-10,20-diphenylporphyrin (3), [48]

Dinitro tetraphenylporphyrin (**2**) (0.4370 g, 0.6201 mmol) was dissolved in 220 mL of concentrated hydrochloric acid under nitrogen. Tin (II) chloride dihydrate

(1.1193 g, 4.9608 mmol) was added to the solution, and the reaction was heated to 65 ^{o}C for 90 min. The porphyrin solution was cooled to room temperature and poured into ice water and was adjusted to pH 8 with concentrated ammonium hydroxide. The aqueous phase was extracted with 5×200 mL portions of CH_2Cl_2, which were combined and dried over anhydrous magnesium sulfate. The organic phase was concentrated on a rotary evaporator to 50 mL and this solution was pre-adsorbed on silica gel. Flash chromatography (silica, 10% EtOAc in CH_2Cl_2) gave compound **3** as the purple crystal (0.3294 g, 28%): m.p. > 300 ^{o}C, IR (KBr): 3381 (NH_2), 3325 (NH), 1512 (NH), 800 (1,4-subst. benzene) cm^{-1}, ^{1}H-NMR (DMSO-d_6) δ: 8.95 (d, J = 4.8 Hz, 4H, β-H), 8.76 (d, J = 4.8 Hz, 4H, β-H), 8.22 (d, J = 7.5 Hz, 4H, aminophenyl), 7.87-7.80 (m,10H, phenyl), 7.03 (d, J = 8.1 Hz, 4H, aminophenyl), 5.59 (s, 4H, NH_2), -2.81 (s, 2H, internal NH) ppm; UV-vis (CH_2Cl_2) λ_{max} (log ε): 423 (5.27), 520 (3.88), 558 (3.75), 595 (3.42), 652 (3.48) nm, ESI-QIT-MS: 645.1 $[M+H]^{+}$ (calculated for $C_{44}H_{32}N_6$: 644.77).

3.5.4 Zinc 5,15-*bis*(4-aminophenyl)-10,20-diphenylporphyrin (4), [14]

To a solution of 190 mL of THF was added compound **3** (638 mg, 0.9895 mmol) and zinc acetylacetonate hydrate (1.276 g, 4.5331 mmol). The solution was refluxed for 4 h, cooled to room temperature, and then the solvent was evaporated. The precipitate was partly dissolved in methanol solution by heating and left overnight at 0 ^{o}C. The resulting violet crystal was collected, washed with methanol, and then dried to afford compound **4** (0.56 g, 80%): m.p. >300 ^{o}C, ^{1}H-NMR (DMSO-d_6) δ: 8.91 (d, J = 4.5 Hz, 4H, β-H), 8.75 (d, J = 4.5 Hz, 4H, β-H), 8.19 (d, J = 7.2 Hz,

4H, aminophenyl), 7.84-7.78 (m,10H, phenyl), 6.99 (d, J = 8.1 Hz, 4H, aminophenyl), 5.45 (s, 4H, NH_2) ppm; UV-vis (CH_2Cl_2) λ_{max} (log ε): 423 (5.47), 550 (4.18), 589 (3.79) nm ESI-QIT-MS: 709.2 $[M+H]^+$ (calculated for $C_{44}H_{30}N_6Zn$: 708.14).

3.5.5 Synthesis of 3,6-*bis*(3-trifluoromethylphenyl)pyrromillitic dianhydride (7), [49]

The 3,6-diaryl durene (**5**) (18.164 g, 0.043 mol) was dissolved in pyridine (220 mL) and water (110 mL). The solution was heated until reflux and then potassium permanganate (27.01 g, 0.1709 mol) was then added. After heating at reflux until the purple color vanished, the formed MnO_2 was removed by filtration and the solvents were evaporated. The residue was dissolved in a 10% NaOH (270 mL) and again treated with potassium permanganate (35 g). The reaction was stopped by adding some ethanol, and the mixture was filtered to remove the MnO_2. The filtrate was acidified with HCl and the white tetracarboxylic acid (**6**) precipitate was collected by filtration. After drying in an oven, the tetracarboxylic acid was carefully sublimated at 160 ^oC under reduced pressure to afford white crystals 3FPMDA (**7**) (12.1 g, 55%): m.p. 193-195 °C. ^{1}H-NMR (δ, DMSO-d_6): 8.06-7.75 (m, 8H, benzene).

3.5.6 Synthesis of 2,2′-*bis*(trifluoromethyl)-4,4′-diaminobiphenyl (9)

To a three neck round bottom flask fitted with a nitrogen inlet, a mechanical stirrer and a reflux condenser, $SnCl_2.2H_2O$ (8.0 g, 35.4 mmol), 2,2′-*bis*(trifluoromethyl)-4,4′-dinitrobiphenyl (1.90 g, 5.0 mmol) and 5 mL of ethanol were

added. The mixture was stirred at room temperature while 12 mL of concentrated hydrochloric acid was slowly added. The resulting mixture was heated at reflux for 12 h. After the ethanol was removed on a rotary evaporator, the residue was dissolved in water. The solution was then neutralized with 20% NaOH to provide a white precipitate. The precipitate was collected by filtration and washed three times each with water and with acetone. The solid was recrystallized from a 50:50 (v/v) mixture of chloroform and hexane to give 1.08 g (67%) of white crystals. The compound was further purified by sublimation at 150 ^{o}C under reduced pressure to afford white crystal: m.p. 181-182 ^{o}C (Ref. 180-182 ^{o}C [50]), ^{1}H-NMR (DMSO-d_6) δ: 6.91-6.85 (m, 4H, aromatic), 6.74 (dd, J = 2.1 Hz, 2H, aromatic), 5.53 (s, 4H, NH_2).

3.6 General procedure for polymer syntheses

The dianhydride monomer, 6FDA/3FPMDA (0.93 mmol) was added to the diamine monomer (0.93 mmol), PFMB/*trans*-DATPP/*trans*-ZnDATPP, at various mole ratios (Table 3.1) in dry NMP containing a small amount of isoquinoline under nitrogen at ambient temperature. After the solution was stirred for 8 h, it was heated to reflux and maintained at that temperature for 12 h. After the solution was allowed to cool to ambient temperature, it was slowly added to vigorously stirred methanol. The precipitated polymer was collected by filtration, washed with methanol, and dried under reduced pressure at 200 ^{o}C for 24 h. The polymer was obtained in 90-95 % yield.

Table 3.1 Polyimides at various ratios of monomers

PI	mole in feed (%)				
	6FDA	3FPMDA	PFMB	DATPP	ZnDATPP
Series I					
trans-DATPP					
PI1	100	-	95	5	-
PI2	100	-	90	10	-
PI3	100	-	85	15	-
Series II					
trans-ZnDATPP					
ZPI1	100	-	95	-	5
ZPI2	100	-	90	-	10
ZPI3	100	-	85	-	15
Series III					
trans-DATPP					
WPI1	95	5	95	5	-
WPI2	90	10	90	10	-
WPI3	85	15	85	15	-
Series IV					
trans-ZnDATPP					
ZWPI1	95	5	95	-	5
ZWPI2	90	10	90	-	10
ZWPI3	85	15	85	-	15

CHAPTER IV

RESULTS AND DISCUSSION

4.1 Monomer Syntheses

In this research, 5,15-*bis*(4-aminophenyl)-10,20-diphenylporphyrin (**3**), which is the *trans*-isomer of diaminotetraphenylporphyrin abbreviated as *trans*-DATPP, is required. Normally, *trans*-DATPP can be synthesized by 2 steps, the formation and the subsequent reduction of 5,15-*bis*(4-nitrophenyl)-10,20-diphenylporphyrin (**2**). In this part, all the attempts for the synthesis and structure identification of both compounds **2** and **3** are illustrated.

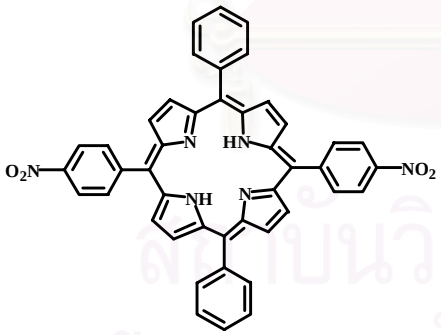

5,10-*bis*(4-nitrophenyl)-10,20-diphenylporphyrin

(**2**)

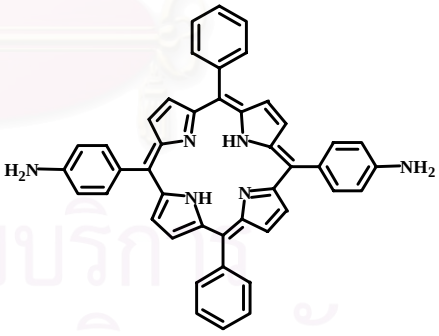

5,10-*bis*(4-aminophenyl)-10,20-diphenylporphyrin

(**3**)

Scheme 4.1 Structure of 5,15-*bis*(4-nitrophenyl)-10,20-diphenylporphyrin (**2**) and 5,15-*bis*(4-aminophenyl)-10,20-diphenylporphyrin (**3**)

4.1.1 Synthesis of 5,15-*bis*(4-nitrophenyl)-10,20-diphenylporphyrin (2)

The formation of **2** can be performed by 3 pathways. The first one is a one-step reaction, which is the condensation reaction of pyrrole, benzaldehyde and 4-nitrobenzaldehyde in propionic acid under refluxing condition (Scheme 4.2). The mixture of mononitro tetraphenylporphyrin and dinitro tetraphenylporphyrins (*cis* and *trans* isomers) was usually obtained and only about 2.2% of the mixture of dinitro tetraphenylporphyrins was achieved [9]. Unfortunately, it was reported that these two isomers could not be separated.

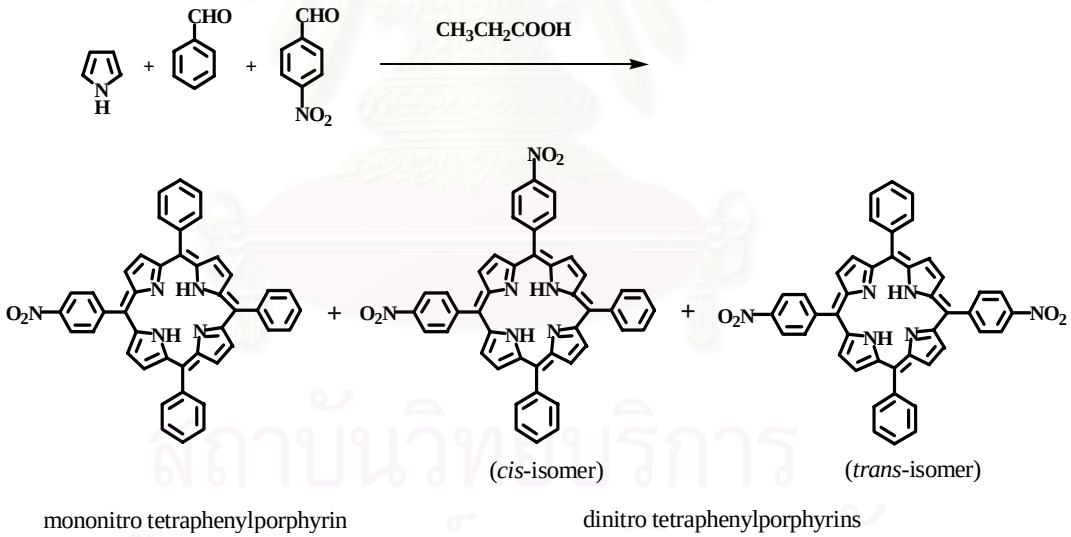

Scheme 4.2 One-step synthesis of the dinitro tetraphenylporphyrin

The second pathway was involved firstly the synthesis of tetraphenylporphyrin and then the nitration reaction of tetraphenylporphyrin with fuming nitric acid

(Scheme 4.3). The mononitro tetraphenylporphyrin and the mixture of the dinitro tetraphenylporphyrin were also obtained and the isomers of the dinitro tetraphenylporphyrin could not be separated [51].

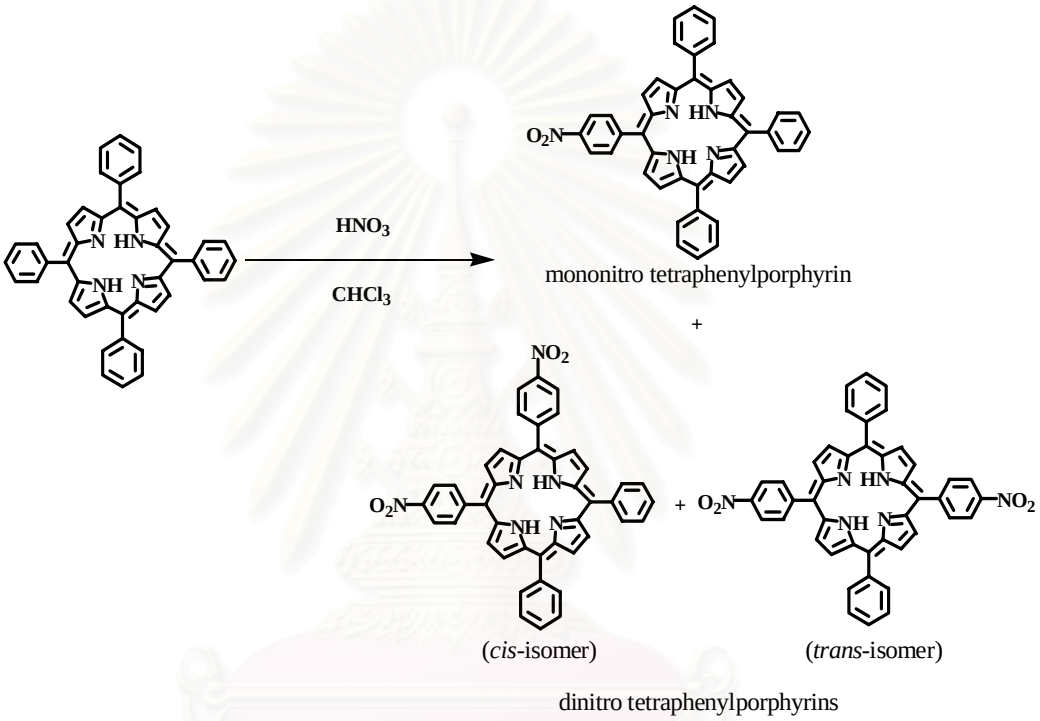

Scheme 4.3 Nitration reaction of tetraphenylporphyrin

The third pathway is the formation of *trans*-substituted *meso*-porphyrin according to the method of Lindsey. He synthesized *meso*-substituted tetraphenylporphyrins *via* *meso*-substituted dipyrromethanes (Scheme 4.4). The dipyrromethanes reacted with an aldehyde under acidic catalytic condition and finally oxidized with oxidizing agent, affording *meso*-substituted porphyrins bearing the substituents in a *trans*-substitution pattern (Scheme 4.5).

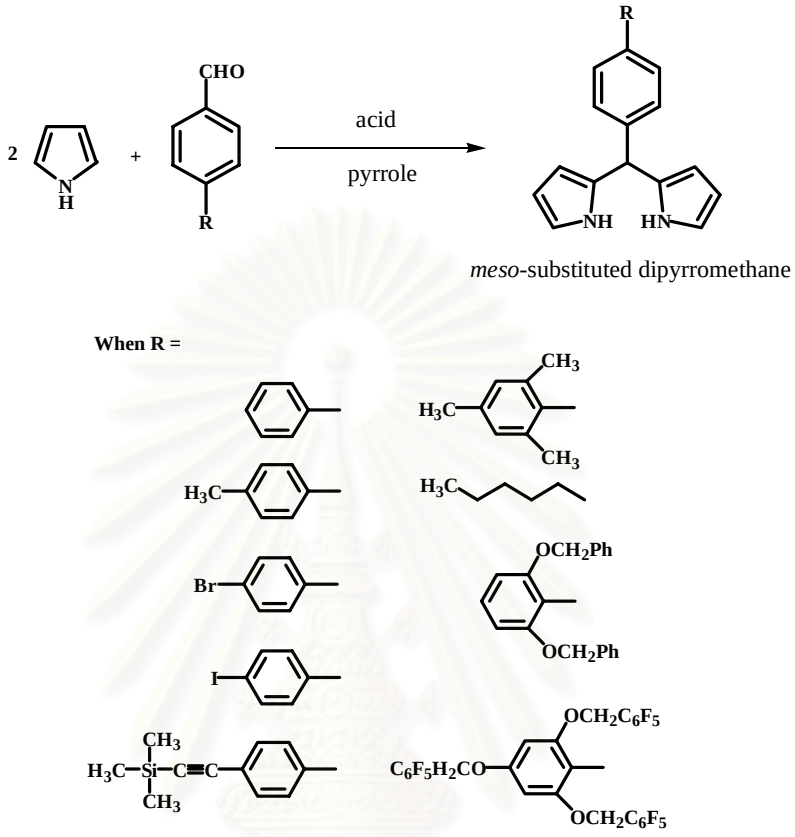

Scheme 4.4 One-step synthesis of *meso*-substituted dipyrromethanes

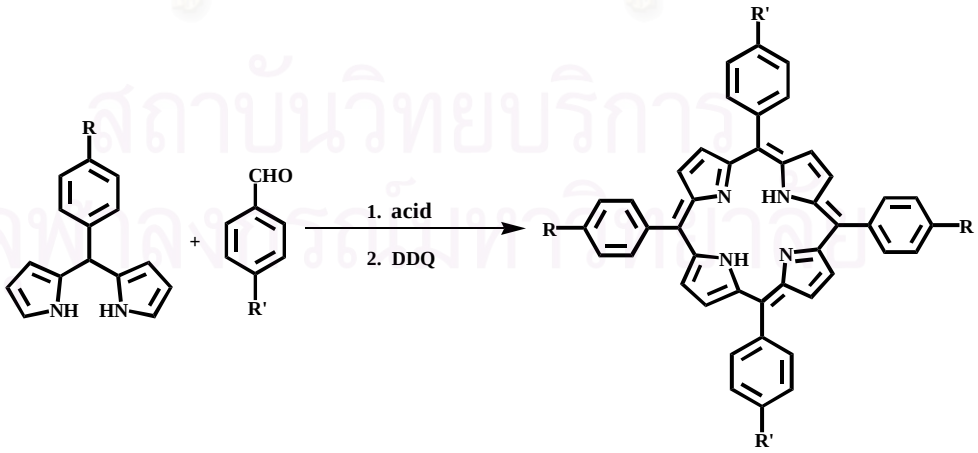

Scheme 4.5 Synthesis of *trans*-substituted *meso*-porphyrins

Since the first two methods provides the mixture of nitro porphyrins while the last method affords only *trans*-substituted *meso*-porphyrins, the modification of the method of Lindsey [46] was chosen for the synthesis of 5,15-*bis*(4-nitrophenyl)-10,20-diphenylporphyrin (**2**) as shown in Scheme 4.6

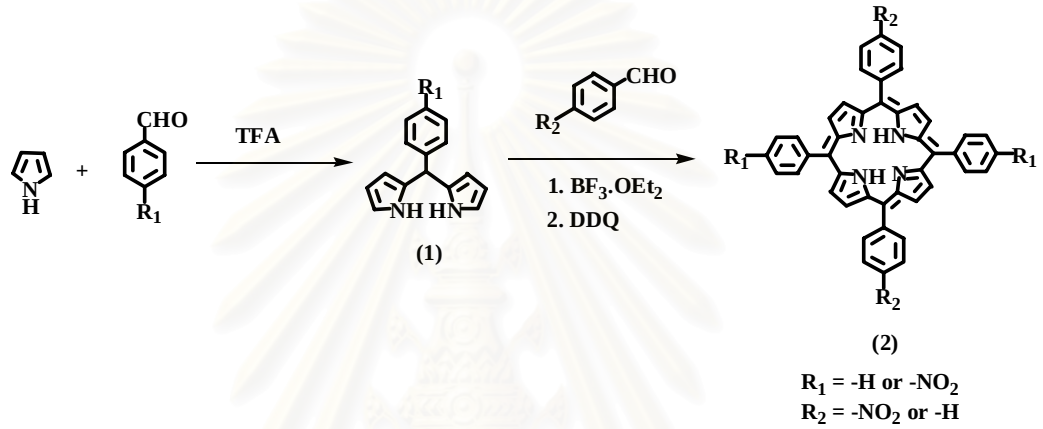

Scheme 4.6 5,15-*bis*(4-nitrophenyl)-10,20-diphenylporphyrin (**2**) formation

4.1.1.1 Synthesis of *meso*-(4-nitrophenyl)dipyrromethane (1b)

The synthesis of *meso*-substituted dipyrromethane **1a** or **1b** (Scheme 4.7) was attempted by starting at the condensation of pyrrole and either benzaldehyde or 4-nitrobenzaldehyde with the catalytic amount of trifluoroacetic acid (TFA) at room temperature. The complete reaction was obtained when no aldehyde left in the reaction as revealed by TLC monitoring. The excess pyrrole was then removed by vacuum distillation at room temperature.

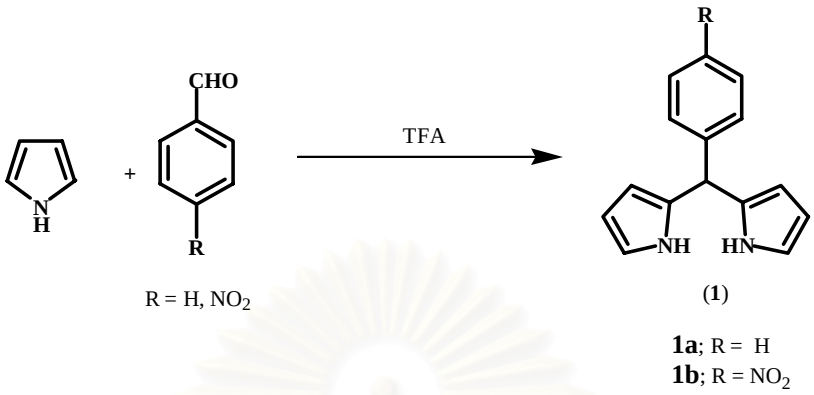

Scheme 4.7 Synthesis of *meso*-substituted dipyrromethane

When benzaldehyde was used, column chromatography on silica was required to isolate the white *meso*-phenyldipyrromethane (**1a**) with 35% yield. The IR spectrum of **1a** showed the strong absorption band at 3343 cm^{-1}, the characteristic N-H stretching of pyrrole (Figure 4.1).

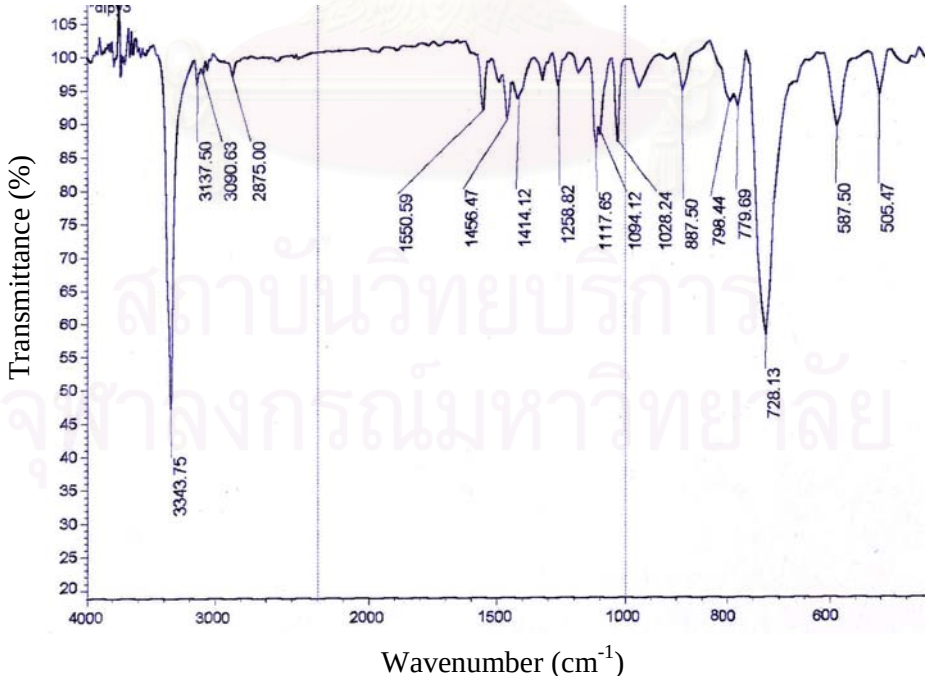

Figure 4.1 IR spectrum of *meso*-phenyldipyrromethane (**1a**).

The 200 MHz ^{1}H-NMR spectrum of **1a** (Figure 4.2) in chloroform-*d* exhibited the 2H broad peak of NH at δ 7.90 ppm. Other chemical shifts were assigned for the corresponding protons of **1a** as revealed in Table 4.1.

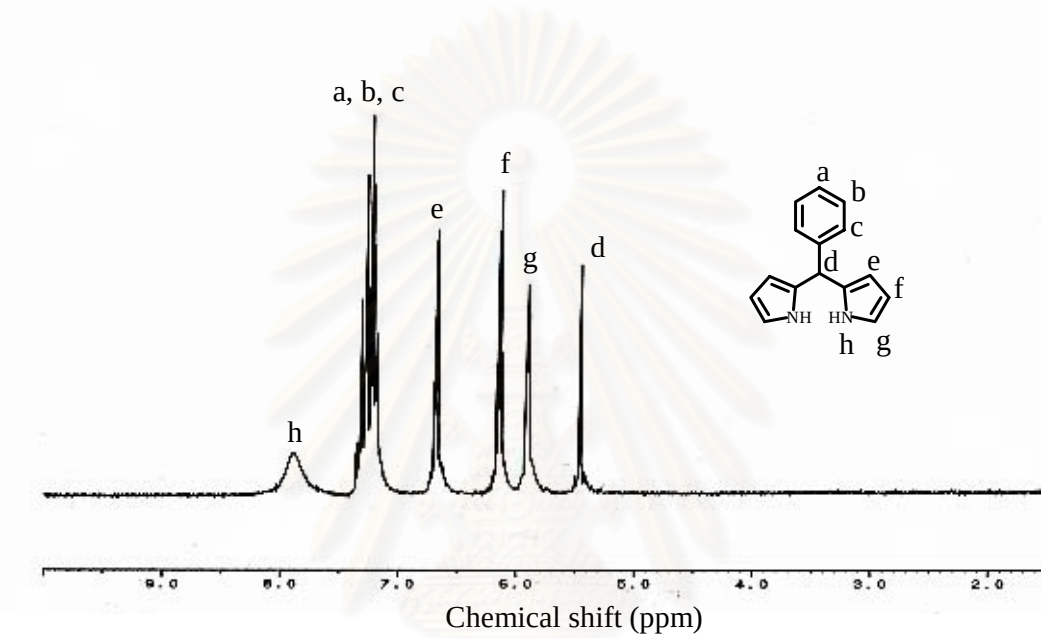

Figure 4.2 ^{1}H-NMR (200 MHz, $CDCl_3$) spectrum of *meso*-phenyldipyrromethane (**1a**).

Table 4.1 ^{1}H-NMR data of *meso*-phenyldipyrromethane (**1a**)

δ (ppm)	Multiplicity (J), number of proton (s), type of proton (position)
7.90	bs, 2H, NH (h)
7.35-7.18	m, 5H, phenyl (a, b, c)
6.70	q (2.4 Hz), 2H, β-H (e)
6.17	q (2.6 Hz), 2H, β-H (f)
5.92-5.89	m, 2H, pyrrole-H (g)
5.47	s, 1H, *meso*-H (d)

The reaction of 4-nitrobenzaldehyde interestingly afforded *meso*-(4-nitrophenyl)-dipyrromethane (**1b**) with 75% yield which was precipitated in CH_2Cl_2/hexane and recrystallized in aqueous ethanol. IR spectrum of **1b** (Figure 4.3) showed the strong

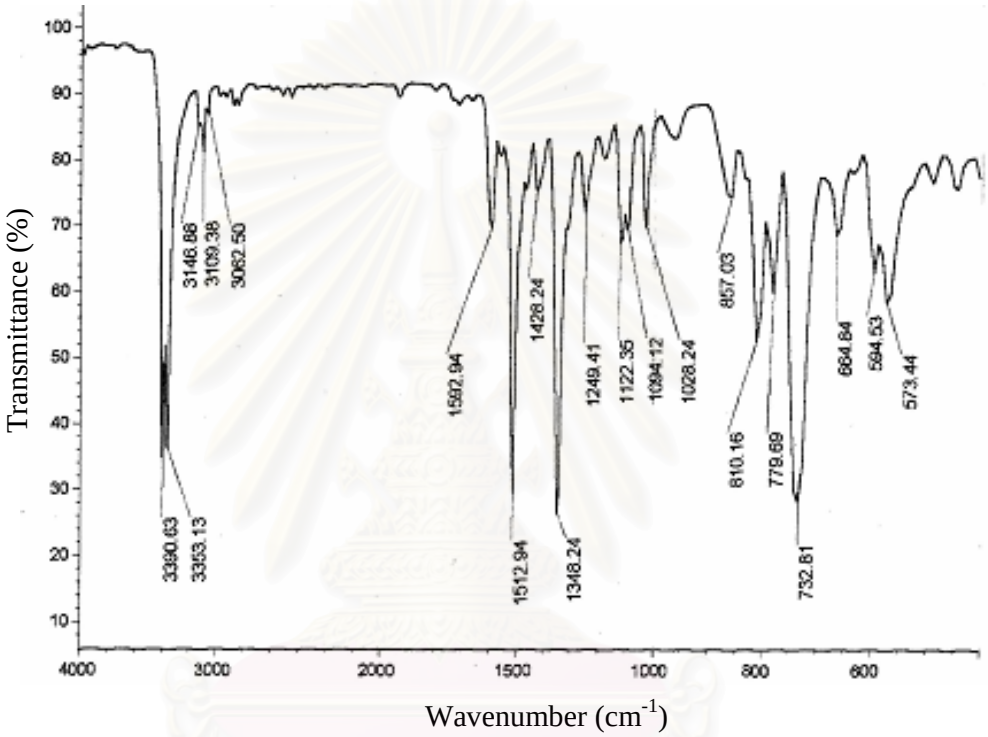

Figure 4.3 IR spectrum of *meso*-(4-nitrophenyl)dipyrromethane (**1b**).

absorptions at 3390 cm^{-1} and 3353 cm^{-1}, the characteristic absorptions of N-H stretching. The absorption of NO_2 stretching was observed around 1512 cm^{-1} and 1348 cm^{-1}. The absorption at 857 cm^{-1} was also found, which indicated the presence of 1,4-substituted benzene in the structure. The 200 MHz ^{1}H-NMR spectrum (Figure 4.4) of **1b** in chloroform-*d* exhibited a broad peak of NH at δ 8.01 ppm. Other chemical shifts were assigned for the corresponding protons of **1b** as revealed in Table 4.2.

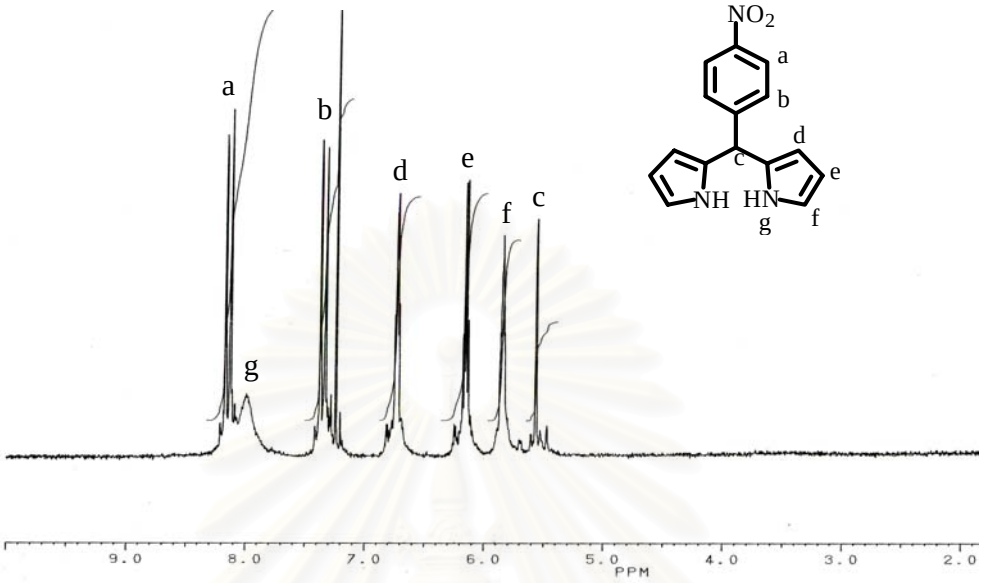

Chemical shift (ppm)

Figure 4.4 ^{1}H-NMR (200 MHz, $CDCl_3$) spectrum of *meso*-(4-nitrophenyl)dipyrromethane (**1b**).

Table 4.2 ^{1}H-NMR data of *meso*-(4-nitrophenyl)dipyrromethane (**1b**)

δ (ppm)	Multiplicity (J), number of proton (s), type of proton (position)
8.17-8.09	d (8.6 Hz), 2H, nitrophenyl (a)
8.01	bs, 2H, NH (g)
7.37-7.29	d (8.8 Hz), 2H, nitrophenyl (b)
6.74-6.71	m, 2H, β-H (d)
6.17	q (2.6 Hz), 2H, β-H (e)
5.86-5.83	m, 2H, pyrrole-H (f)
5.57	s, 1H, *meso*-H (c)

4.1.1.2 5,15-*Bis*(4-nitrophenyl)-10,20-diphenylporphyrin (2)

Since *meso*-(4-nitrophenyl)dipyrromethane (**1b**) could be synthesized with the yield as twice as *meso*-phenyldipyrromethane (**1a**), **1b** was chosen to be the starting material in the next step.

Meso-(4-nitrophenyl)dipyrromethane (**1b**) was reacted with benzaldehyde in the presence of $BF_3.OEt_2$ and then oxidized by DDQ (Scheme 4.8) to obtain 5,15-*bis*(4-nitrophenyl)-10,20-diphenylporphyrin (**2**) with approximately 4% yield.

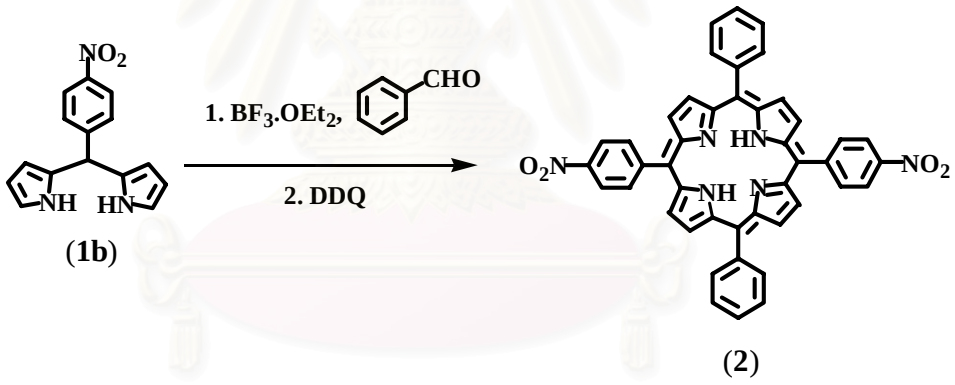

(**1b**) (**2**)

Scheme 4.8 Synthesis of 5,15-*bis*(4-nitrophenyl)-10,20-diphenylporphyrin (**2**)

The IR spectrum of **2** showed the absorption band at 3325 cm^{-1}, which is the characteristic absorption of N-H stretching of the internal NH of porphyrin (Figure 4.5). The symmetric and asymmetric C-NO_2 stretching was confirmed by the absorptions around 1522 cm^{-1} and 1343 cm^{-1}, respectively. The absorptions at 967 cm^{-1} for NO_2 and 847 cm^{-1} for 1,4-substituted benzene were also observed.

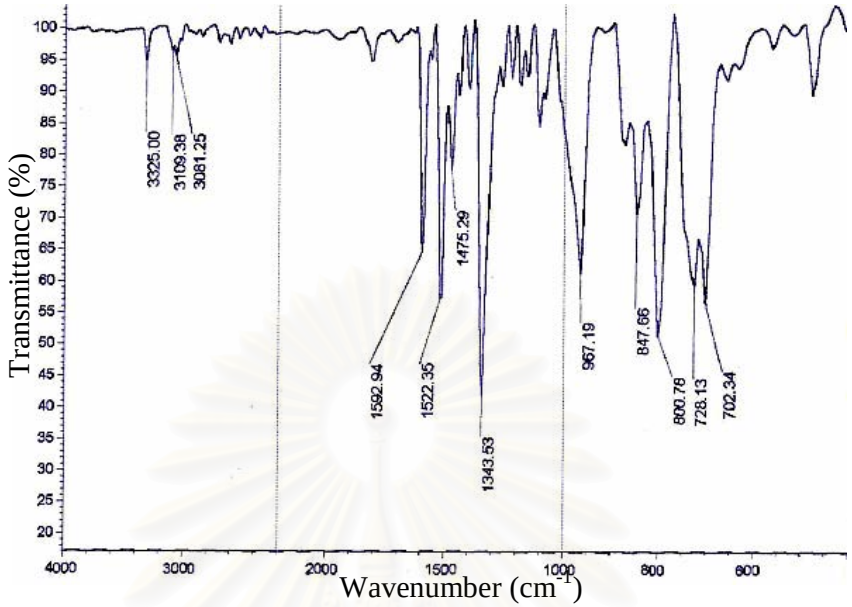

Figure 4.5 IR spectrum of 5,15-*bis*(4-nitrophenyl)-10,20-diphenylporphyrin (**2**).

^{1}H-NMR spectrum of the obtained product (Figure 4.6) confirmed that it was 5,15-*bis*(4-nitrophenyl)-10,20-diphenylporphyrin (**2**). The characteristic internal NH

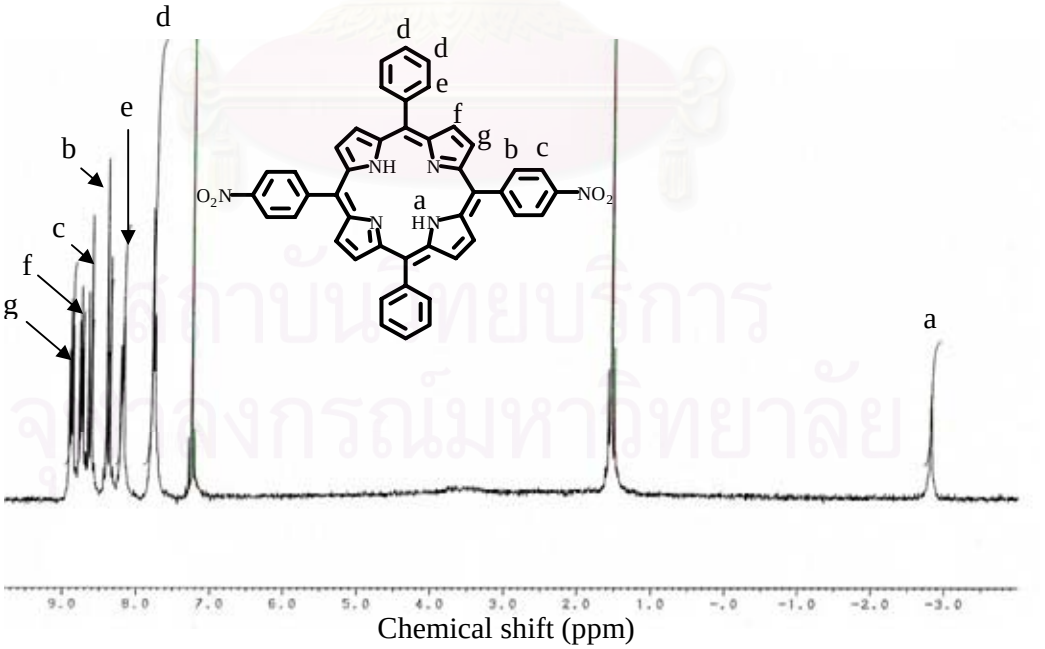

Figure 4.6 ^{1}H-NMR (200 MHz, $CDCl_3$) spectrum of 5,15-*bis*(4-nitrophenyl)-10,20-diphenylporphyrin (**2**).

of porphyrin was observed at δ -2.81 ppm. Other signals appeared at the chemical shifts which were assigned to the corresponding protons as revealed in Table 4.3.

Table 4.3 ^{1}H-NMR data of 5,15-*bis*(4-nitrophenyl)-10,20- diphenylporphyrin (**2**)

δ (ppm)	multiplicity (J), number of proton (s), type of proton (position)
8.90	d (8.8 Hz), 4H, β-H (g)
8.75	d (9.0 Hz), 4H, β-H (f)
8.65	d (8.4 Hz), 4H, nitrophenyl (c)
8.40	d (8.4 Hz), 4H, nitrophenyl (b)
8.21	d (7.4 Hz), 4H, o-phenyl (e)
7.78-7.75	m, 6H, p-, m- phenyl (d)
-2.81	s, 2H, internal NH (a)

4.1.2 Synthesis of 5,15-*bis*(4-aminophenyl)-10,20-diphenylporphyrin (3)

5,15-*Bis*(4-nitrophenyl)-10,20-diphenylporphyrin **2** was reduced in accordance with the method of Kruper [48] by using stannous (II) chloride dihydrate and concentrated hydrochloric acid. The resulting crude product was subsequently subjected to column chromatography to obtain pure 5,15-*bis*(4-aminophenyl)-10,20-diphenylporphyrin (**3**) or *trans*-DATPP with 28% yield (Scheme 4.9).

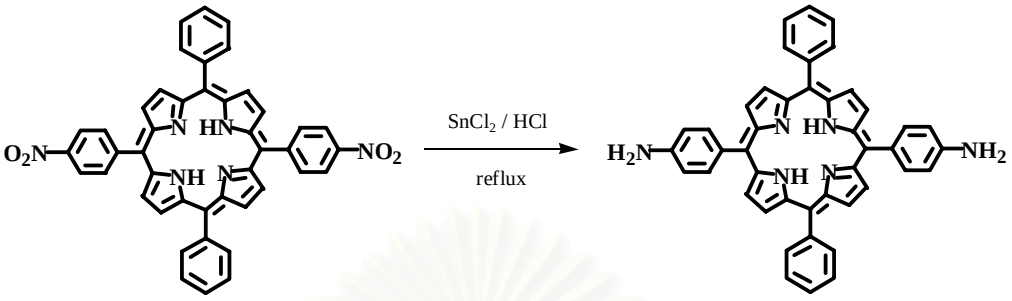

5,15-*bis*(4-nitrophenyl)-10,20-diphenylporphyrin (**2**)

5,15-*bis*(4-aminophenyl)-10,20-diphenylporphyrin or *trans*-DATPP (**3**)

Scheme 4.9 Synthesis of 5,15-*bis*(4-aminophenyl)-10,20-diphenylporphyrin (**3**)

Its structure was identified by FT-IR and ^{1}H-NMR spectroscopy. IR spectrum of *trans*-DATPP (**3**) showed the absorptions at 3381 (NH), 3325 (NH) and 800 cm^{-1} (1,4-substituted benzene) (Figure 4.7).

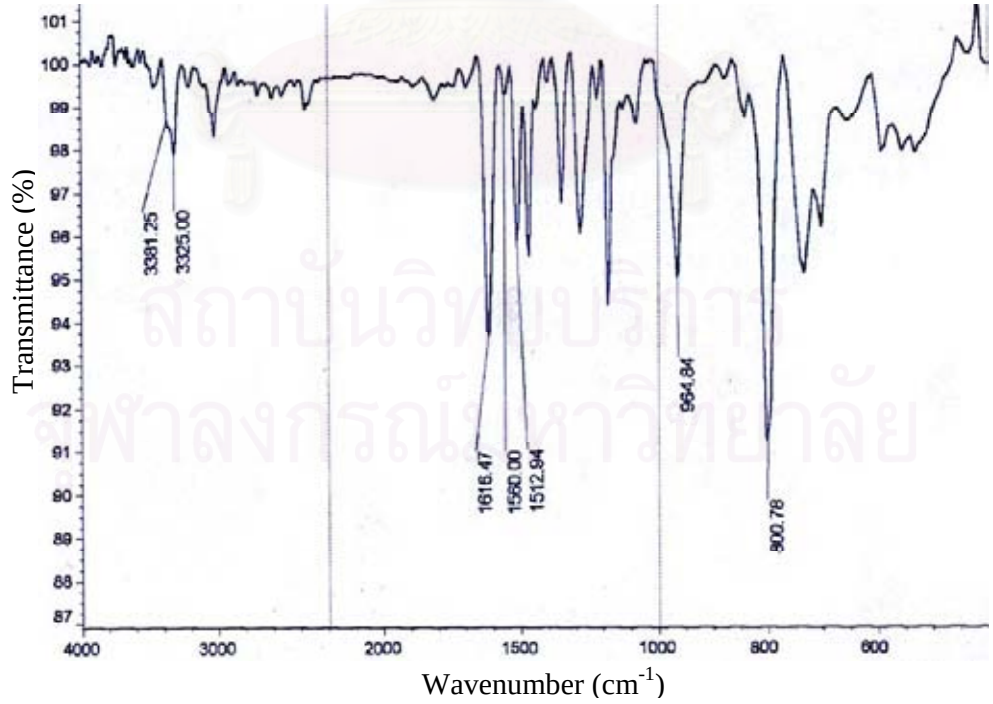

Figure 4.7 IR spectrum of 5,15-*bis*(4-aminophenyl)-10,20-diphenylporphyrin (**3**).

Its structure was further identified by its ^{1}H-NMR spectrum (Figure 4.8) which was interpreted as shown in Table 4.4.

Table 4.4 ^{1}H-NMR data of 5,15-*bis*(4-aminophenyl)-10,20-diphenylporphyrin (**3**)

δ (ppm)	multiplicity (J), number of proton (s), type of proton (position)
8.95	d (4.8 Hz), 4H, β-H (g)
8.76	d (4.8 Hz), 4H, β-H (f)
8.22	d (7.5 Hz), 4H, aminophenyl (d)
7.87-7.80	m,10H, phenyl (e)
7.03	d (8.1 Hz), 4H, aminophenyl (c)
5.59	s, 4H, NH_2 (b)
-2.81	s, 2H, internal NH (a)

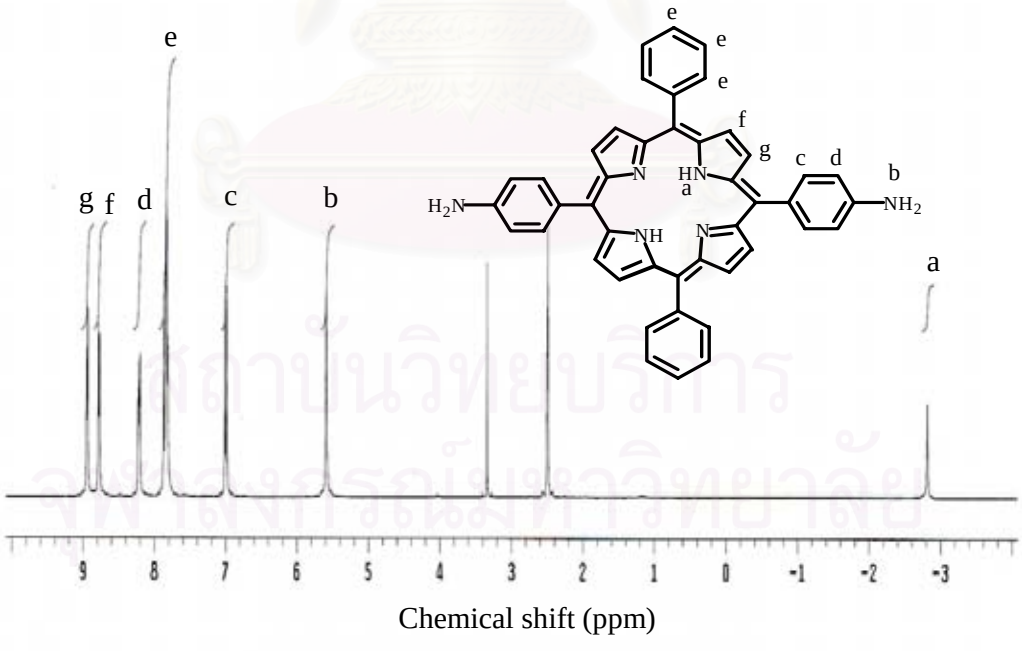

Figure 4.8 ^{1}H-NMR (300 MHz, DMSO-d_6) spectrum of 5,15-*bis*(4-aminophenyl)-10,20-diphenylporphyrin (**3**).

UV-vis absorption spectra of *trans*-DATPP (**3**) comparing to tetraphenylporphyrin (TPP) (Scheme 4.10) in CH_2Cl_2 and DMAc are shown in Appendix A (Figures A.1.1 and A.2.1). There were 5 absorption bands for each compound as detailed in Table 4.5. The UV-vis absorption spectrum of *trans*-DATPP exhibits a typical pattern of free base porphyrin, and is similar to that of TPP. In CH_2Cl_2 the Soret band and Q-band of *trans*-DATPP were observed at slightly lower wavelength when DMAc was used. The cause of the small red-shift of *trans*-DATPP comparing to TPP is due to the electron donating amino groups on benzene rings.

Table 4.5 UV-vis absorption data of TPP and *trans*-DATPP

Compound	CH_2Cl_2		DMAc	
	Soret band (nm)	Q-band (nm)	Soret band (nm)	Q-band (nm)
TPP	417	515 549 590 646	417	514 548 590 646
trans-DATPP	423	520 558 595 652	425	522 567 600 660

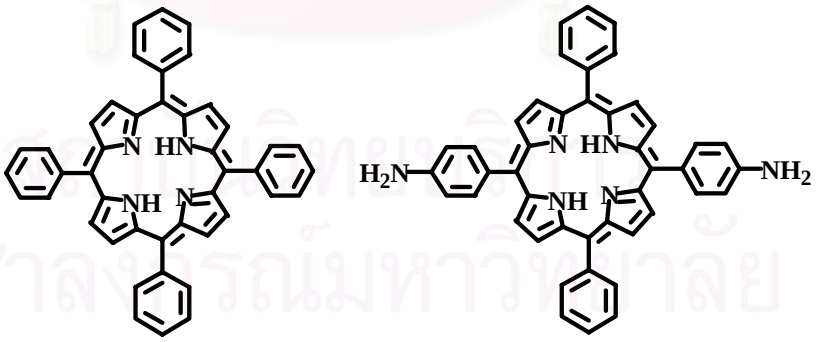

TPP ***trans*-DATPP (3)**

Scheme 4.10 TPP and *trans*-DATPP structures

4.1.3 Synthesis of zinc 5,15-*bis*(4-aminophenyl)-10,20-diphenylporphyrin (4)

The incorporation of zinc into the structure of *trans*-DATPP was performed by reacting *trans*-DATPP with zinc acetylacetonate hydrate (Scheme 4.11) [14].

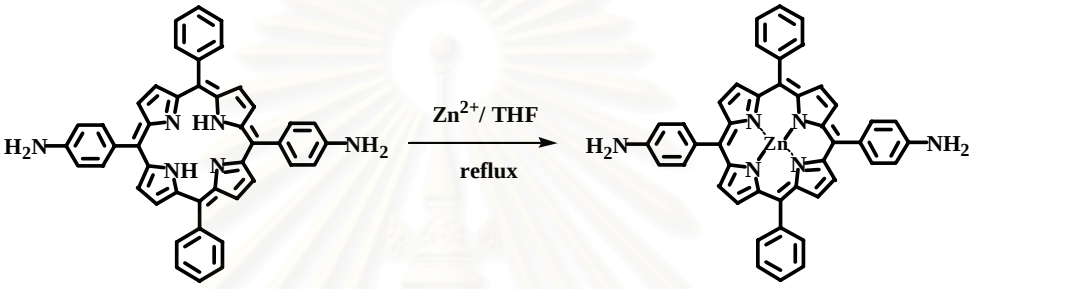

5,15-*bis*(4-aminophenyl)-10,20-diphenylporphyrin or *trans*-DATPP (**3**)

zinc 5,15-*bis*(4-aminophenyl)-10,20-diphenylporphyrin or *trans*-ZnDATPP (**4**)

Scheme 4.11 Synthesis of zinc 5,15-*bis*(4-aminophenyl)-10,20-diphenylporphyrin (**4**)

The formation of zinc 5,15-*bis*(4-aminophenyl)-10,20-diphenylporphyrin (**4**) or *trans*-ZnDATPP was confirmed by its infrared spectrum. The disappearance of the absorption band at 3325 cm^{-1}, which was due to the internal NH stretching for *trans*-DATPP, was observed (Figure 4.9). In addition, the ^{1}H-NMR spectrum of *trans*-DATPP (Figure 4.8) showed the characteristic internal NH at δ -2.81 ppm, while such signal disappeared in the ^{1}H-NMR spectrum of *trans*-ZnDATPP (Figure 4.10). This observation clearly indicated that zinc had bound with *trans*-DATPP. Other signals at various chemical shifts were assigned for the corresponding protons of *trans*-ZnDATPP as revealed in Table 4.6.

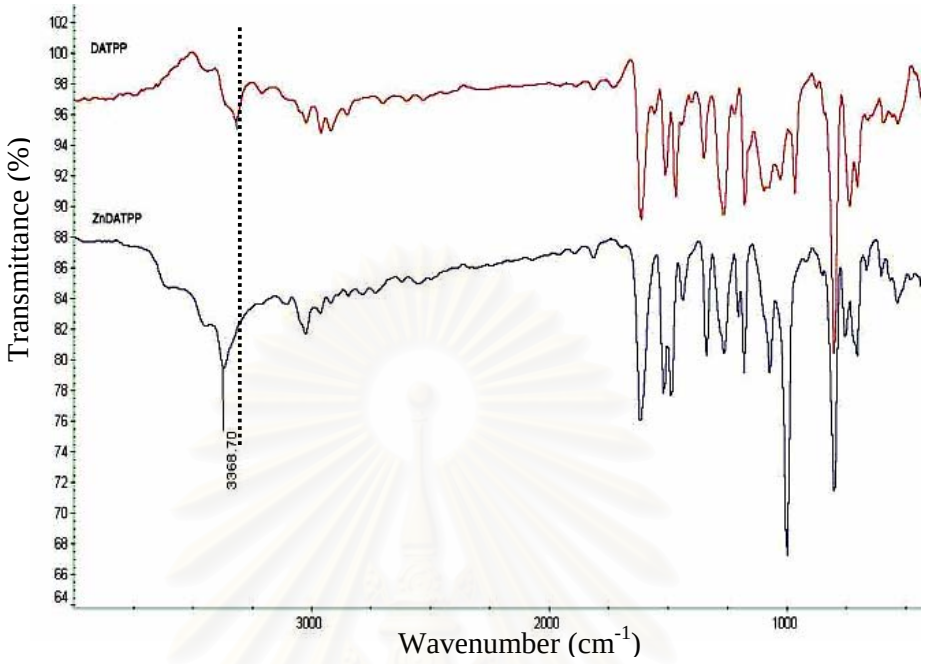

Figure 4.9 IR spectrum of *trans*-DATPP (top) and *trans*-ZnDATPP (below).

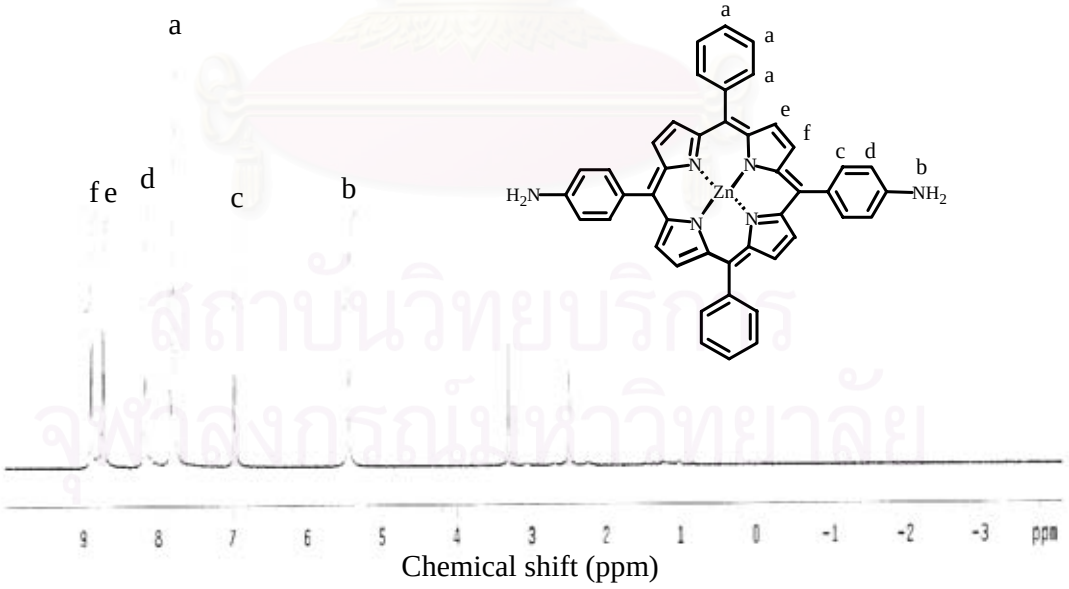

Figure 4.10 ^{1}H-NMR (300 MHz, DMSO-d_6) spectrum of zinc 5,15-*bis*(4-aminophenyl)-10,20-diphenylporphyrin (**4**).

Table 4.6 ^{1}H-NMR data of zinc 5,15-*bis*(4-aminophenyl)-10,20-diphenylporphyrin (**4**)

δ (ppm)	multiplicity (J), number of proton (s), type of proton (position)
8.91	d (4.5 Hz), 4H, β-H (f)
8.75	d (4.5 Hz), 4H, β-H (e)
8.19	d (7.2 Hz), 4H, aminophenyl (d)
7.84-7.78	m,10H, phenyl (a)
6.99	d (8.1 Hz), 4H, aminophenyl (c)
5.45	s, 4H, NH_2 (b)

UV-vis absorption spectra of *trans*-ZnDATPP (**4**) comparing to zinc tetraphenylporphyrin (ZnTPP) (Scheme 4.12) in CH_2Cl_2 and DMAc are shown in Appendix A (Figures A.1.2 and A.2.2).

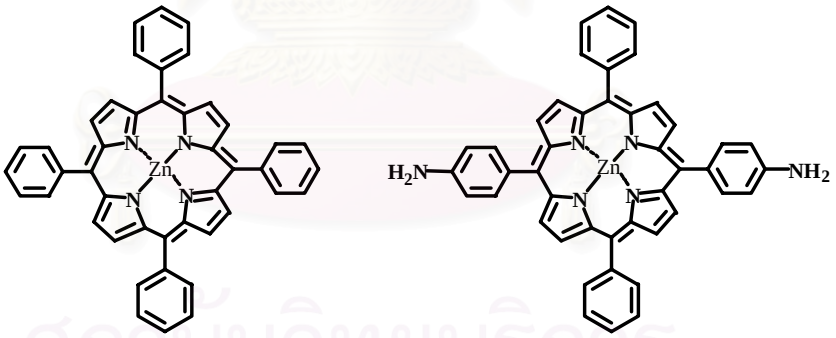

ZnTPP *trans*-ZnTPP (**4**)

Scheme 4.12 ZnTPP and *trans*-ZnDATPP structures

There were 3 absorption bands for each compound as detailed in Table 4.7. The absorption spectrum of *trans*-ZnDATPP showed a typical pattern for porphyrin with metallation which was similar to that of ZnTPP. In CH_2Cl_2 the Soret band for *trans*-ZnDATPP was observed at 423 nm, while ZnTPP absorbs at 418 nm. The cause of

this small red-shift is dependent on both the nature of the end group and the solvent. Upon metallation of *trans*-DATPP, the four Q-bands collapse to two bands. This simplification of the spectrum is known to be a result of the increase in symmetry as the system approaches square planar symmetry [25].

Table 4.7 UV-vis absorption data of ZnTPP and *trans*-ZnDATPP

Compound	CH_2Cl_2		DMAc	
	Soret band (nm)	Q-band (nm)	Soret band (nm)	Q-band (nm)
ZnTPP	418	548 585	426	560 599
trans-ZnDATPP	423	550 589	432	562 607

4.1.4 Synthesis of 3,6-*bis*(3-trifluoromethylphenyl)pyrromellitic dianhydride (7)

Many researchers reported that the polyimide containing 4,4′-hexafluoroisopropylidenediphthalic anhydride (6FDA) can be dissolved in many organic solvents [52-53]. This was attributed to the interference of hexafluoroisopropylidene group to polymer chain packing. Moreover, it was found that polyimide containing 3,6-*bis*(3-trifluoromethylphenyl)pyrromellitic dianhydride (3FPMDA) also enhanced the solubility of the polyimide [44]. Both dianhydrides were then used for condensation polymerization in this research. However, only 6FDA is commercially available. Therefore, 3FPMDA (**7**) was synthesized by starting from 3,6-*bis*(3-trifluoromethylphenyl)durene (**5**) which was available in Harris's laboratory. Compound **5** was oxidized with potassium permanganate according to Marvel *et al.* [49]. The tetracarboxylic acid intermediate (**6**) was then dehydrated to 3FPMDA (**7**) by sublimation (Scheme 4.13).

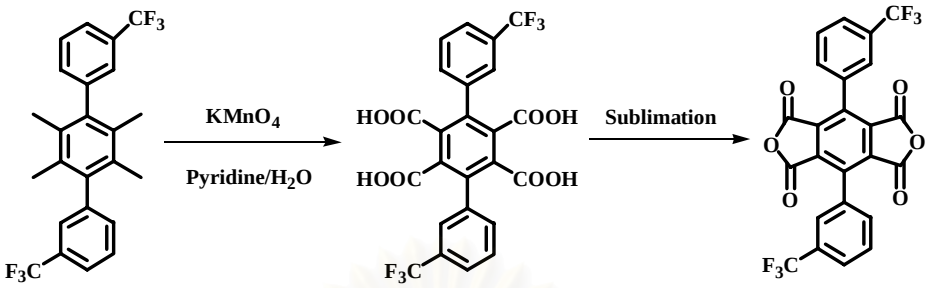

3,6-*bis*(3-trifluoromethylphenyl)-durene (**5**)

tetracarboxylic acid intermediate (**6**)

3,6-*bis*(3-trifluoromethylphenyl)-pyrromellitic dianhydride (**7**)

Scheme 4.13 Synthesis of 3,6-*bis*(3-trifluoromethylphenyl)pyrromellitic dianhydride (**7**)

Its structure was confirmed by ^{1}H-NMR spectroscopy, the ^{1}H-NMR pattern of the resulting product was the same as 3FPMDA which was reported in the literature [44]. Only one multiplet at δ 8.06-7.75 ppm appeared in the spectrum and no appearance of carboxylic proton was observed (Figure 4.10).

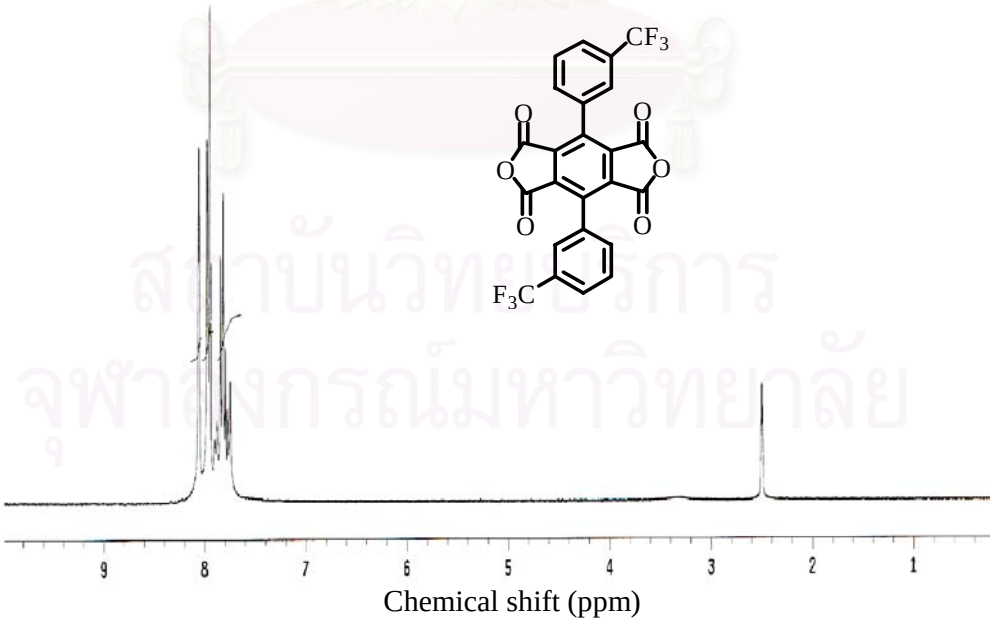

Figure 4.11 ^{1}H-NMR (300 MHz, DMSO-d_6) spectrum of 3,6-*bis*(3-trifluoromethyl-phenyl) pyrromellitic dianhydride (**7**).

4.1.5 Synthesis of 2,2′-*bis*(trifluoromethyl)-4,4′-diaminobiphenyl (9)

Soluble polyimides prepared from diamines containing twisted structure, such as 2,2′-*bis*(trifluoromethyl)-4,4′-diaminobiphenyl (PFMB, **9**) had also been reported [2,53]. Therefore, 2,2′-*bis*(trifluoromethyl)-4,4′-diaminobiphenyl (PFMB, **9**) was prepared by starting from 2,2′-*bis*(trifluoromethyl)-4,4′-dinitrobiphenyl (**8**) which was available in Harris's laboratory. Compound **8** was reduced with stannous (II) chloride dihydrate in the presence of acid to PFMB, **9** (Scheme 4.14). The product was recrystallized from a 50:50 (v/v) mixture of chloroform and hexane. The ^{1}H-NMR pattern (Figure 4.12) of the resulting product was the same as PFMB which was reported in the literature [50]. The chemical shifts were assigned for the corresponding protons of **9** as revealed in Table 4.8.

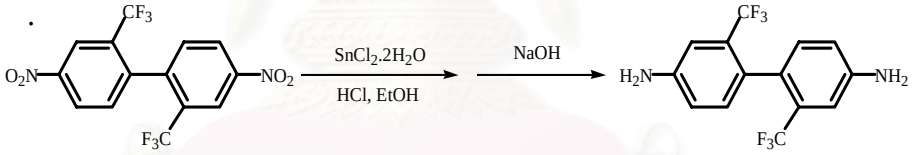

(**8**) (**9**)

Scheme 4.14 Synthesis of 2,2′-*bis*(trifluoromethyl)-4,4′-diaminobiphenyl (**9**)

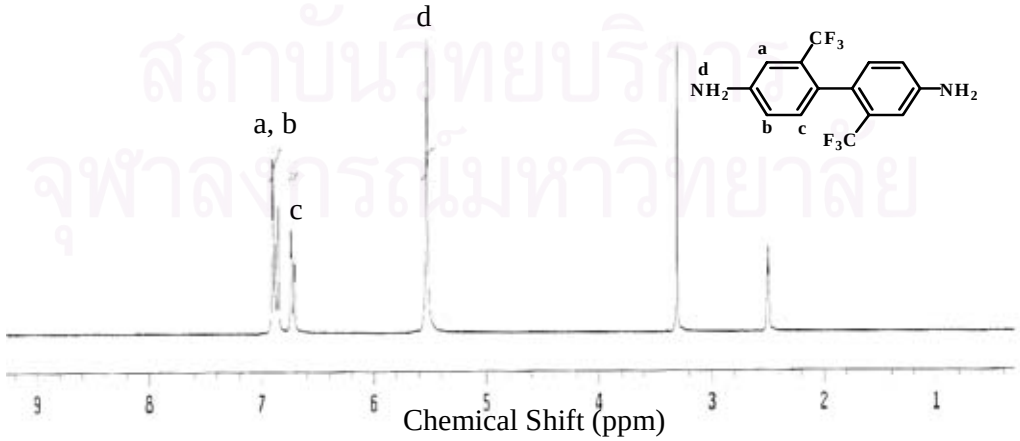

Figure 4.12 ^{1}H-NMR (300 MHz, DMSO-d_6) spectrum of 2,2′-*bis*(trifluoromethyl)-4,4′-diaminobiphenyl (**9**).

Table 4.8 ^{1}H-NMR data of 2,2′-*bis*(trifluoromethyl)-4,4′-diaminobiphenyl (**9**)

δ (ppm)	Multiplicity (J), number of proton, type of proton (position)
6.91-6.85	m, 4H, aromatic (a, b)
6.74	dd (2.1 Hz), 2H, aromatic (c)
5.53	s, 4H, NH_2 (d)

4.2 Polymer Syntheses

4.2.1 Syntheses of polyimides

As mentioned earlier in Chapter II, polyimides were synthesized *via* the isolation of poly(amic acid) which was then thermally or chemically imidized in place. In this research, the designed polyimides based on 6FDA and PFMB were synthesized using one-step method which would be able to dissolve in common organic solvents [2,50,52,53]. However, the small amount of the other dianhydride (3FPMDA) and diamines (*trans*-DATPP and *trans*-ZnDATPP) were added so that these polyimides could behave as the electron donor materials. The polymerization was carried out with the solid content 8-10% (w/v) in the presence of catalytic amount of isoquinoline. The reaction mixture was stirred at room temperature for approximately 8 h and then gradually heated to reflux and held there for 12 h. The water generated by imidization was allowed to distil out of the reaction mixture to favor the polyimide formation. The polyimide product, which remained in solution throughout the polymerization, was isolated by precipitating in methanol.

Four series of polyimides were prepared from dianhydride and diamine compounds at various mole percents. The first series of polyimides (PI1-PI3) was synthesized by the condensation reaction between 6FDA, the dianhydride, and two diamines, PFMB and *trans*-DATPP, as shown in Scheme 4.15. The second series of

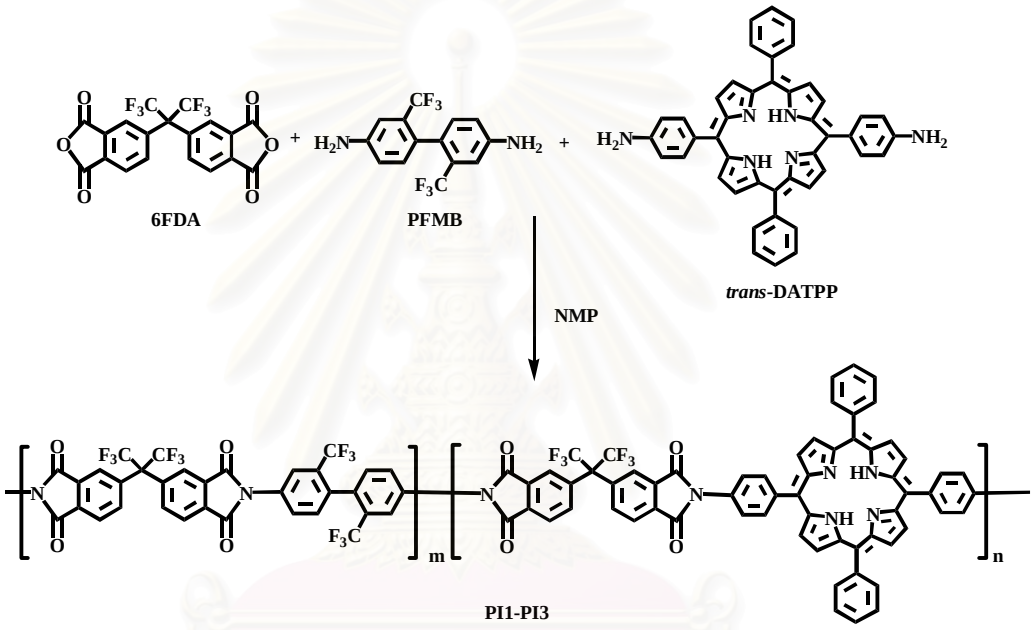

Scheme 4.15 Syntheses of polyimides in series I

polyimides (ZPI1-ZPI3) was prepared by the same reaction but the different porphyrin monomer, *trans*-ZnDATPP, was used instead of *trans*-DATPP as shown in Scheme 4.16. For the third and fourth series of polyimides, (WPI1-WPI3) and (ZWPI1-ZWPI3), the same condensation reaction as series I and II, respectively, were carried out but with the additional dianhydride, 3FPMDA, as shown in Schemes 4.17 and 4.18.

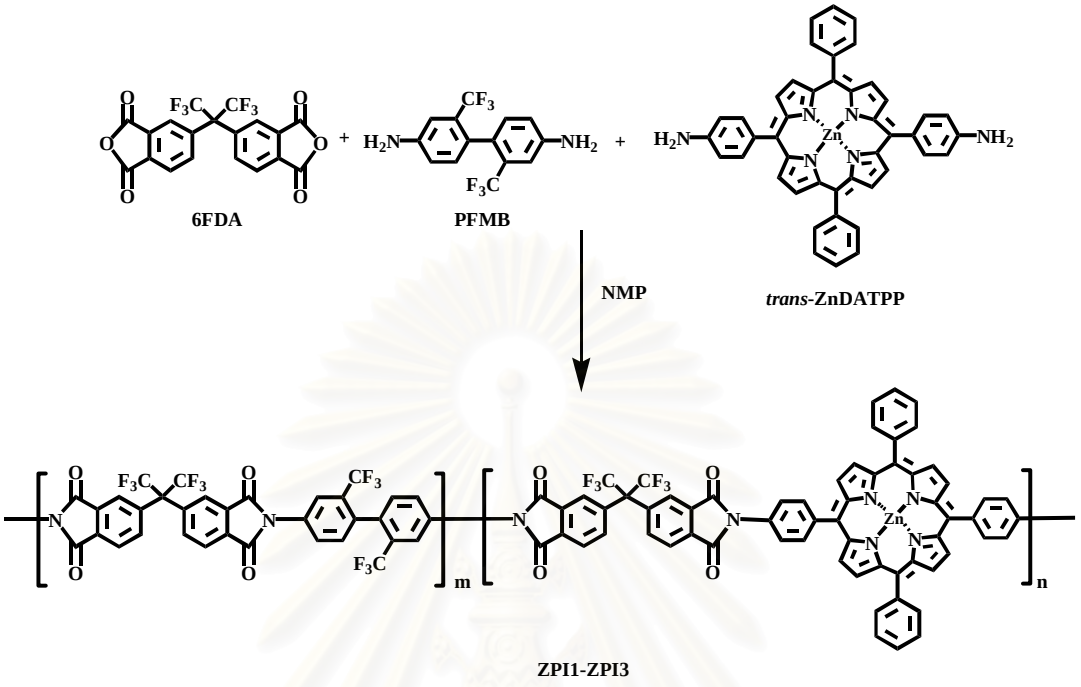

Scheme 4.16 Syntheses of polyimides in series II

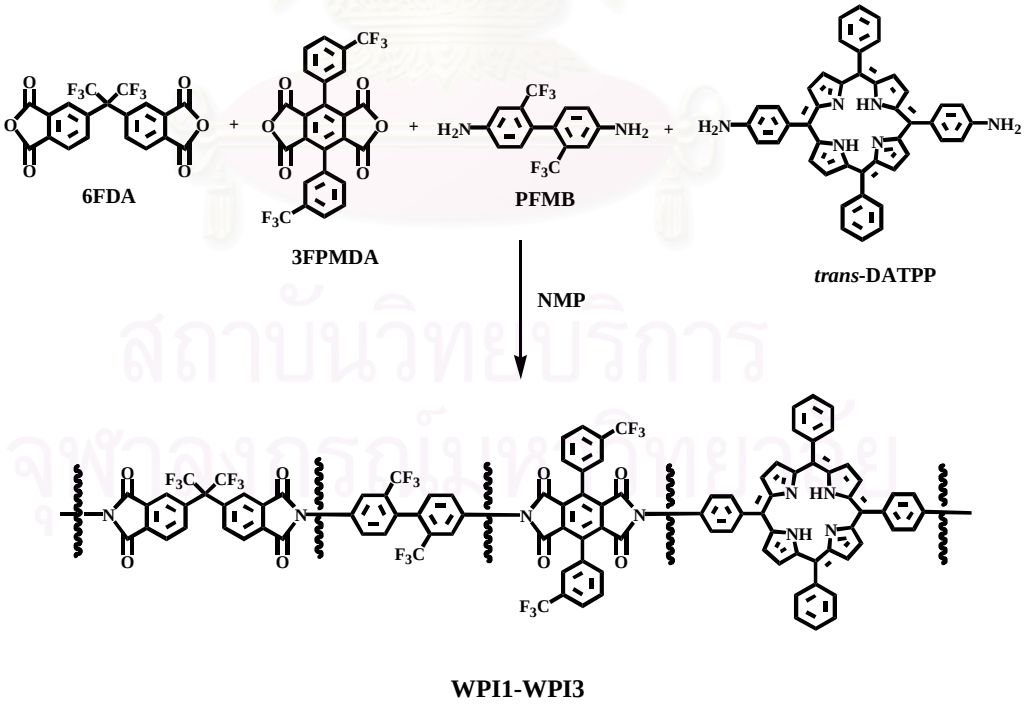

Scheme 4.17 Syntheses of polyimides in series III

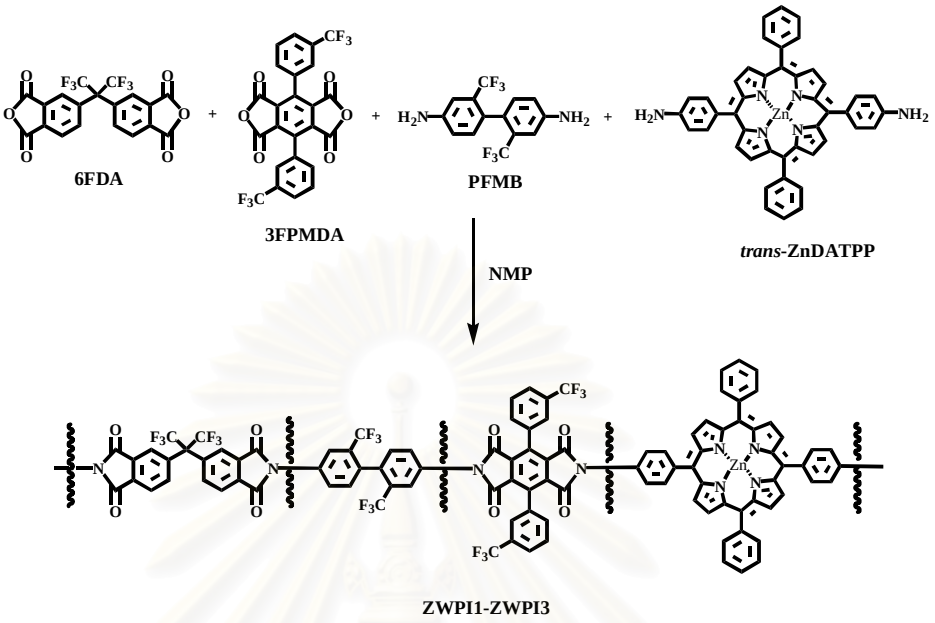

Scheme 4.18 Syntheses of polyimides in series IV

The mole percent of monomers in the feed used for preparing all polyimides and percent yield of these polyimides were shown in Table 4.9. The polyimide without porphyrin moiety (PI0) was also prepared from 6FDA and PFMB for comparison as shown in Scheme 4.19.

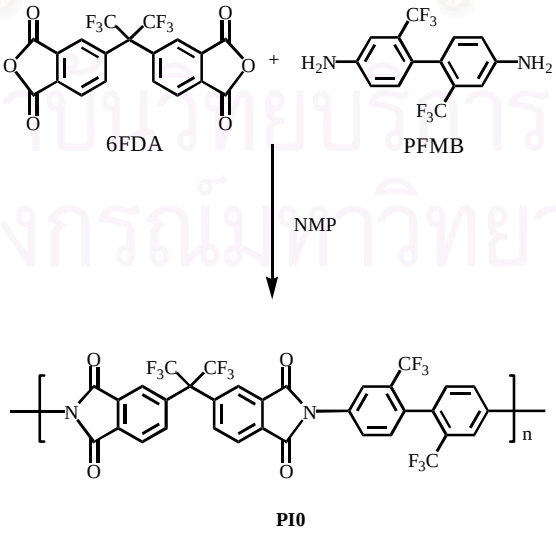

Scheme 4.19 Synthesis of polyimide without porphyrin

Table 4.9 Four series of polyimides

PI	mole in feed (%)					Yield (%)
	6FDA	3FPMDA	PFMB	DATPP	ZnDATPP	
Series I						
trans-DATPP						
PI1	100	-	95	5	-	95
PI2	100	-	90	10	-	94
PI3	100	-	85	15	-	90
Series II						
trans-ZnDATPP						
ZPI1	100	-	95	-	5	94
ZPI2	100	-	90	-	10	93
ZPI3	100	-	85	-	15	90
Series III						
trans-DATPP						
WPI1	95	5	95	5	-	95
WPI2	90	10	90	10	-	90
WPI3	85	15	85	15	-	91
Series IV						
trans-ZnDATPP						
ZWPI1	95	5	95	-	5	93
ZWPI2	90	10	90	-	10	92
ZWPI3	85	15	85	-	15	90

4.2.2 Identification of polyimides

4.2.2.1 Infrared spectroscopy

The IR spectra of all polyimides were shown in Appendix B. Figure 4.13 exhibits the representative IR spectra of the polyimides (PI3, ZPI3, WPI3, ZWPI3). It clearly revealed that there were no characteristic absorption bands of amine indicating that no amine monomers left in the resulting products. In addition, no absorption bands of amide as well as carboxylic acid of poly(amic acid) intermediate appeared in the spectra. It indicated that the poly(amic acid) had been converted completely to the corresponding polyimides during refluxing. This was proved by the appearance of the absorption bands at 1787 (asymmetric stretching C=O), 1732 (symmetric stretching C=O), 1367 (stretching C-N) and 721 cm^{-1} (bending C=O), which were the characteristic absorption bands of polyimide. Polyimide

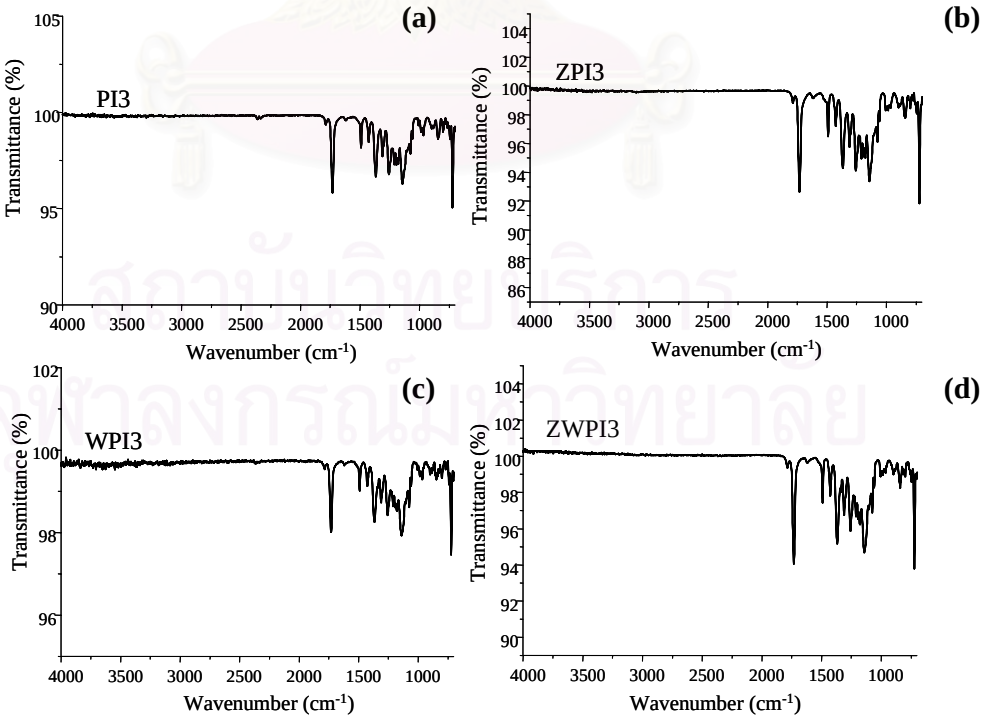

Figure 4.13 IR spectra of polyimides; (a) PI3, (b) ZPI3, (c) WPI3 and (d) ZWPI3.

in series I and III, containing *trans*-DATPP or free-base porphyrin, had the internal NH in the structure. However, the characteristic internal NH absorption band was not observed in these spectra. This must be due to the rigid structure of the polymer chain which made it difficult for N-H vibration.

4.2.2.2 Proton-Nuclear magnetic resonance (^{1}H-NMR)

^{1}H-NMR spectroscopic technique was employed to differentiate the polyimides containing *trans*-DATPP and *trans*-ZnDATPP. ^{1}H-NMR spectra of polyimides PI3, ZPI3, WPI3 and ZWPI3 were shown in Figure 4.14. All spectra of polyimides showed the signal at δ 8.90 ppm, which was due to the protons at β positions on pyrrole rings of porphyrin moiety. It was also observed that only polyimides PI3 and WPI3, which containied *trans*-DATPP or free-base porphyrin, showed the signal of internal NH at δ –2.80 ppm. In case of polyimides containing *trans*-ZnDATPP, ZPI3 and ZWPI3, no appearance of this characteristic internal NH signal was observed and the rest of the spectra was similar to polyimide containing *trans*-DATPP, PI3 and WPI3, respectively. Therefore, these ^{1}H-NMR results confirmed the incorporation of porphyrin into polymer structure.

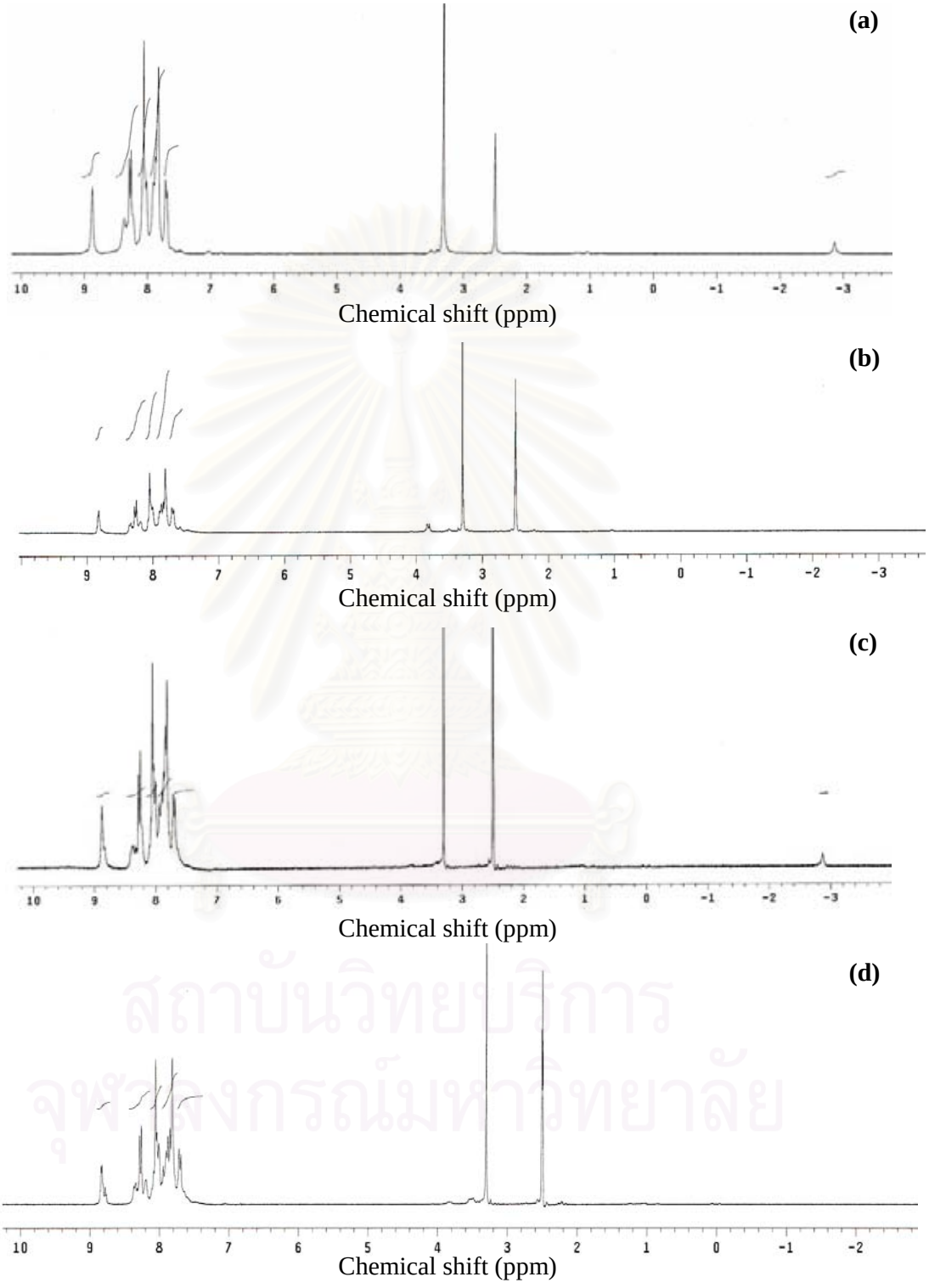

Figure 4.14 ^{1}H-NMR (300 MHz, DMSO-d_6) of polyimides; (a) PI3, (b) ZPI3, (c) WPI3 and (d) ZWPI3.

4.2.2.3 Determination of porphyrin content in polyimides

Trans-DATPP and *trans*-ZnDATPP content in the polymer structure can be determined by UV-visible spectroscopy (Appendix C). Table 4.10 showed the calculated results of porphyrin content in polyimides as the weight percent. The determination was performed by measuring the optical density of the polyimides in CH_2Cl_2 at the Soret band, λ_{max} = 419 nm for series I and III and λ_{max} = 420 nm for series II and IV. These were the characteristic absorption bands of porphyrin moieties which were not interfered by the absorption of other parts of the polyimides.

Table 4.10 Porphyrin content in polyimides

PI	weight of porphyrin (%)	
	in feed	in polymer
Series I		
PI1	4.13	3.87
PI2	8.08	7.27
PI3	11.87	9.21
Series II		
ZPI1	4.50	4.05
ZPI2	8.78	8.26
ZPI3	12.88	11.03
Series III		
WPI1	4.11	3.77
WPI2	8.71	6.25
WPI3	11.73	9.90
Series IV		
ZWPI1	4.49	3.25
ZWPI2	8.74	7.68
ZWPI3	12.74	9.82

The results demonstrated that *trans*-DATPP and *trans*-ZnDATPP were incorporated into the polymer backbones as expected. In the calculation, it was assumed that all the other monomers were completely incorporated into polymer structure. However, it was postulated that some monomers must be lost during the experiment. Therefore, porphyrin content in polyimides should be slightly higher than the calculation.

4.3 Polymer Properties

4.3.1 Solution viscosity

There were a few reports on the synthesis of polyimides containing porphyrin *via* poly(amic acid) [9-15]. Those polyimides were unfortunately insoluble in all organic solvents, which made it difficult to determine their properties. Usually the properties of the corresponding intermediate, poly(amic acid), were studied instead. For example, the inherent viscosity (η_{inh}) of poly(amic acid) solution was measured and reported in a way that was related to the corresponding polyimides. In this research, the soluble porphyrin-containing polyimides were successfully prepared and the intrinsic viscosity [η] of these polyimides was thus able to be determined directly.

4.3.1.1 Viscosity of polyimides in series I and II

Table 4.11 showed the intrinsic viscosity of the porphyrin-containing polyimides measured in NMP at 35 ^{o}C (Appendix D). All the polyimides in series I and II had higher viscosity than the polyimide without porphyrin (PI0) which was

synthesized from the same dianhydride and diamine at the same condition except no porphyrin monomer. These results indicated that the incorporated porphyrin must

Table 4.11 The physical property data of polyimides

PI	$[\eta]^a$ (dL/g)	$T_g{}^b$ (^oC)	TGA[c] (^oC)	
			N_2	Air
PI0	0.72	284	492	462
Series I				
trans-DATPP				
PI1	1.10	294	492	487
PI2	0.94	301	502	475
PI3	0.89	310	501	467
Series II				
trans-ZnDATPP				
ZPI1	0.99	316	488	455
ZPI2	0.80	318	477	456
ZPI3	0.76	326	486	449
Series III				
trans-DATPP				
WPI1	0.89	241	491	481
WPI2	0.77	286	502	417
WPI3	0.64	290	499	444
Series IV				
trans-ZnDATPP				
ZWPI1	0.75	268	472	439
ZWPI2	0.61	296	485	444
ZWPI3	0.56	305	465	413

[a]Intrinsic viscosity determined in NMP at 35 ^oC.

[b]Temperature at which change in slope occurred on a plot of film dimensional change vs temperature obtained by TMA with a heating rate of 10 ^oC/min. Films were subjected to three initial stresses and the results were extrapolated to zero stress.

[c]Tempeature at which 5% weight loss occurred when polymers were subjected to TGA with a heating rate of 10 ^oC/min.

play a role for the significant increase in viscosity. It is possible that much higher molecular weights of polymers were obtained when porphyrins were incorporated into polyimide chains. Indeed, it has been reported that strong attractive interactions between porphyrins can lead to aggregation in solution [54]. Intrachain aggregation within the polyimide *via* pi-pi interactions of porphyrins on the same chain is expected to result in a decrease in viscosity with increasing porphyrin content (greater coiling), whereas interchain aggregation is expected to result in an increase in viscosity through increased chain entanglement (Scheme 4.20). Therefore both intra- and inter- interactions of polyimide chains would attribute to the higher viscosity compared to the polyimide without porphyrin. A decrease in viscosity with increasing porphyrin content in both series I and II was observed, indicating probable intrachain interactions (*i.e.*, coiling). It is noted that solution viscosities are dependent in part on the size of polymer molecules that expanded in solvent. Another consequence of our results is that polyimides in series II had lower viscosity than polyimides in series I at the same level of porphyrin content. This can be attributed to ligation of the zinc porphyrin with either the polymer or the solvent [54, 55, 56, 57] (Scheme 4.20).

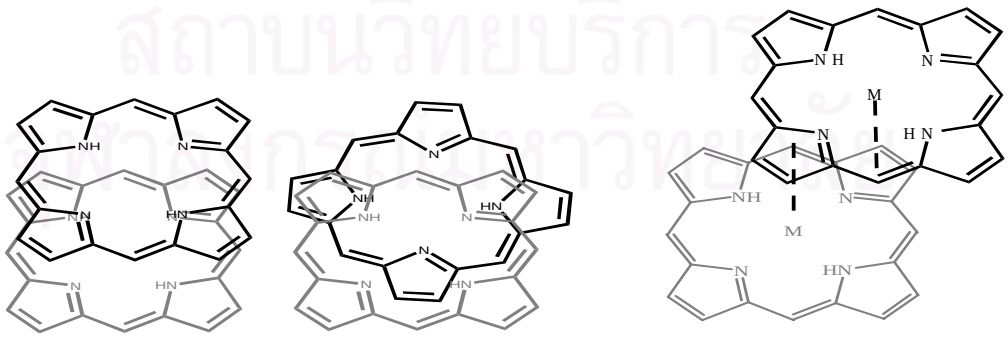

pi-pi interaction **metal ligation**

Scheme 4.20 pi-pi interaction and metal ligation in porphyrin

4.3.1.2 Viscosity of polyimides in series III and IV

The intrinsic viscosity of polyimides in series III and IV were shown in Table 4.11. It was also observed that these polyimides exhibited the tendency of decreasing in viscosity with higher content of porphyrin similar to polyimides in series I and II, respectively. Two reasons for such decreases could be described. These results were firstly caused by pi-pi interaction of porphyrin in polymer structure as explained in 4.3.1.1. In addition, polyimides in series III and IV had incorporated 3FPMDA as the extra dianhydride comparing to polyimides in series I and II. 3FPMDA had two trifluoromethylphenyl groups in the structure which caused the steric effect to the polymerization. The low molecular weights of polyimides in series III and IV were expected, and low viscosities were observed. To illustrate this postulation, another two polyimides were synthesized separately. The polyimides prepared from 3FPMDA and PFMB had number average molecular weight (Mn) 18,710 g/mol and weight average molecular weight (Mw) 24,720 g/mol. When 6FDA reacted with PFMB, the polyimide with Mn 29,560 g/mol and Mw 41,820 g/mol were resulted. Furthermore, the first polyimide was rather a powder but the second one was in the fiber form. Consequently, the incorporation of 3FPMDA into porphyrin-containing polyimides would give lower molecular weight and thus lower viscosity.

4.3.2 Thermal properties of polymers

4.3.2.1 Glass transition temperature (T_g)

The glass transition temperatures (T_gs) of the polyimides were determined by thermomechanical analysis (TMA) of thin films. The films were prepared by casting THF solutions of porphyrin-containing polyimide on a glass plates, followed by drying at room temperature for 24 h and at 200 ^oC under reduced pressure for 24 h. Each film was then tested at three different applied stresses with heating rate of 10 ^oC/min. The T_g at each stress was taken as the temperature at which a dramatic change in slope of the plot of film dimensional change versus temperature occurred. The T_g at each stress was then extrapolated to the T_g at zero stress, as shown in Appendix E. The T_gs of polyimides are listed in Table 4.11. It is well known that T_g is closely related to chain rigidity and free volume. An increase in rigidity tends to increase T_g, while increasing free volume decreases T_g. The polyimides containing lower porphyrin content have more flexible linkages per repeating unit than those containing higher porphyrin content. Therefore the lower T_g had observed as expected. It was found that the T_gs of all polyimides containing *trans*-ZnDAPP were higher than the polyimides containing *trans*-DATPP at the same amount of porphyrin. This is due to the incorporation of *trans*-ZnDATPP in polymer structure resulting in an increase in chain rigidity, which should increase T_g. Polyimides in series III and IV, which had the additional 3FPMDA unit in the structure, showed lower T_gs than polyimides in series I and II, probably due to higher free volume of polyimides containing 3FPMDA. It was also observed that polyimide without porphyrin showed the lower T_g than polyimide containing porphyrin. This could be attributed to the higher polymer chain flexibility.

4.3.2.2 Decomposition temperature

These porphyrin-containing polyimides displayed good thermal and thermooxidative stabilities. The decomposition temperatures of the polyimides were determined by TGA (Appendix F) in both nitrogen and air and were taken as the temperature at which 5% weight loss occurred (Table 4.11). The polyimides in series I and III, which contained *trans*-DATPP, seem slightly more stable than polyimides in series II and IV, which contained *trans*-ZnDATPP, at the same level of porphyrin content. From the TGA data, it was found that the existence of *trans*-DATPP or *trans*-ZnDATPP in the polymer did not significantly affect the thermal stabilities of these polyimides as comparing to polyimide without porphyrin.

4.3.3 Polymer solubility

To determine the solubility of these porphyrin-containing polyimides, they were dissolved in seven different solvents. The solubility behavior of the polyimides is summarized in Table 4.12. All four series of polyimides were apparently soluble in the polar aprotic solvent (NMP, DMAc, DMSO, DMF), THF, acetone and CH_2Cl_2.

Table 4.12 Solubility[a] of polyimides

PI	NMP	DMAc	DMSO	DMF	THF	Acetone	CH_2Cl_2
Series I							
PI1	++	++	++	++	++	++	+
PI2	++	++	++	++	++	++	+
PI3	++	++	++	++	++	++	+
Series II							
ZPI1	++	++	++	++	++	++	+
ZPI2	++	++	++	++	++	++	+
ZPI3	++	++	++	++	++	++	+
Series III							
WPI1	+++	+++	+++	+++	++	++	+
WPI2	+++	+++	+++	+++	++	++	+
WPI3	+++	+++	+++	+++	++	++	+
Series IV							
ZWPI1	+++	+++	+++	+++	++	++	+
ZWPI2	+++	+++	+++	+++	++	++	+
ZWPI3	+++	+++	+++	+++	++	++	+

[a]Solubility was performed at the concentration 4% (w/v) at room temperature

+++ : completely soluble in 1 hour

++ : completely soluble in 5 hour

+ : completely soluble overnight

However, the polyimides seemed not readily soluble in CH_2Cl_2, and took longer time for dissolving than in polar aprotic solvents, THF or acetone. The excellent solubility of these polyimides compared to normal aromatic polyimides caused by the presence of hexafluoroisopropylidene group in 6FDA in their polymer structures. This flexible group interrupts chain packing. The decrease in chain packing leads to an increase in free volume, which allows small solvent molecules to penetrate the polymer chain. Furthermore, the increase in solubility can also be attributed to the twisted biphenyl

structure of PFMB unit. As stated earlier, this type of structure hinders chain packing because of the non-coplanarity of the two phenyl rings. The decrease in chain packing leads to an increase in free volume. The similar phenomenon has already been reported by other research groups [2, 45, 58, 59, 60]. In addition, polyimides in series III and IV, which had the additional 3FPMDA unit in the structure, showed the high solubility in polar aprotic solvents, THF or acetone. This was attributed to higher free volume of polyimides containing 3FPMDA.

4.3.4 Spectroscopic properties of polyimides

Due to the good solubility of these polymers, the photophysical process of these polymers (*i.e.*, absorption, excitation and photoinduced electron transfer processes) can be investigated.

4.3.4.1 Absorption properties of polyimides

The tetrapyrrolic macrocycles in which the nucleus is fully conjugated can be regarded a characteristic absorption. The absorption spectra of these aromatic tetrapyrrolic macrocycles display an intense band in the region of 400 nm. This absorption is called the Soret band and has a strong absorption with a high molar extinction coefficient. Porphyrins also display four accompanying bands, commonly referred to as the Q-band, of lower intensity between 450-650 nm. Upon metallation of the porphyrin, the four Q-bands collapse to two [25].

Absorption spectra (Appendix A, Table 4.13) obtained from polyimides containing *trans*-DATPP (series I and III) and *trans*-ZnDATPP (series II and IV) are similar to tetraphenylporphyrin (TPP) and zinc tetraphenylporphyrin (ZnTPP), respectively. However, they are slightly different from the corresponding porphyrin monomers (*trans*-DATPP and *trans*-ZnDATPP, respectively). The absorption spectra obtained from polyimides in series I, III and II, IV, showed Soret transitions that were substantially blue-shifted from *trans*-DATPP and *trans*-ZnDATPP, respectively. The shift of the absorption bands to higher energy was also observed in the Q-band region. The source of this blue-shift is surely related to the nature of the structure of porphyrin incorporated into polymer chain. They, *trans*-DATPP and *trans*-ZnDATPP, after incorporation into polyimides, exhibited the absorption in the same manner as TPP and ZnTPP did, respectively. The Soret bands for polyimides in series I and III are observed at 419 nm in CH_2Cl_2 and 418 nm in DMAc, while TPP absorbs at 417 nm in both CH_2Cl_2 and DMAc. In case of polyimides in series II and IV, the Soret bands are observed at 420 nm in CH_2Cl_2 and 427 nm in DMAc, while ZnTPP is observed at 418 nm in CH_2Cl_2 and 426 nm in DMAc.

Table 4.13 UV-vis absorption maxima of polyimides in CH_2Cl_2 and DMAc

Compound	CH_2Cl_2		DMAc	
	Soret band (nm)	Q-band (nm)	Soret band (nm)	Q-band (nm)
TPP	417	515 549 590 646	417	514 548 590 646
trans-DATPP	423	520 558 595 652	425	522 567 600 660
ZnTPP	418	548 585	426	560 599
trans-ZnDATPP	423	550 589	432	562 607
Series I				
PI1	419	515 550 590 646	418	515 550 590 646
PI2	419	515 550 590 646	418	515 550 590 646
PI3	419	515 550 590 646	418	515 550 590 646
Series II				
ZPI1	420	548 588	427	560 600
ZPI2	420	548 588	427	560 600
ZPI3	420	548 588	427	560 600
Series III				
WPI1	419	515 550 590 646	418	515 550 590 646
WPI2	419	515 550 590 646	418	515 550 590 646
WPI3	419	515 550 590 646	418	515 550 590 646
Series IV				
ZWPI1	420	548 588	427	560 600
ZWPI2	420	548 588	427	560 600
ZWPI3	420	548 588	427	560 600

The absorption spectra of all porphyrin-containing polyimide films were also recorded (Table 4.14). The films were prepared by casting THF solutions of porphyrin-containing

Table 4.14 UV-vis absorption maxima of polyimide films compared to polyimides solution

PI	Solution/film	Q-band (nm)			
PI1	CH_2Cl_2	515	550	590	646
	DMAc	515	550	590	646
	Film	518	554	594	649
PI2	CH_2Cl_2	515	550	590	646
	DMAc	515	550	590	646
	Film	516	553	593	649
PI3	CH_2Cl_2	515	550	590	646
	DMAc	515	550	590	646
	Film	515	555	593	649
ZPI1	CH_2Cl_2	548	558		
	DMAc	560	600		
	Film	557	599		
ZPI2	CH_2Cl_2	548	558		
	DMAc	560	600		
	Film	559	599		
ZPI3	CH_2Cl_2	548	558		
	DMAc	560	600		
	Film	561	599		
WPI1	CH_2Cl_2	515	550	590	646
	DMAc	515	550	590	646
	Film	518	554	594	650
WPI2	CH_2Cl_2	515	550	590	646
	DMAc	515	550	590	646
	Film	516	554	594	650
WPI3	CH_2Cl_2	515	550	590	646
	DMAc	515	550	590	646
	Film	512	553	594	650
ZWPI1	CH_2Cl_2	548	558		
	DMAc	560	600		
	Film	557	599		
ZWPI2	CH_2Cl_2	548	558		
	DMAc	560	600		
	Film	556	599		
ZWPI3	CH_2Cl_2	548	558		
	DMAc	560	600		
	Film	560	599		

containing polyimides (4% w/v) with on a glass plates, followed by drying at room temperature for 24 h and at 200 ^{o}C under reduced pressure for 24 h. Since Soret band in these spectra are far out of scale and cannot be recorded. Four absorption bands in Q-band region were observed. It was found that the absorptions in Q-band region in both solution and film of porphyrin-containing polyimides similar to each other. This result was contradictory to the report of Zhu *et al*. [12]. They prepared different free base porphyrin-containing polyimide films by two-step method, *via* poly(amic acid) intermediates. Then they observed that 4 absorption bands in Q-band region of porphyrin moiety in poly(amic acid) solution was changed to 2 absorption bands after poly(amic acid) and polyimide films were formed. These results could not be compared directly with the result in this study. Since the methods for preparing polyimides and films formation in this study are different from Zhu's work. From this point, the combination of four bands to two bands in Q-band region will be studied as a future work.

4.3.4.2 Fluorescence properties of polyimides

Steady state fluorescence measurements of both polyimides containing *trans*-DATPP and *trans*-ZnDATPP were performed. Similarly a little change in emission spectra is observed in the energies of the fluorescence bands for polyimides containing *trans*-DATPP (series I and III) which have fluorescence bands 650 nm and 714 nm in CH_2Cl_2, 650 and 715 nm in DMAc (Appendix G, Table 4.15). These bands are nearly identical to those observed for TPP in the same solvents (649 nm and 714 nm in CH_2Cl_2, 650 nm and 715 nm in DMAc).

Table 4.15 Fluorescence maxima of polyimides in CH_2Cl_2 and DMAc

Compound	CH_2Cl_2	DMAc
TPP	649 714	650 715
trans-DATPP	662 721	677
ZnTPP	593 643	604 660
trans-ZnDATPP	601 647	622 667
Series I		
PI-1	650 714	650 715
PI-2	650 714	650 715
PI-3	650 714	650 715
Series II		
PI-4	596 643	606 660
PI-5	596 643	606 660
PI-6	596 643	606 660
Series III		
WPI1	650 714	650 715
WPI2	650 714	650 715
WPI3	650 714	650 715
Series IV		
ZWPI1	596 643	606 660
ZWPI2	596 643	606 660
ZWPI3	596 643	606 660

The fluorescence spectra of the polyimides containing *trans*-ZnDATPP (series II and IV) showed a red-shift in the fluorescence maxima from that of ZnTPP (593 and 643 nm in CH_2Cl_2, 604 and 660 nm in DMAc). Polyimides in series II and IV had (Appendix G, Table 4.15) the fluorescence maxima at 596 and 643 nm are found for polyimides in CH_2Cl_2, and maxima at 606 and 660 nm were observed in DMAc. These spectral shifts are unlike those observed for polyimides in series I and III, which showed only very little change in fluorescence maxima.

The quantum yields (Φ_{Fl}) for these polyimides were determined, and are shown in Table 4.16. Because substitution on the porphyrin changes the quantum yield of the standard porphyrins (TPP and ZnTPP) substantially (Appendix H), relative quantum yields ($\Phi_{n\text{-}PI}/\Phi_{trans\text{-}DATPP}$ and $\Phi_{zn\text{-}PI}/\Phi_{trans\text{-}ZnDATPP}$, where n-PI = PI1-PI3, WPI1-WPI3 for the *trans*-DATPP-containing polyimides and zn-PI= ZPI1-ZPI3, ZWPI1-ZWPI3 for the *trans*-ZnDATPP-containing polyimides) are also shown in Table 4.16. The fluorescence quantum yields of polyimides in CH_2Cl_2 and DMAc were determined by using TPP (Φ_{Fl}= 0.11 in CH_2Cl_2, Φ_{Fl}= 0.15 in DMAc) and ZnTPP (Φ_{Fl}= 0.03 in both CH_2Cl_2 and DMAc) as a standard [61]. As expected, the fluorescence quantum yields ($\Phi_{n\text{-}PI}$) for polyimides in series I increased slightly with an increasing content of *trans*-DATPP in both CH_2Cl_2 and DMAc. In CH_2Cl_2, the quantum yields are decreased substantially relative to TPP (19-35%), indicating significant quenching of the porphyrin fluorescence that is attributed to electron transfer from a porphyrin donor to diimide acceptor group. The relative quantum yield data indicates quenching *via* electron transfer is ~44-56% efficient. In contrast, the quantum yields in DMAc are slightly larger than that of TPP; the relative quantum yield data indicates only a small (0-15%) amount of fluorescence quenching compared to the starting porphyrin.

Fluorescence quantum yields of polyimides in series II show substantial fluorescence quenching in both solvents. In CH_2Cl_2, the amount of quenching is 29-43% of ZnTPP and ~60-70% of that of the monomeric porphyrin, *trans*-ZnDATPP, and in DMAc the quenching is 26-43% of ZnTPP and ~33-49% of the monomer.

Table 4.16 Quantum yields of polyimides

Compound	CH_2Cl_2		DMAc	
	Φ_{Fl}	$\Phi_{n\text{-}PI}/\Phi_{trans\text{-}DATPP}$ or $\Phi_{zn\text{-}PI}/\Phi_{trans\text{-}ZnDATPP}$	Φ_{Fl}	$\Phi_{n\text{-}PI}/\Phi_{trans\text{-}DATPP}$ or $\Phi_{zn\text{-}PI}/\Phi_{trans\text{-}ZnDATPP}$
TPP	0.110		0.150	
trans-DATPP	0.160		0.190	
ZnTPP	0.030		0.030	
trans-ZnDATPP	0.054		0.033	
Series I				
PI1	0.071	0.444	0.159	0.835
PI2	0.084	0.526	0.181	0.952
PI3	0.089	0.559	0.191	1.006
Series II				
ZPI1	0.021	0.396	0.022	0.670
ZPI2	0.020	0.364	0.020	0.613
ZPI3	0.017	0.314	0.017	0.516
Series III				
WPI1	0.073	0.459	0.163	0.856
WPI2	0.070	0.437	0.153	0.808
WPI3	0.061	0.380	0.140	0.739
Series IV				
ZWPI1	0.019	0.343	0.018	0.546
ZWPI2	0.014	0.263	0.014	0.423
ZWPI3	0.011	0.201	0.012	0.371

The quantum yields of polyimides in series III decreased with the increasing of *trans*-DATPP content. This could be attributed to the quenching effect of 3FPMDA that incorporated into polymer backbone. Fluorescence quantum yields of polyimides in series III show substantial fluorescence quenching in both CH_2Cl_2 and DMAc solvents. In CH_2Cl_2, the amount of quenching is 33-45% of TPP and ~54-62% of that of the monomeric porphyrin, *trans*-DATPP. In contrast, some of the quantum yields in DMAc are slightly larger than that of TPP (polyimides WPI1 and WPI2); the

relative quantum yield data indicates quenching *via* electron transfer is ~13-25% efficient.

The fluorescence quantum yields of polyimides in series IV show substantial fluorescence quenching in both solvents. In CH_2Cl_2, the quantum yields are decreased substantially relative to ZnTPP (38-64%). The relative quantum yield data indicates quenching *via* electron transfer is ~66-80% efficient. In DMAc, the quenching is 40-60% of ZnTPP and 45-63% of the monomeric porphyrin.

4.3.5 Electrochemical properties of polyimides

The electrochemical properties of the selected polyimides (PI3, ZPI3, WPI3, ZWPI3) were studied by cyclic voltammetry (CV) (Appendix I). The reduction potentials, $E_{1/2}$ (red), for these polymers were recorded. Unfortunately, the corresponding oxidation potential, $E_{1/2}$ (ox), for these polymers could not be determined, possibly because the porphyrin moieties were not accessible to the electrode surface [56]. The free energy of electron transfer (ΔG_{ET}) was therefore calculated using the first singlet excited state energy of the porphyrin donor, the values of $E_{1/2}$ (red) determined in this research and $E_{1/2}$ (ox) from literature [56, Appendix I]. Polyimides PI3 and WPI3 had reduction potential of -1.25 V and -1.19 V, respectively, while ZPI3 and ZWPI3 which contained *trans*-ZnDATPP had the reduction potential of -1.14 V and -1.06 V, respectively. ΔG_{ET} of polyimides PI3 and WPI3 are estimated to be endothermic by ~0.37 and ~0.31 eV, respectively, whereas the corresponding values for the polyimides containing *trans*-ZnDATPP, ZPI3 and

ZWPI3, were calculated to be exothermic by -0.17 and -0.25 eV, respectively (Table 4.17).

Table 4.17 Free energy of electron transfer for PI3, ZPI3, WPI3 and ZWPI3

Polyimide	ΔG_{ET}[a] (eV)
PI3	0.37
ZPI3	-0.17
WPI3	0.31
ZWPI3	-0.25

[a]Estimated using the Weller Equation (See Appendix I)

However, ΔG_{ET} of polyimides WPI3 and ZWPI3 which had the additional 3FPMDA in the polymer structure showed the lower ΔG_{ET} than polyimides PI3 and ZPI3, which could be attributed to the quenching effect of 3FPMDA. The energy diagrams of polymers are shown in Figure 4.15 are reasonable representations of the energetic processes describing the photophysics of polymers containing *trans*-DATPP and *trans*-ZnDATPP (Appendix I).

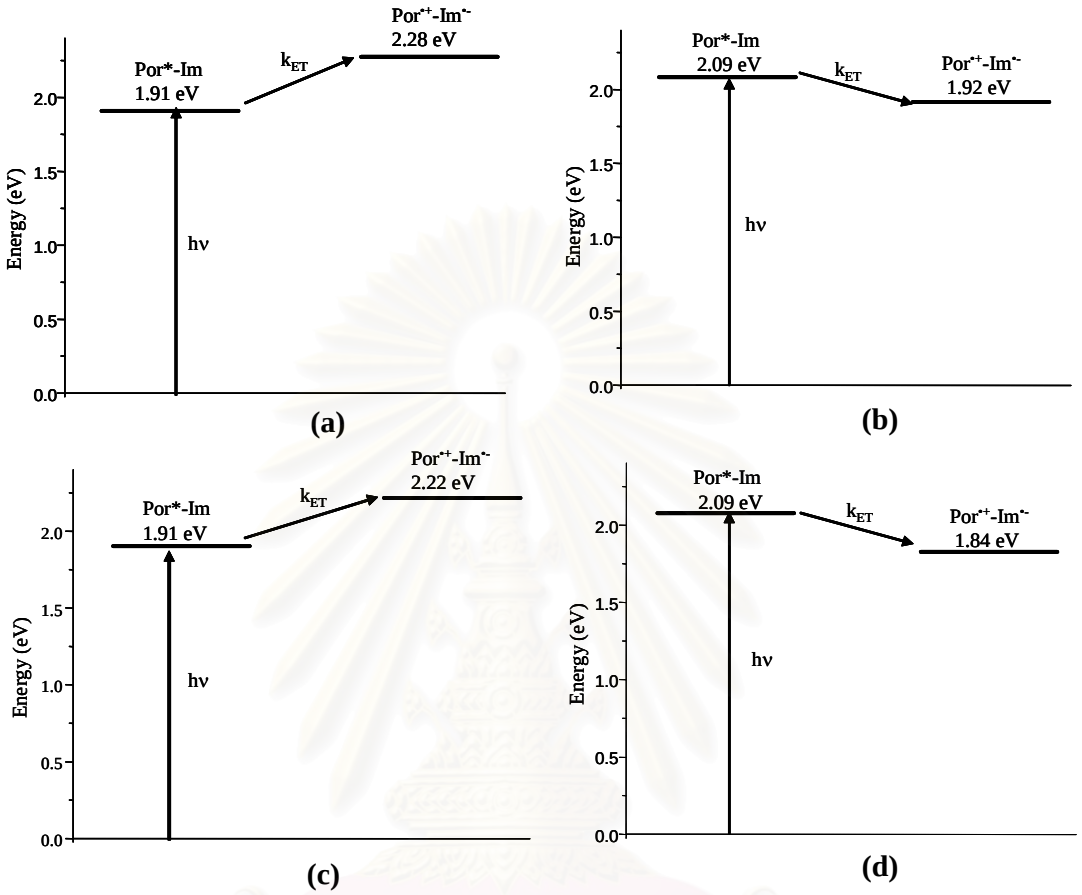

Figure 4.15 Energy diagram of polyimides; (a) PI3, (b) ZPI3, (c) WPI3 and (d) ZWPI3.

4.3.6 Fluorescence lifetimes of polyimides

Fluorescence lifetimes (τ_{Fl}) of some selected polyimides (PI3, ZPI3, WPI3, ZWPI3) were determined using the time-correlated single photon counting (TCSPC) technique and are shown in Table 4.18. Most of the fluorescence lifetimes were found to be best to a two-component exponential decay composed of one major component and one minor component. The values of τ_{Fl} for those polymers were uniformly

smaller than those of standard porphyrins (TPP and ZnTPP). The major component for PI3 was found to be 8.22 ns in CH_2Cl_2 and 10.70 ns in DMAc, both values of which are smaller than those of TPP (9.25 ns in CH_2Cl_2 and 12.2 ns in DMAc), while the major component in polymer WPI3 was 8.00 ns in CH_2Cl_2 and 11.60 ns in DMAc. The major component for ZPI3 was found to be 1.51 ns in CH_2Cl_2 and 1.53 ns in DMAc (compared to 1.78 ns for ZnTPP in CH_2Cl_2 and 1.92 ns in DMAc), while the major component in polymer ZWPI3 was 1.51 ns in CH_2Cl_2 and 1.46 ns in DMAc (Table 4.18).

Table 4.18 Summary of photophysical data of polyimides

Compound	Solvent	τ_1[a] (ns)	τ_2[a] (ns)	τ_3[a] (ns)	k_{ET} (s^{-1})
TPP	CH_2Cl_2	9.25[b]			
ZnTPP	CH_2Cl_2	1.78[b]			
PI3	CH_2Cl_2	8.22 (99.02%)	0.94 (0.98%)		1.46×10^7
ZPI3	CH_2Cl_2	1.51 (96.75%)	0.37 (3.25%)		1.17×10^8
WPI3	CH_2Cl_2	8.00 (93.95%)	1.94 (4.24%)	0.29 (1.81%)	2.34×10^7
ZWPI3	CH_2Cl_2	1.51 (97.18%)	0.28 (2.82%)		1.16×10^8
TPP	DMAc	12.2[c]			
ZnTPP	DMAc	1.92[c]			
PI3	DMAc	10.70 (98.38%)	1.74 (1.62%)		1.28×10^7
ZPI3	DMAc	1.53 (96.99%)	0.48 (3.01%)		1.47×10^8
WPI3	DMAc	11.60 (75.68%)	5.79 (24.32%)		1.62×10^7
ZWPI3	DMAc	1.46 (97.18%)	0.15 (2.82%)		1.82×10^8

[a] Values in parentheses are the relative contribution from each component. [b] See ref 56. [c] See ref 56.

From these lifetimes, the electron transfer rate constants (k_{ET},) of each polymer were determined by using the following equation as described in experimental section, assuming electron transfer is the sole method of excited state decay other than fluorescence (Table 4.18).

$$k_{ET} = \frac{1}{\tau_{PI}} - \frac{1}{\tau_{ref}}$$

From this data it is seen that the rate constants determined for polyimides containing *trans*-DATPP (PI3, WPI3) are similar to one another in both solvents, but are approximately an order of magnitude smaller than those of polyimides containing *trans*-ZnDATPP (ZPI3, ZWPI3). The fluorescence quantum yield and lifetime data can now be assessed in terms of the corresponding electrochemical data. The endothermic value of ΔG_{ET} obtained for polyimides containing *trans*-DATPP indicates the electron transfer (ET) is unlikely in these polyimides. Nonetheless, a small to moderate decrease in both Φ_{Fl} and τ_{Fl} is observed for polyimides in series I and III. A possible explanation for these values is that chain coiling in CH_2Cl_2 leads to a favorable spatial arrangement of the donor porphyrin and the acceptor diimide group for ET. More extensive chain coiling is expected in a poor solvent, wherein the polyimide is better solvated by itself than by the solvent. The poorer solubility of the polyimide in CH_2Cl_2, that leads to lower values of Φ_{Fl} and more rapid k_{ET}, supports this explanation. Alternatively, the aforementioned aggregation effects might serve to change the local environment around the porphyrin macrocycle in the polyimide, making ET more favorable than calculated in Table 4.17. In the case of polyimides containing *trans*-ZnDATPP (ZPI3, ZWPI3), electron transfer is clearly a favorable

pathway for excited state decay. The lower values of Φ_{Fl} and more rapid k_{ET} in CH_2Cl_2 relative to DMAc for the zinc porphyrin-containing polymers appears to support the first interpretation, where coiling effects have a much larger impact on electron transfer.

CHAPTER V

CONCLUSION AND SUGGESTIONS

5.1 Conclusions

Four series of polyimides containing either *trans*-DATPP or *trans*-ZnDATPP were synthesized and found to be soluble in most common organic solvents, which was the first time ever reported. Porphyrin-containing polyimides based on 6FDA, series I and II, exhibited significantly higher viscosities than polyimide without porphyrin. It was postulated that the aggregation of polyimide chains might occur *via* pi-pi interaction of porphyrin units, and in case of zinc porphyrin-containing polyimides, axial ligation to the zinc porphyrin was additionally influence on the decrease in viscosity. Porphyrin-containing polyimides based on 6FDA and 3FPMDA, series III and IV, showed lower viscosity with increasing 3FPMDA comparing to the polyimides in series I and II at the same level of porphyrin content. This result was concluded that low viscosity was caused by steric hindrance of two trifluoromethylphenyl groups of 3FPMDA in addition to pi-pi interaction of porphyrins. Because of the good solubility of these polyimides, it provides several advantages comparing to the insoluble porphyrin-containing polyimides. Besides the easier and more convenient fabrication process, their photophysical properties can be determined in solution. Steady state and time-resolved fluorescence measurements on these polyimides in CH_2Cl_2 and DMAc revealed moderate quenching of the fluorescence

that was attributed to photoinduced electron transfer from excited porphyrin units within the polymer to diimide acceptor groups. The incorporation of 3FPMDA into porphyrin-containing polyimides had increased the exothermicity while the rate of electron transfer constant was the same comparing to porphyrin-containing polyimides without 3FPMDA. Accordingly, these polyimides have great potential in photonic applications.

5.2 Suggestions for further work

1. Because of the good solubility of these polyimides, it can be studied other properties of these polyimides in the solution such as molecular weight determination by gel permeation chromatography (GPC).

2. Study the combination of four bands to two bands in Q-band region.

3. Optimize both the electron transfer properties of these polymers by modifying the acceptor group as well as the ratio of porphyrin/acceptor within the copolymer.

REFERENCES

1. Arnold Jr, F.E. Cheng, S. Z. D., Hsu, S. L. -C., Lee, C. J. and Harris, F. W. “Organo-Soluble, Segmented Rigid-Rod Polyimide Films: 2. Properties for microelectronic Application” *Polymer* 1992, 33, 5179.
2. Harris, F. W., Lin, S. -H., Li, F. and Cheng, S. Z. D. “Organo-Soluble Polyimides: Synthesis and Polymerization of 2,2′-Disubstituted-4,4′,5,5′-biphenyltetra-carboxylic Dianhydrides” *Polymer* 1996, 37, 5049.
3. Lin, S. –H., Li, F., Cheng, S. Z. D. and Harris, F. W. “Organo-Soluble Polyimides: Synthesis and Polymerization of 2,2′-Bis(trifluoromethyl)-4,4′,5,5′-Biphenyl-tetracarboxylic Dianhydride” *Macromolecules* 1998, 31, 2080.
4. Harris, F. W. in *Polyimides* (Eds D. Wilson, H. D. Stenzenberger and P. M. Hergenrother), Blackie and Son, New York, 1990, pp. 1-37.
5. Chou, J. –H., Kosal, M. E., Nalwa, H. S., Rakow, N. A. and Suslick, K. S. in *The Porphyrin Handbook* (Eds Kadish, K., Smith, K. and Guilard, R.), Academic Press, New York, 2000, (vol. 6, chapter 41), pp.43-131.
6. Bao, Z. N., Chen, Y. M. and Yu, L. P. “New Metalloporphyrin Containing Polymers from the Heck Coupling Reaction” *Macromolecules* 1994, 27, 4629.
7. Peng, Z. –H, Bao, Z. N. and Yu, L. P. “Large Photorefractivity in an Exceptionally Thermostable Multifunctional Polyimides” *J. Am. Chem. Soc.* 1994, 116 6003.
8. Wagner, R. W. and Lindsey, J. S. “A Molecular Photonic Wire” *J. Am. Chem. Soc.* 1994, 116, 9759.
9. Nisiukata, Y., Morikawa, A., Kakimoto, M. –A., Imai, Y., Nishiyama, K. and Fujihira, M. “Preparation and Photocurrent Properties of Tin Dioxide Electrode Modified by

Polyimide Langmuir Blodgett Films Possessing Tetraphenylporphyrin Unit" *Polymer J.* 1990, 22, 593.

10. Xu, Z. –K., Zhu, B. –K., and Xu, Y. –Y. "Photoinductivity of Copolyimide Films Containing Tetraphenylporphyrin and Carbazole Moieties" *Chem. Mater*. 1998, 10, 1350.
11. Zhu, B. –K., Xu, Z. –K., and Xu, Y. –Y. "Synthesis and Electrophotographic Properties of Copolyimides Containing Tetraphenlyporphyrin" *European Polymer Journal* 1999, 35, 77.
12. Zhu, B. –K., Xu, Y. –Y., Wei, X. –Z. and Xu, Z. –K. "Synthesis and Photoconductive Characteristics of Biphenylporphyrin-Containing Poly(amic acid)s and Polyimides" *Polym. Int.* 2004, 53, 708.
13. Iwamoto, M. and Xu, X. "Transient Photoinduced Voltage in Hetero-structured Polyimide Langmuir-Blodgett films" *Thin Solid Films* 1996, 284-285, 936.
14. Ohkita, H., Ogi, T., Kinoshita, R., Ito, S., and Yamamoto, M. "Photoinduced Electron Transfer in Nanostructures of Ultrathin Polyimide Films Containing Porphyrin Moieties" *Polymer* 2002, 43, 3571.
15. Ogi, T., Kinoshita, R. and Ito, S. "Spectroscopic and Optical Characterization of Porphyrin Chromophores Incorporated into Ultrathin Polyimide Films" *Journal of Colloid and Interface Science* 2005, 286, 280.
16. Grubba, T. L., Ulerya, V. L., Smitha, T. J., Tullosa, G. L., Yagcia, H., Mathiasa, L. J., and Langsamb, M. "Highly Soluble Polyimides from Sterically Hindered Diamines" *Polymer* 1999, 40, 4279.
17. Zhang, S., Li, Y., Wang, X., Zhao, X., Shao, Y., Yin, D. and Yang, S. "Synthesis and Properties of Novel Polyimides Derived from 2,6-*Bis*(4-aminophenoxy-40-benzoyl)pyridine with some of Dianhydride monomers" *Polymer* 2005, 46, 11986.

18. Butt, M. S., Akhtar, Z., Zaman, Z. U. and Munir, A. “Synthesis and Characterization of some Novel Aromatic Polyimides” *Eur. Polym. J.* 2005, 41, 1638.

19. Leu, W. –T. and Hsiao, S. –H. “Synthesis and Properties of Novel Aromatic Poly(ester-imide)s Bearing 1,5-*Bis*(benzoyloxy)naphthalene Units” *Eur. Polym. J.* 2006, 42, 328.

20. Banihashemi, A. and Abdolmaleki, A. “Novel Aromatic Polyimides Derived from Benzofuro-[2,3-β]benzofuran-2,3,8,9-tetracarboxylicbdianhydride (BBTDA)” *Eur. Polym. J.* 2004, 40, 1629.

21. Qiua, Z. and Zhanga, S. “Synthesis and Properties of Organosoluble Polyimides Based on 2,20-Diphenoxy-4,4′,5,5′-biphenyltetracarboxylic Dianhydride” *Polymer* 2005, 46, 1693.

22. Liaw, D. -J., Liaw, B. –Y. and Yu, C. –W. “Synthesis and Characterization of New Organosoluble Polyimides Based on Flexible Diamine” *Polymer* 2001, 42, 5175.

23. Su, Y. Y. and Yang, C. P. “Properties of Organosoluble Aromatic Polyimides from 3′-Trifluoromethyl-3,4′-oxydianiline” *Polymer* 2003, 44, 6311.

24. Leu, W. –T. and Hsiao, S. –H. “Synthesis and Properties of Novel Aromatic Poly(ester-imide)s bearing 1,5-*Bis*(benzoyloxy)naphthalene Units” *Eur. Polym. J.* 2006, 42, 328.

25. MacAlpine, J. “Chemistry at the Porphyrin Periphery” *Thesis*; Ph.D. Department of Chemistry, The University of British Columbia 1999.

26. Takahashi, K., Takano, Y., Yamaguchi, T., Nakamura, J. –I, Yokoe, C. and Murata, K. “Porphyrin Dye-Sensitization of Polythiophene in a Conjugated Polymer/TiO_2 p–n Hetero-junction Solar Cell” *Synthetic Metals* 2005, 155, 51.

27. Takechi, K., Shiga, T., Motohiro, T., Akiyamab, T., Yamada, S., Nakayama, H. and Kohama, K. “Solar Cells Using Iodine-Doped Polythiophene–Porphyrin Polymer Films” *Solar Energy Materials & Solar Cells*, Article in press.

28. Aida, T. and Inoue, S. “Metalloporphyrins as Initiators for Living and Immortal Polymerizations” *Acc. Chem. Res.* 1996, 29, 39.

29. Johanson, U., Marandi, M. Sammelselg, V. and Tamm, J. “Electrochemical Properties of Porphyrin-Doped Polypyrrole Films” *Journal of Electroanalytical Chemistry* 2005, 575, 267.

30. Nowakowska, M., Kataoka, F. and Guillet, J. E. “Photoinduced Electron Transfer in Porphyrin-Quinone End-Capped Poly(methacrylic acid). 1. Photophysical Studies” *Macromolecules* 1996, 29, 1600.

31. Jiang, B., Yang, S. –W. and Jones, W. E., Jr. “Conjugated Porphyrin Polymers: Control of Chromophore Separation by Oligophenylenevinylene Bridges” *Chem. Mater.* 1997, 9, 2031.

32. Udal′tsov, A. V. “Characteristics of Donor-Acceptor Complexes Formed in Porphyrin-Polymer Systems and Their Photoactivation in Electron Transfer Photoreaction” *Journal of Photochemistry and Photobiology B: Biology* 1997, 37, 31.

33. Nowakowska, M., Karewicz, A., Klos, M. and Zapotoczny, S. “Synthesis and Properties of Water-Soluble Poly(sodium styrenesulfonate-*block*-5-(4-acryloyl-oxyphenyl)-10,15,20-tritolylporphyrin) by Nitroxide-Mediated Free Radical Polymerization” *Macromolecules* 2003, 36, 4134.

34. Jiménez, H. R. and Momenteau, M. “Synthesis and Characterization of Superstructured Rhodium Porphyrins” *Inorganica Chimica Acta* 1996, 244, 171.

35. You, W. Y., Wang, L., Wang, Q. and Yu, L. “Synthesis and Structure/Property Correlation of Fully Functionalized Photorefractive Polymers” *Macromolecules* 2002, 35, 4636.

36. McEwan, K., Lewis, K., Yang, G. –Y., Chng, L. –L., Lee, Y. –W., Lau, W. –P. and Lai, K. –S. “Synthesis, Characterization, and Nonlinear Optical Study of Metalloporphyrins” *Adv. Funct. Mater*. 2003, 13, 863.

37. Yamada, S., Kuwata, K., Yonemura, H. and Matsuo, T. “Second-Order Nonlinear Optical Properties of Amphiphilic Porphyrins in Langmuir-Blodgett Monolayer Assemblies” *J. Photochem. Photobiol. A: Chem.* 1995, 87, 115.

38. Spanggaard, H. and Krebs, F. C. “A Brief History of the Development of Organic and Polymeric Photovoltaics” *Solar Energy Materials & Solar Cells* 2004, 83, 125.

39. Sendhil, K. Vijayan, C. and Kothiya, M. P. “Nonlinear Optical Properties of a Porphyrin Derivative Incorporated in Nafion Polymer” *Optical Materials* 2005, 27, 1606.

40. Jiang, L., Lu, F., Gao, Y., Song, Y., Liu, H., Gan, H., Jiu, T., Li, Y., Li, Y., Wang, S. and Zhu, D. “Nonlinear Optical Properties of an Ultrathin Film Containing Porphyrin and Poly(phenylenevinylene) Units” *Thin Solid Films* 2006, 496, 311.

41. Shimidzu, T. and Segawa, H. “Porphyrin Arrays Connected with Molecular Wire” *Thin Solid Films* 1996, 273, 14.

42. Jiang, B., Yang, S. W., Bailey, S. L., Hermans, L. G., Niver, R. A., Bolcar, M. A. and Jones, W. E., Jr. “Toward Transparent Molecular Wires: Electron and Energy Transfer in Transition Metal Derivatized Conduction Polymers” *Coordination Chemistry Reviews* 1998, 171, 365.

43. Negi, Y. S., Suzuki, Y. –I., Kawamura, I., Hagiwara, T., Takahashi, Y., Ijima, M., Kakimoto, M. –A. and Imai, Y. “Synthesis and Properties of Polyimides Based on

2,2′-*Bis*[4-(4-Aminophenoxy)phenyl)]propane and 2,2′-*Bis*[4-(4-Aminophenoxy)-phenyl]hexafluoropropane" *J. Polym. Sci. A: Polymer Chemistry* 1992, 30, 2281.

44. Tomikawa, M., Harris, F. W., Cheng, S. Z. D. and Galentier, E. "Synthesis and Photo-induced Solution Properties of New Rigid-Rod Polyimides" Reactive & Functional *Polymers* 1996, 30, 101.

45. Lin, S. –H., Li, F., Cheng, S. Z. D., and Harris, F. W. "Organo-Soluble Polyimides: Synthesis and Polymerization of 2,2′-*Bis*(trifluoromethyl)-4,4′,5,5′-Biphenyl-tetracarboxylic Dianhydride" *Macromolecules* 1998, 31, 2080.

46. Lee, C. –H. and Lindsey, J. S. "One-Flask Synthesis of *Meso*-Substituted Dipyrromethanes and Their Application in the Synthesis of *Trans*-Substituted Porphyrin Building Blocks" *Tetrahedron* 1994, 50, 11427.

47. Littler, B. J., Miller, M. A. Hung, C. –H., Wagner, R. W., ÓShea, D. F., Boyle, P.D. and Lindsey, J. S. "Refiend Synthesis of 5-Substituted Dipyrromethane" *J. Org. Chem*. 1999, 64, 1391.

48. Kruper Jr, W. J., Chamberlin, T. A. and Kochanny, M. "Regiospecific Aryl Nitration of *Meso*-Substituted Tetraarylporphyrins: A Simple Route to Bifunctional Porphyrins" *J. Org. Chem.* 1989, 54, 2753.

49. Marvel, C. S. and Rassweiler, J. H. "Polymeric Phthanocyanines" *J. Am. Chem. Soc*. 1958, 80, 1197.

50. Shiang, W. R. and Woo, E. P. "Soluble Copolyimides with High Modulus and Low Moisture Absorption" *J. Polym. Sci. A: Polymer Chemistry* 1993, 31, 2081.

51. Hayvali, M., Gündüz, H., Gündüz, N., Kiliç, Z. and Hökelek, T. "Synthesis and Characterization of Unsymmetrically Tetrasubstituted Porphyrin and Their Nickel (II) Complexes with the Crystal Structure of 5, 15-*Bis*(4-aminophenyl)-10,20-diphenylporphyrinatonickel (II)" *Journal of Molecular Structure* 2000, 525, 215.

52. Yin, J., Ye, Y. –F. and Wang, Z. –G. “Study on Preparation and Properties of Polyimides Containing Long Flexible Chain in the Backbone” *Eur. Polym. J*. 1998, 34, 1839.

53. Li, F., Fang, S., Ge, J. J., Honigfort, P. S., Chen, J. –C., Harris, F. W. and Cheng, S. Z. D. “Diamine Architecture Effects on Glass Transitions, Relaxation Processes and Other Material Properties in Organo-Soluble Aromatic Polyimide Films” *Polymer* 1999, 40, 4571.

54. Hunter, C. A. and Sanders, J. K. M. “The Nature of π-π Interactions” *J. Am. Chem. Soc*. 1990, 112, 5525.

55. Yamamoto, T., Fukushima, N., Nakajima, H., Maruyama, T. and Yamaguchi, I. “Synthesis and Chemical Properties of π-Conjugated Zinc Porphyrin Polymers with Arylene and Aryleneethylene Groups between Zinc Porphyrin Units” *Macromolecules* 2000, 33, 5988.

56. Rajesh, C. S., Capitosti, G. J., Cramer, S. J. and Modarelli, D. A. “Photoinduced Electron-Transfer within Free Base and Zinc Porphyrin Containing Poly(Amides) Dendrimers” *J. Phys. Chem. B* 2001, 105, 10175.

57. Nappa, M. and Valentine, J. S. “The Influence of Axial Ligands on Metalloporphyrin Visible Absorption Spectra: Complexes of Tetraphenylporphinatozinc” *J. Am. Chem. Soc.* 1978, 100, 5075.

58. Karangu, N. T., Rezac, M. E. and Beckham, H. W. “Synthesis and Properties of Processable Polyimides Containing Diacetylene Groups” *Chem. Mater*. 1998, 10, 567.

59. Chung, I. S. and Kim, S. Y. “Soluble Polyimides from Unsymmetrical Diamine with Trifluoromethyl Pendent Group” *Macromolecules* 2000, 33, 3190.

60. Harris, F. W., Sakaguchi, Y., Shibata, M. and Cheng, S. Z. D. “Organo-Soluble Polyimides: Synthesis and Characterization of Polyimides Containing Phenylated *p*-Biphenyl and *p*-Terphenyl Units” *High Perform. Polym*. 1997, 9, 251.

61. Murov, S. L., Carmichael, I. And Hug, G. L. *Handbook of Photochemistry*; Marcel Dekker, Inc: New York, 1993.

APPENDICES

APPENDIX A

Absorption spectra of polyimides

A.1 Absorption spectra of porphyrins and polyimides in CH_2Cl_2

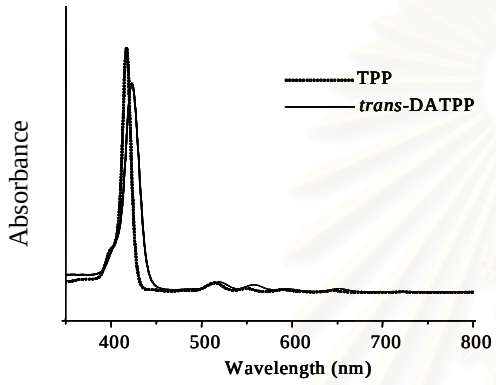

Figure A.1.1 Absorption spectra of TPP and *trans*-DATPP.

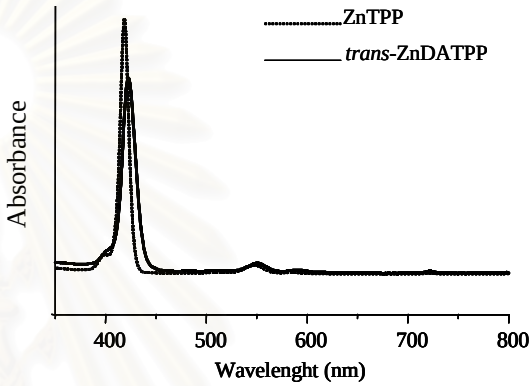

Figure A.1.2 Absorption spectra of ZnTPP and *trans*-ZnDATPP.

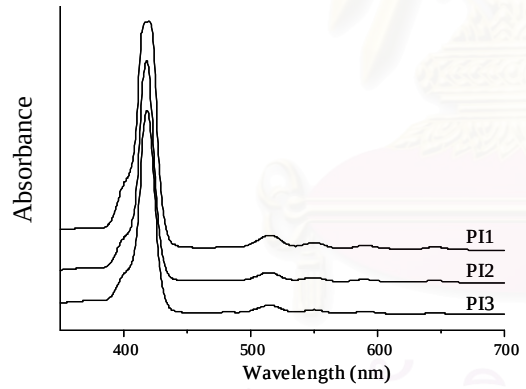

Figure A.1.3 Absorption spectra of polyimides in series I.

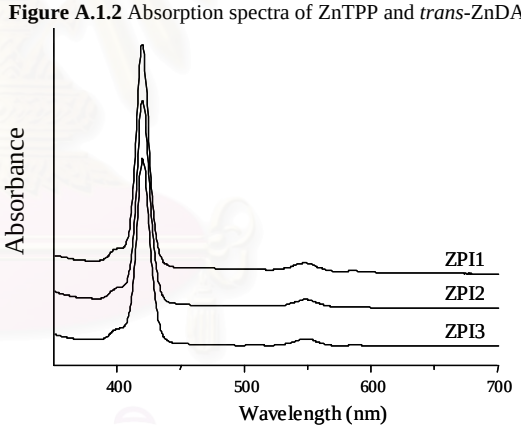

Figure A.1.4 Absorption spectra of polyimides in series II.

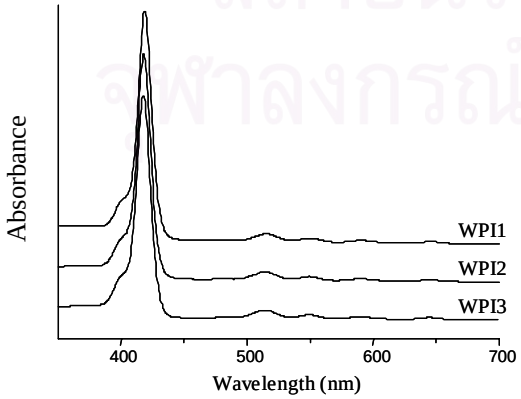

Figure A.1.5 Absorption spectra of polyimides in series III.

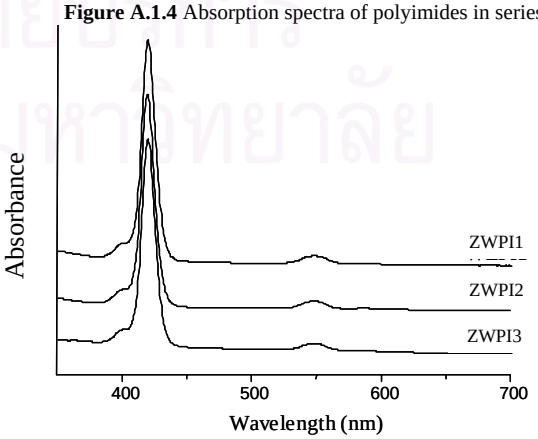

Figure A.1.6 Absorption spectra of polyimides in series IV.

A.2 Absorption spectra of porphyrins and polyimides in DMAc

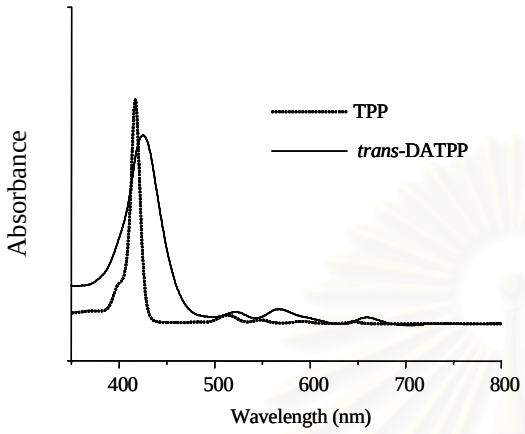

Figure A.2.1 Absorption spectra of TPP and *trans*-DATPP.

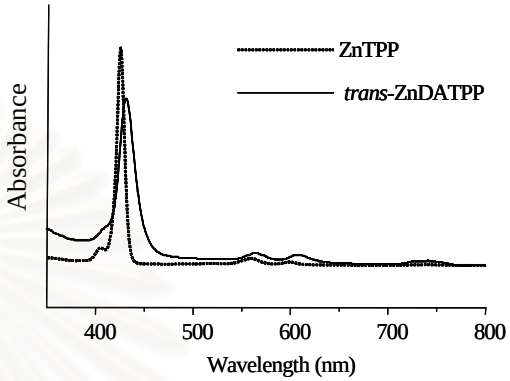

Figure A.2.2 Absorption spectra of ZnTPP and *trans*-ZnDATPP.

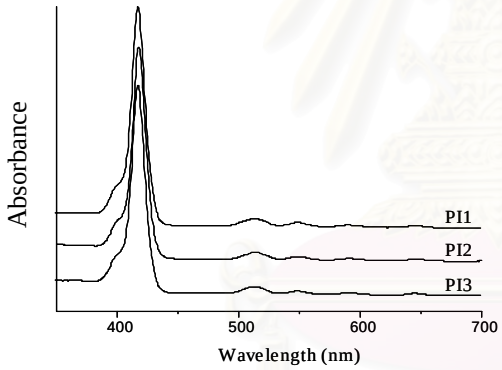

Figure A.2.3 Absorption spectra of polyimides in series I.

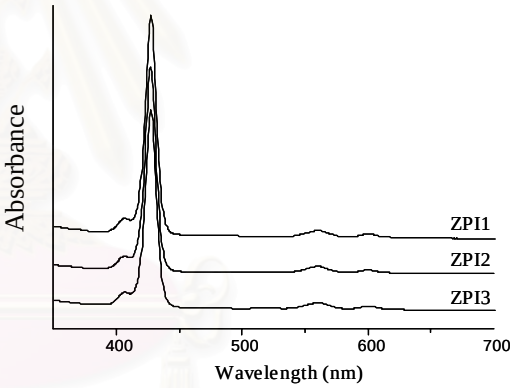

Figure A.2.4 Absorption spectra of polyimides in series II.

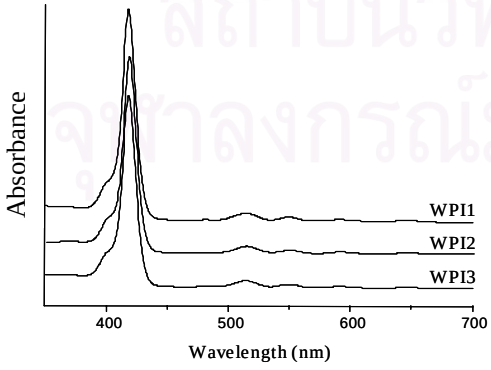

Figure A.2.5 Absorption spectra of polyimides in series III.

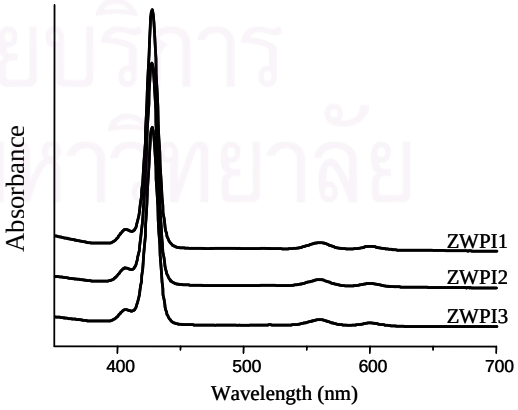

Figure A.2.6 Absorption spectra of polyimides in series IV.

APPENDIX B

Infrared spectra of polyimides

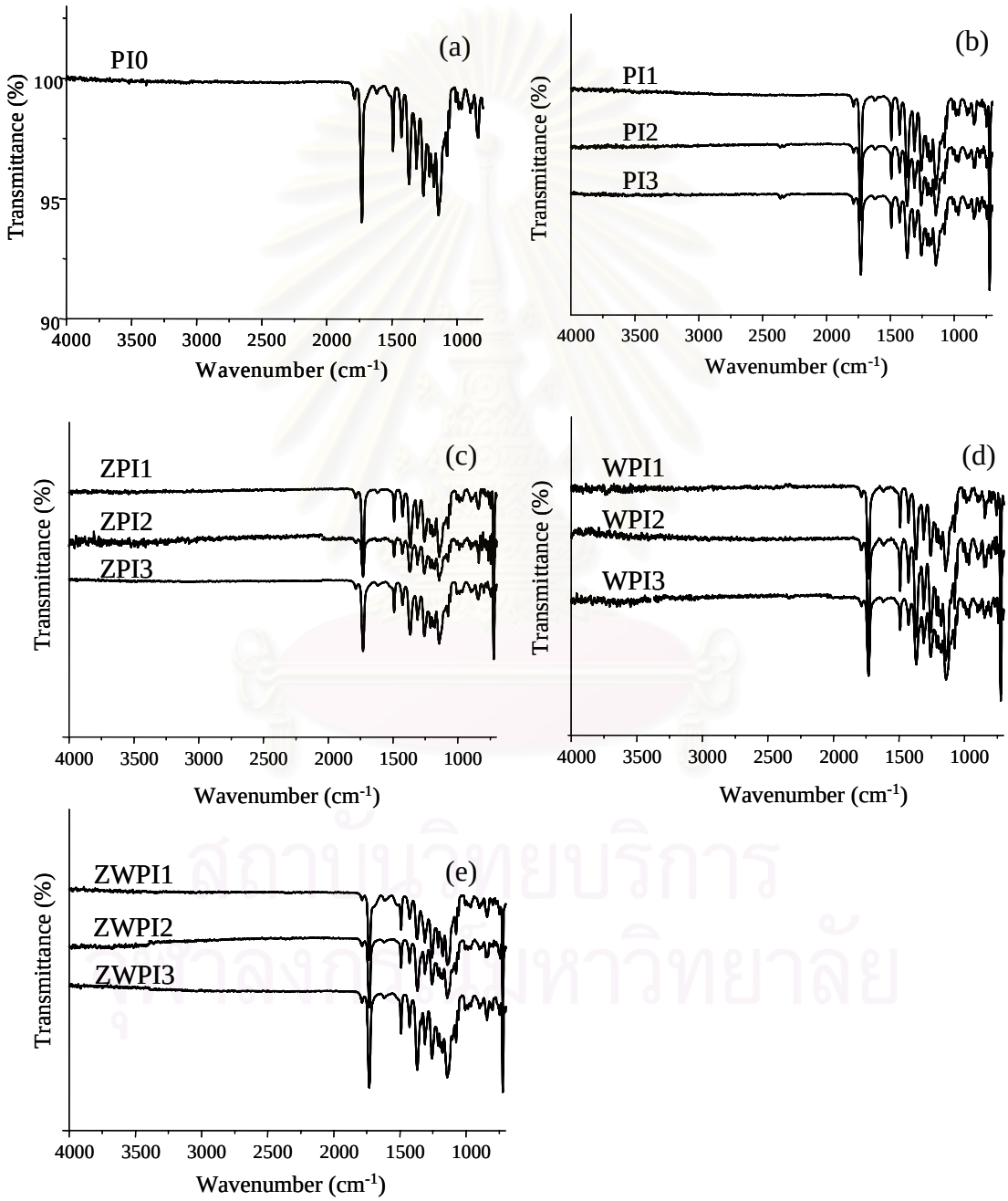

Figure B.1 IR spectra of polyimides; (a) PI0, (b) series I, (c) series II, (d) series III and (e) series IV.

APPENDIX C

Determination of porphyrin content in polyimides

The concentration of porphyrin monomers can be obtained by using equation C.1.

$$A = \varepsilon bc \qquad (C.1)$$

Where A = absorbance (optical density)

ε = molar extinction coefficient

b = path length through the sample

c = concentration of solute

Table C.1 Concentration of porphyrin in polyimides

PI	absorbance	ε^a ($M^{-1}.cm^{-1}$)	concentration	mole of porphyrin
PI1	0.899	542000	3.48321E-05	1.74161E-07
PI2	1.630	542000	6.31550E-5	3.15775E-07
PI3	1.770	542000	6.85793E-05	3.42897E-07
ZPI1	0.827	626300	1.71659E-05	8.58295E-08
ZPI2	1.461	626300	3.03257E-05	1.51629E-07
ZPI3	1.463	626300	3.73751E-05	1.86875E-07
WPI1	0.831	542000	2.45314E-05	1.22657E-07
WPI2	0.860	542000	1.74539E-05	8.72694E-08
WPI3	1.792	542000	4.29815E-05	2.14908E-07
ZWPI1	0.898	626300	2.29411E-05	1.14705E-07
ZWPI2	1.568	626300	3.25467E-05	1.62734E-07
ZWPI3	1.194	626300	3.05030E-05	1.52515E-07

[a] ε (CH_2Cl_2) = ε_{TPP} = 542000 for polyimides containing free base porphyrin,
= ε_{ZnTPP} = 626300 for polyimdies containing zinc porphyrin

Table C.2 Weight percent of porphyrin in feed and polyimides

PI	weight of polymer (mg)	weight of porphyrin in feed (%)	weight of porphyrin in polymer (%)
PI1	2.9	4.13	3.87
PI2	2.8	8.08	7.27
PI3	2.4	11.87	9.21
ZPI1	1.5	4.50	4.05
ZPI2	1.3	8.78	8.26
ZPI3	1.2	12.88	11.03
WPI1	2.1	4.11	3.77
WPI2	0.9	8.71	6.25
WPI3	1.4	11.73	9.90
ZWPI1	2.5	4.49	3.25
ZWPI2	1.5	8.74	7.68
ZWPI3	1.1	12.74	9.82

APPENDIX D

Intrinsic viscosity measurement

The intrinsic viscosity is determined experimentally by measurements of flow times of solvent (t_0) and a series of dilute polymer concentrations of known concentration (t_c) in a standard capillary viscosity. The specific viscosity is calculated from the equation

$$\eta_{sp} = \frac{\eta_c - \eta_0}{\eta_0} = \frac{t_c - t_0}{t_0} \qquad \text{(D.1)}$$

and from the Huggins equation

$$\frac{\eta_{sp}}{c} = [\eta] + k^1[\eta]^2 c \qquad \text{(D.2)}$$

where k^1 is a positive constant, the intrinsic viscosity is obtained by plotting η_{sp}/c versus c and extrapolating to zero concentration (Figure D.1).

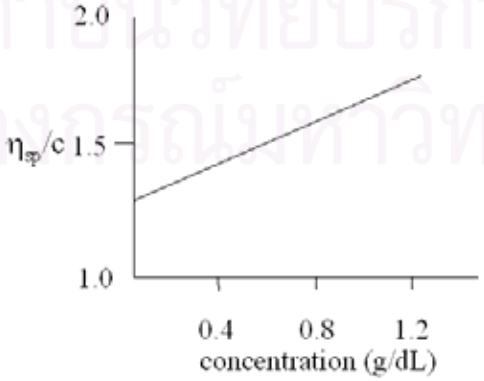

Figure D.1 Dilute solution viscometry: Huggins plot of η_{sp}/c against concentration.

Table D.1 Average flow times of polyimides.

PI	concentration[a] (g/dL)	t_1 (s)	t_2 (s)	t_3 (s)	t_{ave} (s)
PI0	0.20	55.34	55.37	55.29	55.33
	0.39	62.35	62.19	62.22	62.25
	0.60	70.81	70.69	70.66	70.72
	0.80	80.41	80.79	80.37	80.52
	1.00	90.60	91.16	90.87	90.88
PI1	0.20	59.35	59.35	59.22	59.31
	0.40	70.94	71.44	71.09	71.16
	0.60	84.72	84.97	84.69	84.79
	0.80	101.53	102.06	102.16	101.92
	1.00	120.32	120.59	120.31	120.41
PI2	0.21	58.53	58.28	58.35	58.39
	0.38	68.31	68.03	68.25	68.20
	0.59	81.44	80.81	80.97	81.07
	0.82	96.59	97.16	97.06	96.94
	1.00	112.91	112.84	112.72	112.82
PI3	0.20	57.26	57.26	57.36	57.29
	0.41	67.40	67.47	67.60	67.49
	0.61	79.09	79.06	78.97	79.04
	0.81	93.62	93.72	93.16	93.50
	1.02	107.84	107.47	107.50	107.60
ZPI1	0.20	57.90	58.15	57.94	58.00
	0.39	67.66	67.16	67.56	67.46
	0.61	79.59	79.31	79.56	79.49
	0.79	90.13	90.31	90.87	90.44
	1.01	106.97	106.50	106.28	106.58
ZPI2	0.20	55.91	56.25	56.07	56.08
	0.39	63.91	63.97	63.94	63.94
	0.59	72.94	72.44	72.82	72.73
	0.80	84.04	84.41	84.00	84.15
	1.00	94.34	94.66	94.25	94.42
ZPI3	0.20	55.10	55.84	56.03	55.66
	0.39	63.81	63.15	63.37	63.44
	0.60	72.56	71.96	72.41	72.31
	0.80	82.44	81.75	82.87	82.35
	1.00	92.13	92.21	92.44	92.26
WPI1	0.20	56.41	56.47	56.43	56.44
	0.40	66.37	66.56	66.62	66.52
	0.59	76.34	76.50	76.50	76.45
	0.79	86.53	86.09	86.69	86.44
	1.00	98.06	98.40	98.88	98.45

PI	concentration[a] (g/dL)	t_1 (s)	t_2 (s)	t_3 (s)	t_{ave} (s)
WPI2	0.21	55.40	55.82	55.75	55.66
	0.39	62.78	62.78	62.97	62.84
	0.59	70.94	70.66	70.38	70.66
	0.79	78.88	78.57	78.28	78.58
	0.99	86.82	86.97	86.19	86.66
WPI3	0.20	54.06	54.06	54.28	54.13
	0.39	61.22	61.47	61.19	61.29
	0.58	68.03	68.12	68.21	68.12
	0.80	76.19	76.32	76.28	76.26
	0.99	85.62	85.72	85.57	85.64
ZWPI1	0.20	55.54	55.86	55.77	55.72
	0.39	63.12	63.88	63.54	63.51
	0.61	73.41	73.34	73.47	73.41
	0.78	82.56	82.81	82.74	82.70
	1.01	94.34	94.50	94.45	94.43
ZWPI2	0.18	53.66	53.59	53.64	53.63
	0.38	60.12	60.41	60.34	60.29
	0.60	68.03	67.90	68.04	67.99
	0.80	76.37	76.53	76.82	76.57
	0.99	86.03	86.21	86.17	86.14
ZWPI3	0.19	53.37	53.79	53.46	53.54
	0.39	59.64	59.94	59.73	59.77
	0.59	66.81	68.60	67.62	67.68
	0.80	77.60	75.63	75.66	76.30
	0.99	86.25	87.34	87.94	87.18

[a] in NMP and flow time were measured at 35±0.1 ^{o}C

Table D.2 Specific viscosity and the ratio of specific viscosity to concentration of polyimide.

PI	concentration (g/dL)	η^{a}_{sp}	η_{sp}/c
PI0	0.20	0.156	0.764
	0.39	0.300	0.774
	0.60	0.477	0.795
	0.80	0.682	0.851
	1.00	0.898	0.895
PI1	0.20	0.239	1.207
	0.40	0.486	1.222
	0.60	0.771	1.286
	0.80	1.129	1.408
	1.00	1.515	1.509
PI2	0.21	0.220	1.027
	0.38	0.425	1.106
	0.59	0.694	1.172
	0.82	1.025	1.253
	1.00	1.357	1.357
PI3	0.20	0.196853	0.984263
	0.41	0.40986	0.994806
	0.61	0.651139	1.070951
	0.81	0.953207	1.1739
	1.02	1.247824	1.223357
ZPI1	0.20	0.211545	1.047253
	0.39	0.409233	1.054725
	0.61	0.660469	1.089883
	0.79	0.889214	1.125587
	1.01	1.226516	1.214373
ZPI2	0.20	0.171437	0.848696
	0.39	0.335701	0.860771
	0.59	0.519393	0.880327
	0.80	0.757886	0.942644
	1.00	0.972356	0.970415
ZPI3	0.20	0.162663	0.797367
	0.39	0.325326	0.829912
	0.60	0.510549	0.850916
	0.80	0.720354	0.902699
	1.00	0.927303	0.931027

PI	concentration (g/dL)	η^{a}_{sp}	η_{sp}/c
WPI1	0.20	0.178957	0.913045
	0.40	0.389527	0.968973
	0.59	0.596964	1.015245
	0.79	0.805654	1.025005
	1.00	1.056542	1.056542
WPI2	0.21	0.162663	0.774585
	0.39	0.312792	0.797938
	0.59	0.476081	0.804191
	0.79	0.64146	0.816106
	0.99	0.81032	0.821825
WPI3	0.20	0.13084	0.66081
	0.39	0.280412	0.715337
	0.58	0.423021	0.72435
	0.80	0.593134	0.739569
	0.99	0.788942	0.793705
ZWPI1	0.20	0.164055	0.804193
	0.39	0.326788	0.833642
	0.61	0.533459	0.868825
	0.78	0.727665	0.928144
	1.01	0.972634	0.966833
ZWPI2	0.18	0.120326	0.653945
	0.38	0.259453	0.675658
	0.60	0.420305	0.698181
	0.80	0.59961	0.753279
	0.99	0.799387	0.805834
ZWPI3	0.19	0.118446	0.630031
	0.39	0.24859	0.640696
	0.59	0.413759	0.701287
	0.80	0.593831	0.740437
	0.99	0.821113	0.829407

[a] Calculated from equation D.1, where t_0= 47.87.

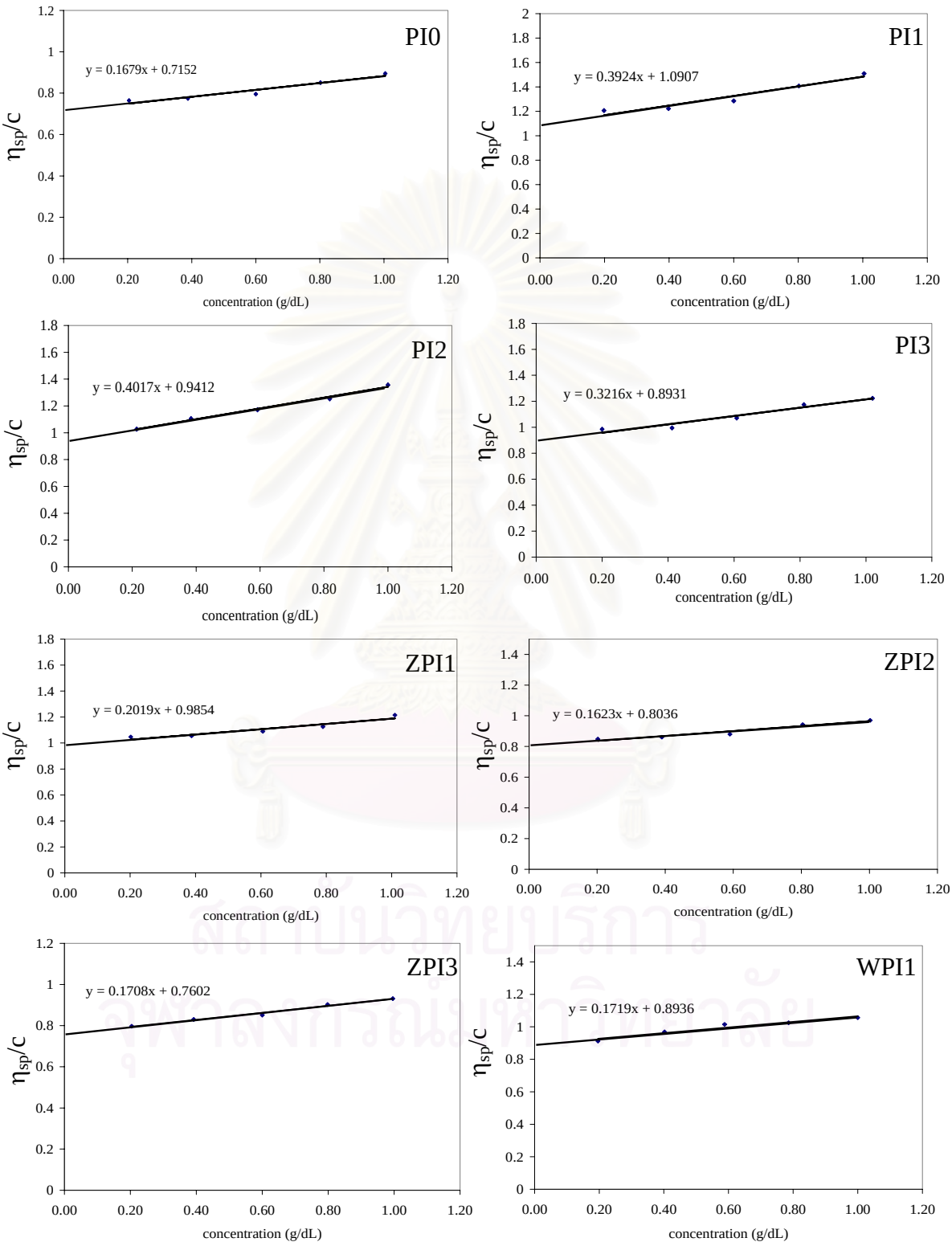

Figure D.2 Intrinsic viscosities of polyimides.

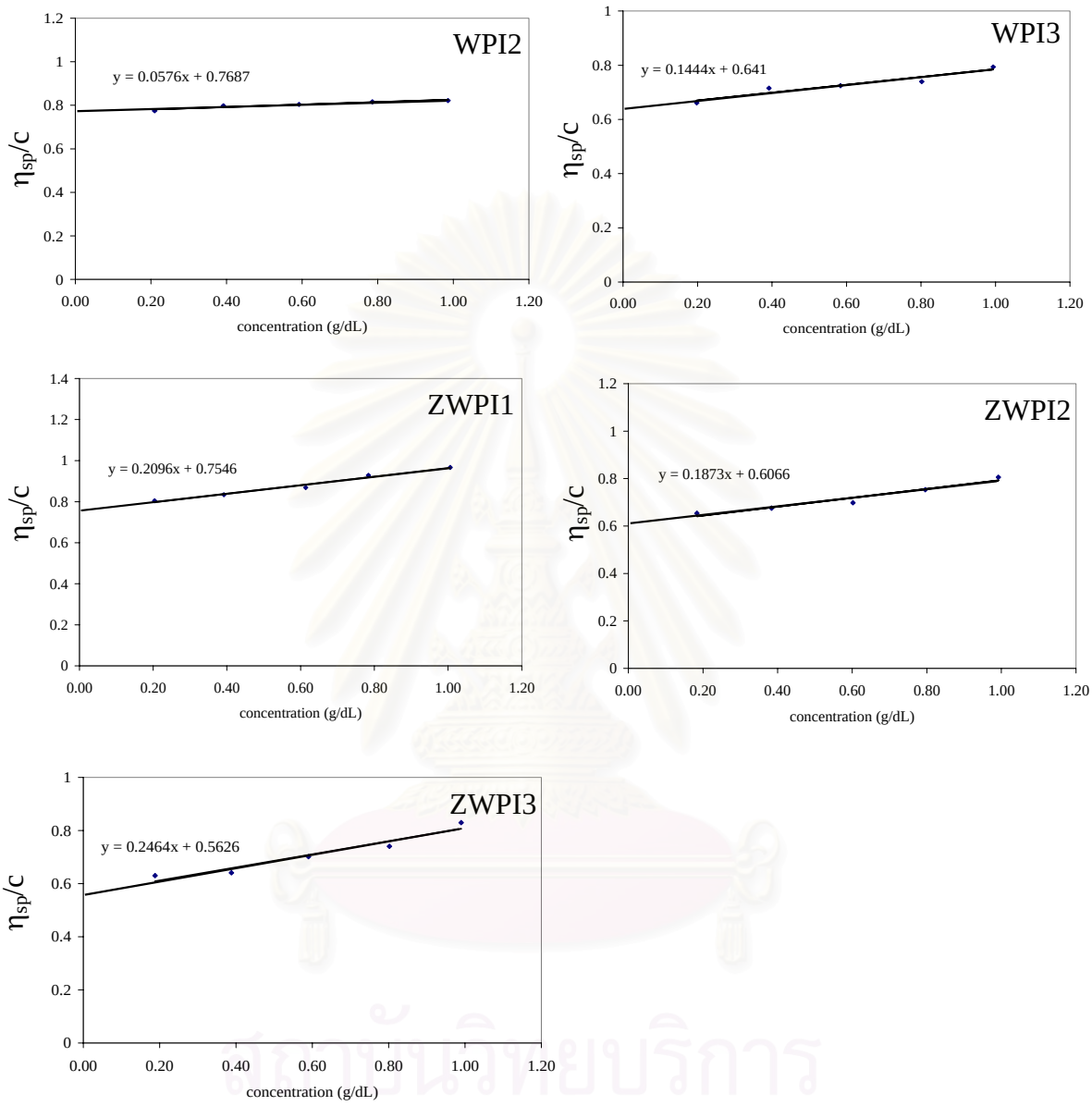

Figure D.2 (continued) Intrinsic viscosities of polyimides.

APPENDIX E

Glass transition temperature of polyimides

Table E.1 Glass transition temperatures of polyimides.

PI	Stress (MPa)	T_g^a (^oC)	T_g^b
PI0	1.801	254.64	284
	3.602	227.84	
	5.403	196.88	
PI1	3.125	270.50	294
	6.250	240.04	
	9.375	220.29	
PI2	3.472	266.51	301
	6.944	250.57	
	10.417	206.28	
PI3	4.464	274.33	310
	8.929	253.22	
	13.393	210.86	
ZPI1	3.834	268.27	316
	7.669	227.07	
	11.503	175.4	

PI	Stress (MPa)	T_g^a (^oC)	T_g^b
ZPI2	5.081	275.19	318
	10.163	236.06	
	15.244	190.73	
ZPI3	7.184	280.21	326
	17.368	237.78	
	21.552	190.73	
WPI1	6.944	207.96	241
	13.889	185.54	
	16.667	160.98	
WPI2	4.808	259.15	286
	9.615	216	
	12.821	210.3	
WPI3	4.921	265.34	290
	9.843	220.31	
	14.764	205.56	

PI	Stress (Mpa)	T_g[a] (^oC)	T_g[b]
ZWPI1	2.341	238.41	268
	3.745	207.61	
	5.618	190.72	
ZWPI2	2.803	270.14	296
	5.605	239.93	
	8.408	215.52	

PI	Stress (Mpa)	T_g[a] (^oC)	T_g[b]
ZWPI3	6.944	278.32	305
	13.889	229.48	
	20.833	213.71	

[a]Temperature at which change in slope occurred on a plot of film dimensional change vs temperature.

[b]Temperature obtained from a plot of stress vs temperature[a] that extrapolated to zero stress.

APPENDIX F

Thermogravimetric analysis (TGA)

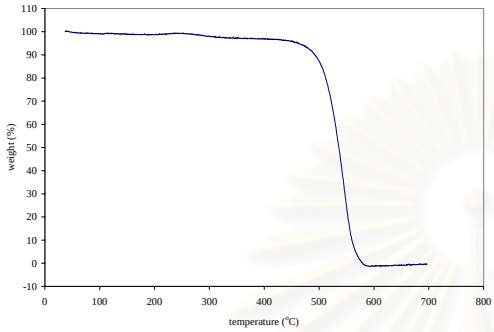

Figure F.1 TGA thermogram of polyimide PI0 in Air.

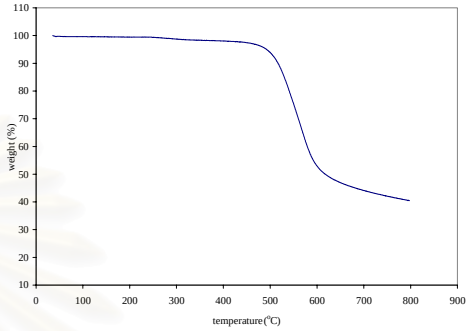

Figure F.2 TGA thermogram of polyimide PI0 in N_2.

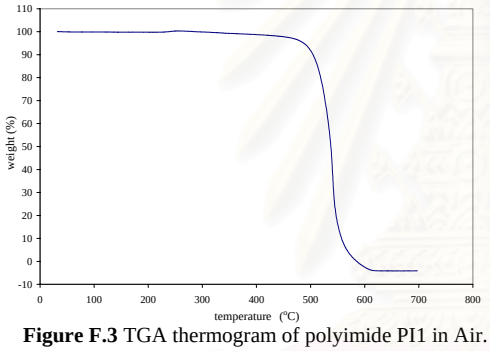

Figure F.3 TGA thermogram of polyimide PI1 in Air.

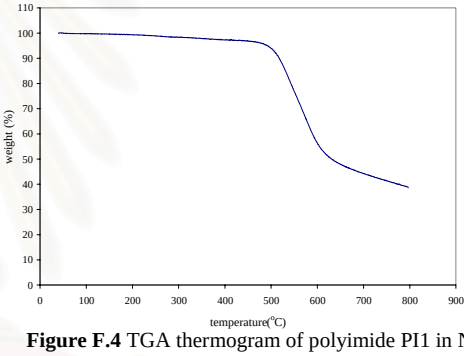

Figure F.4 TGA thermogram of polyimide PI1 in N_2.

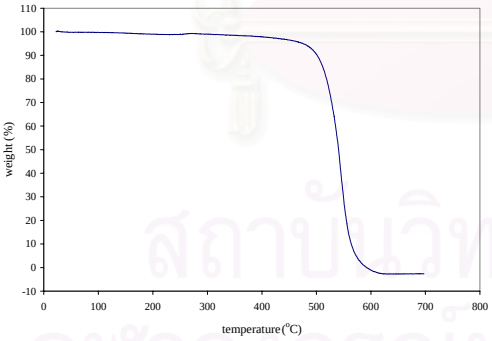

Figure F.5 TGA thermogram of polyimide PI2 in Air.

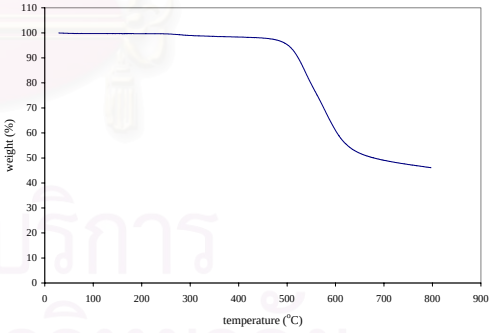

Figure F.6 TGA thermogram of polyimide PI2 in N_2.

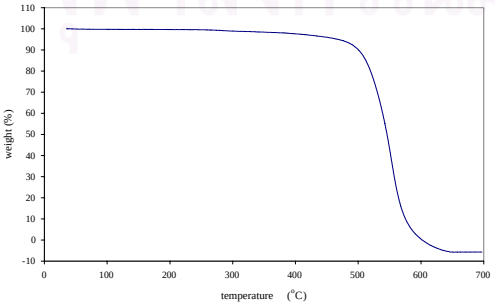

Figure F.7 TGA thermogram of polyimide PI3 in Air.

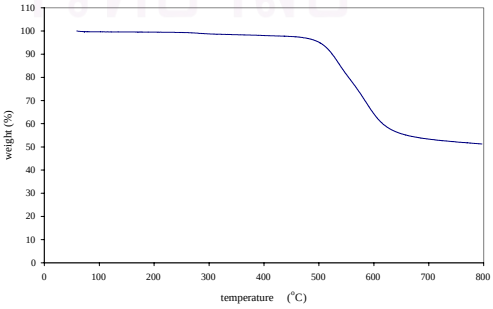

Figure F.8 TGA thermogram of polyimide PI3 in N_2.

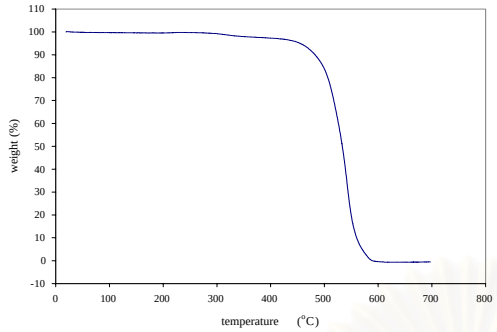

Figure F.9 TGA thermogram of polyimide ZPI1 in Air.

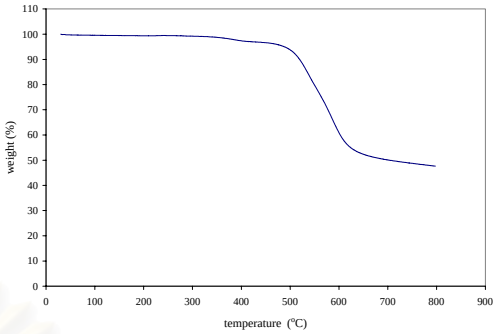

Figure F.10 TGA thermogram of polyimide ZPI1 in N_2.

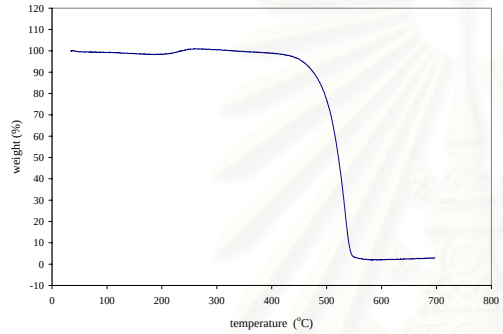

Figure F.11 TGA thermogram of polyimide ZPI2 in Air.

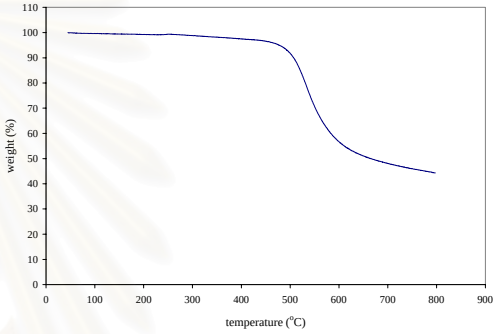

Figure F.12 TGA thermogram of polyimide ZPI2 in N_2.

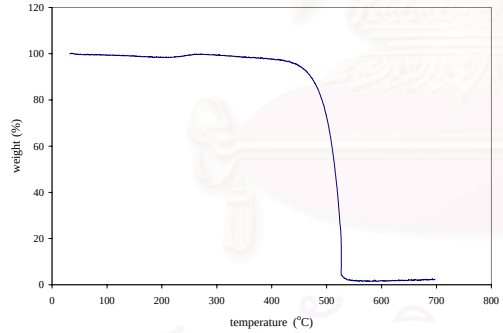

Figure F.13 TGA thermogram of polyimide ZPI3 in Air.

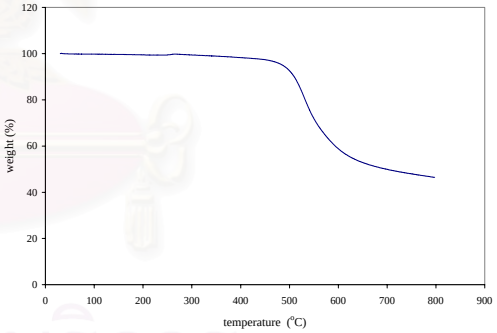

Figure F.14 TGA thermogram of polyimide ZPI3 in N_2.

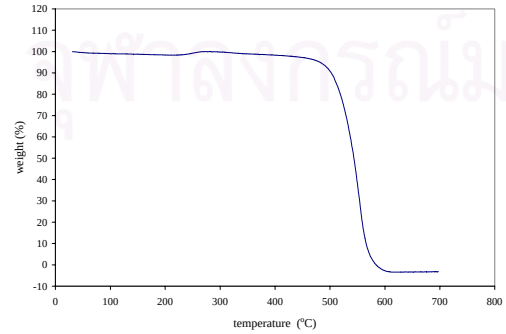

Figure F.15 TGA thermogram of polyimide WPI1 in Air.

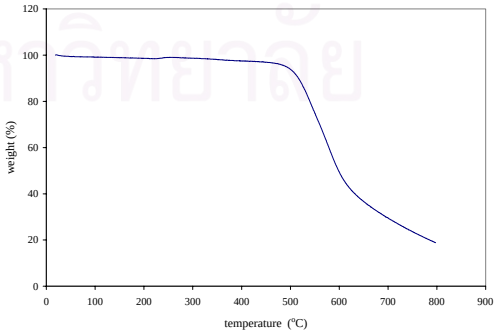

Figure F.16 TGA thermogram of polyimide WPI1 in N_2.

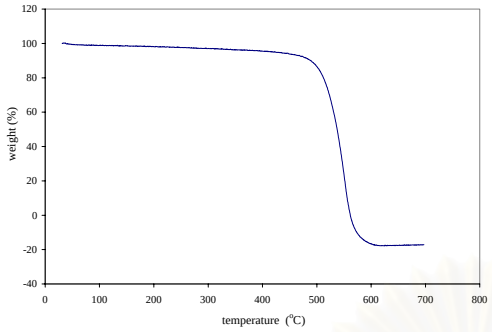

Figure F.17 TGA thermogram of polyimide WPI2 in Air.

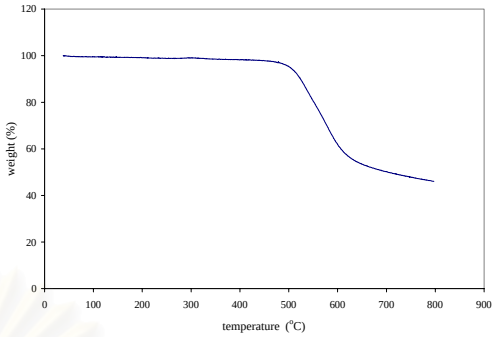

Figure F.18 TGA thermogram of polyimide WPI2 in N_2.

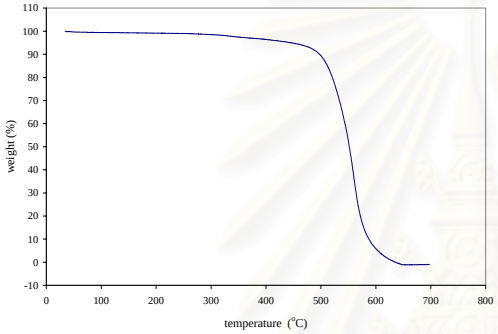

Figure F.19 TGA thermogram of polyimide WPI3 in Air.

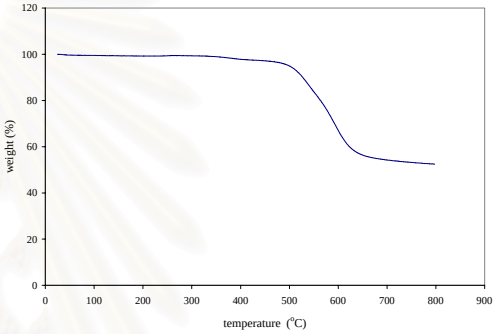

Figure F.20 TGA thermogram of polyimide WPI3 in N_2.

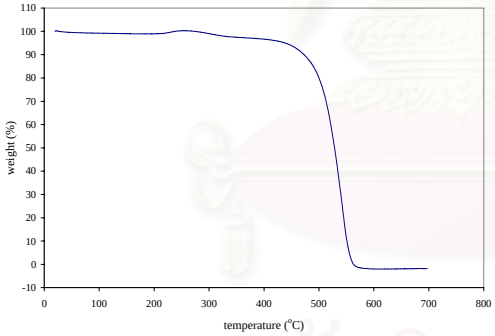

Figure F.21 TGA thermogram of polyimide ZWPI1 in Air.

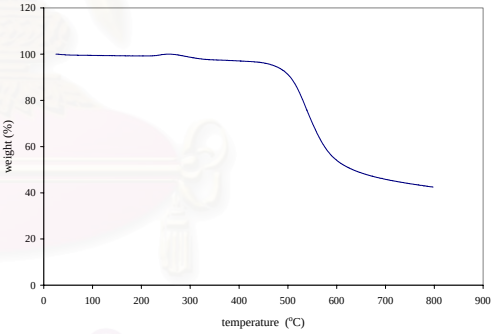

Figure F.22 TGA thermogram of polyimide ZWPI1 in N_2.

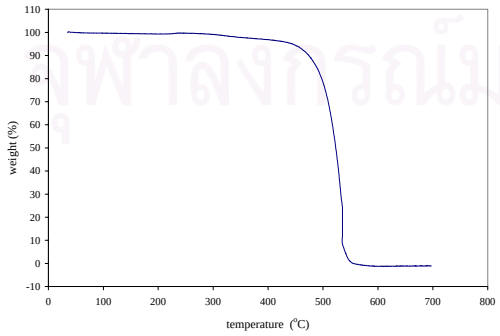

Figure F.23 TGA thermogram of polyimide ZWPI2 in Air.

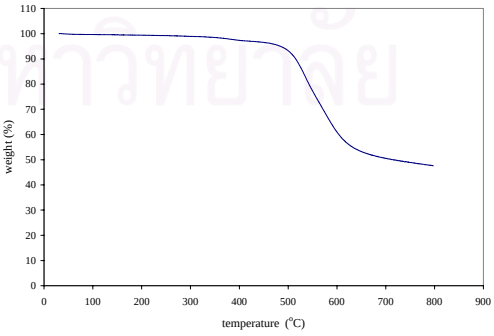

Figure F.24 TGA thermogram of polyimide ZWPI2 in N_2.

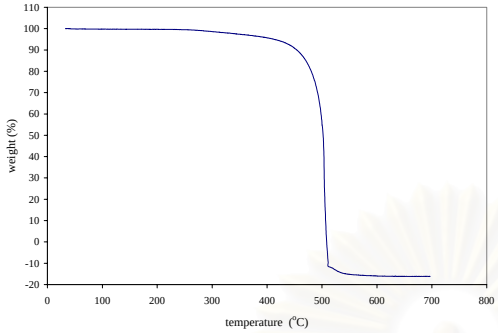

Figure F.25 TGA thermogram of polyimide ZWPI3 in Air.

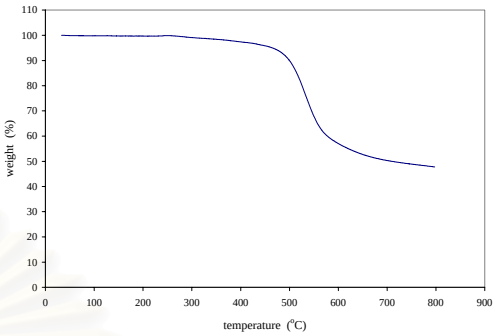

Figure F.26 TGA thermogram of polyimide ZWPI3 in N_2.

APPENDIX G

Fluorescence spectra of porphyrins and polyimides

G.1 Fluorescence spectra of porphyrins and polyimides in CH_2Cl_2

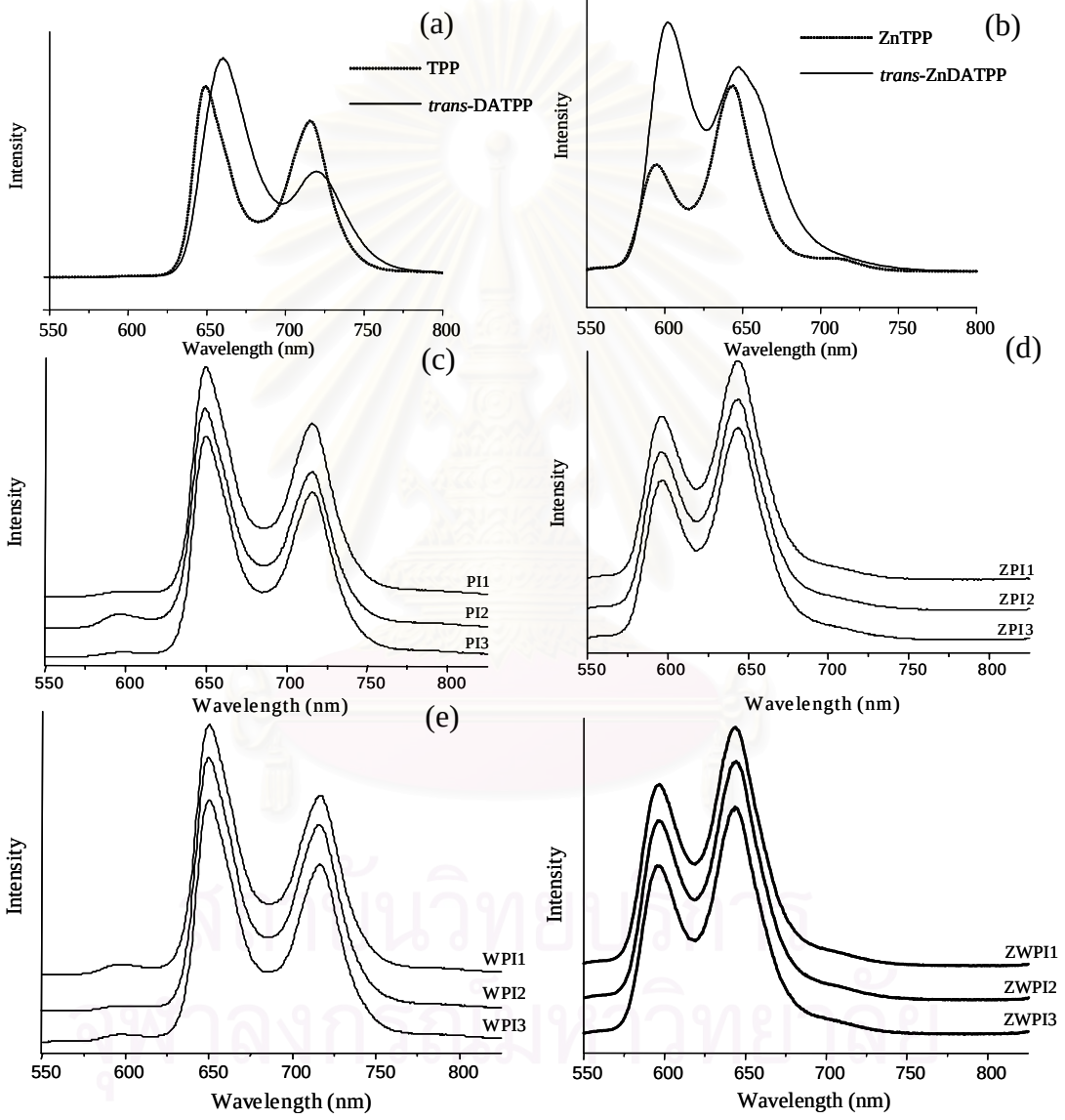

Figure G.1 Fluorescence spectra in CH_2Cl_2 of (a) free base porphyrins, (b) zinc porphyrins, (c) polyimides in series I, (d) polyimides in series II, (e) polyimides in series III and (f) polyimides in series IV.

G.2 Fluorescence spectra of porphyrins and polyimides in DMAc

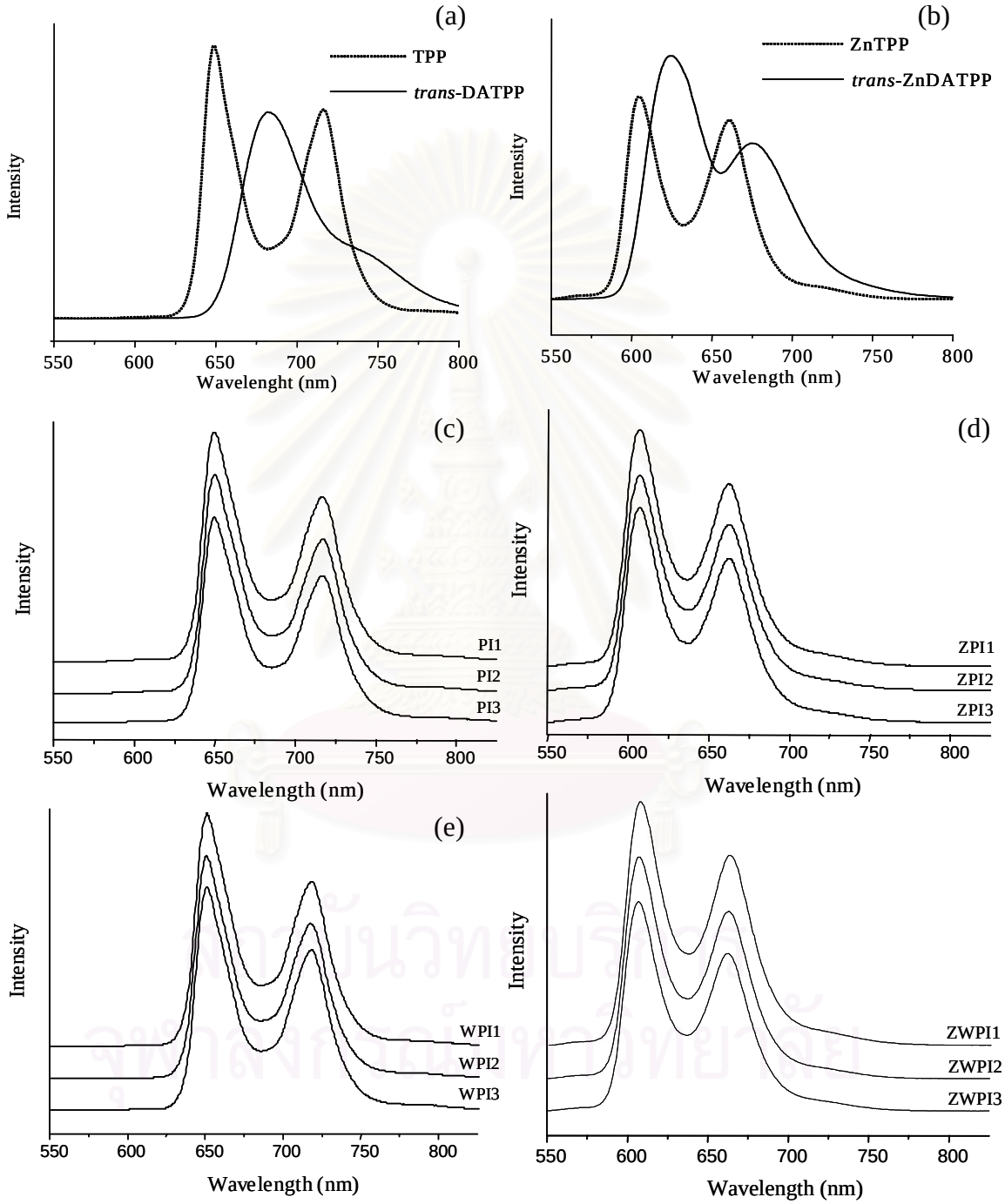

Figure G.2 Fluorescence spectra in DMAc of (a) free base porphyrins, (b) zinc porphyrins, (c) polyimides in series I, (d) polyimides in series II, (e) polyimides in series III and (f) polyimides in series IV.

APPENDIX H

Quantum yield calculation

The quantum yields (Φ_{Fl}) for these polymers were determined by using equations H.1 and H.2

$$\Phi_{PI} = \frac{[(Abs)_{PI} \times (I)_{TPP}]}{[(I)_{PI} \times (Abs)_{TPP}]} \times \Phi_{TPP} \qquad (H.1)$$

$$\Phi_{ZPI} = \frac{[(Abs)_{ZPI} \times (I)_{ZnTPP}]}{[(I)_{ZPI} \times (Abs)_{ZnTPP}]} \times \Phi_{ZnTPP} \qquad (H.2)$$

where Abs = the optical density at excitation wavelength,

I = the area of the emission spectrum

Φ_{TPP} = 0.11 in CH_2Cl_2, 0.15 in DMAc

ΦZn_{TPP} = 0.03 in both CH_2Cl_2 and DMAc

the subscript PI, ZPI refer to the sample *trans*-DATPP or *trans*-ZnDATPP containing polyimides and TPP, ZnTPP refer to standard porphyrin (TPP or ZnTPP).

APPENDIX I

Electrochemical data and electron transfer free energy of polyimides

I.1 Free energy of electron transfer calculation

From the literature values of $E_{1/2}$ (ox) for TPP and ZnTPP [56] and the value of $E_{1/2}$ (red) determined in this research, value of ΔG_{ET} were determined by using Weller equation (equation I.1).

$$\Delta G_{ET} = E_{ox} - E_{red} - E_g \qquad \text{(I.1)}$$

Table I.1 Electrochemical data[a] for TPP, ZnTPP, PI3, ZPI3, WPI3 and ZWPI3

Compound	$E_{1/2}$ (ox)[b]	$E_{1/2}$ (red)[c]	E_g[d] (eV)	ΔG_{ET} (eV)
TPP	1.03[e]		1.91	
ZnTPP	0.78[e]		2.10	
PI3		-1.25	1.91	0.37
ZPI3		-1.14	2.09	-0.17
WPI3		-1.19	1.91	0.31
ZWPI3		-1.06	2.09	-0.25

[a] in CH_2Cl_2, TBAP as an electrolyte. [b]Volts. [c]Volts, reference VS SCE reference electrode. [d]Estimated in the usual manner from the wavelengths of the longest Q-band absorption and $S_1 \rightarrow S_0$ emission. [e]See ref. 56.

I.2 Energy band gap calculation

Table I.2 Energy band gaps (E_gs) of porphyrin derivatives and polyimides in CH_2Cl_2.

Compound	E_g (nm)	E_g (cm^{-1})	E_g[a] (eV)
TPP	647.50	1.5444×10^4	1.91
ZnTPP	589	1.6978×10^4	2.10
trans-DATPP	657	1.5221×10^4	1.89
trans-ZnDATPP	595	1.6807×10^4	2.08
PI1	648	1.5432×10^4	1.91
PI2	648	1.5432×10^4	1.91
PI3	648	1.5432×10^4	1.91

ZPI1	592	1.6892×10^4	2.09
ZPI2	592	1.6892×10^4	2.09
ZPI3	592	1.6892×10^4	2.09
WPI1	648	1.5432×10^4	1.91
WPI2	648	1.5432×10^4	1.91
WPI3	648	1.5432×10^4	1.91
ZWPI1	592	1.6892×10^4	2.09
ZWPI2	592	1.6892×10^4	2.09
ZWPI3	592	1.6892×10^4	2.09

[a] Estimated in the usual manner from the wavelengths of the longest Q-band absorption and $S_1 \rightarrow S_0$ emission.

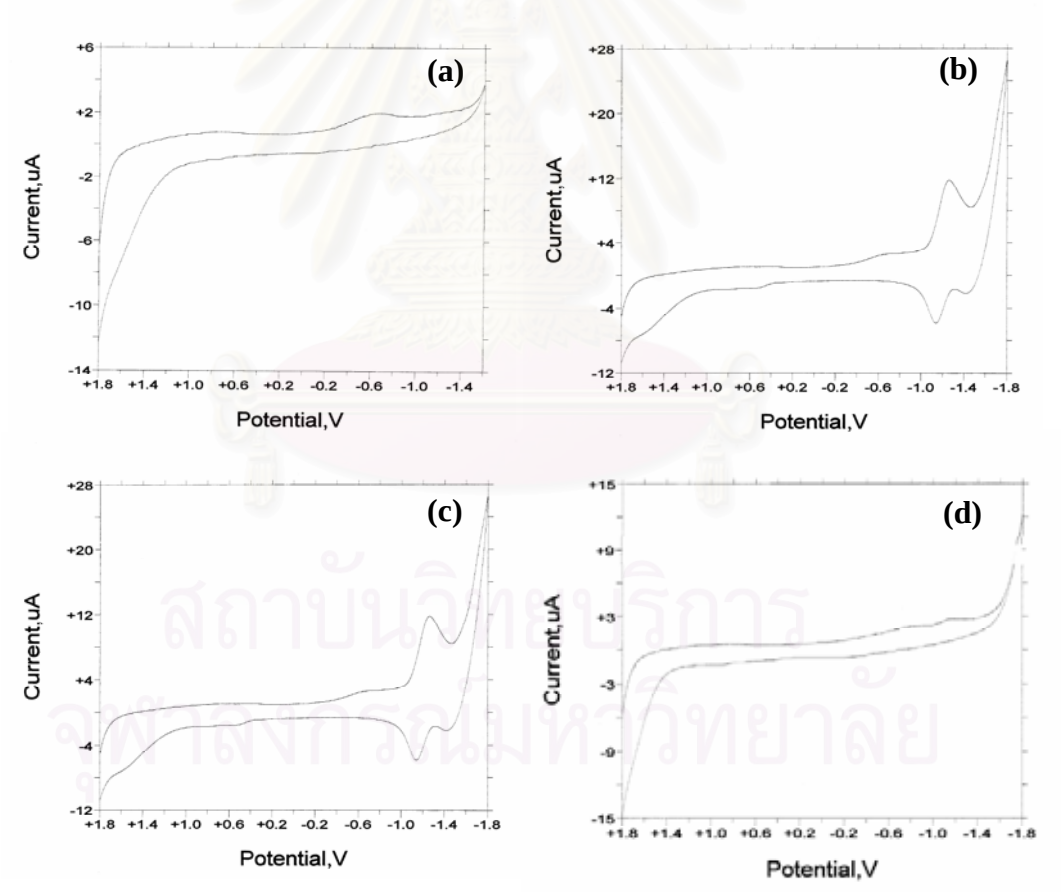

Figure I.1 Cyclic voltammograms; (a) polyimide PI3, (b) polyimide ZPI3, (c) polyimide WPI3 and (d) polyimide ZWPI3.

VITAE

Miss Watchara Anannarukan was born on September 26, 1977 in Mukdahan. She graduated with a Bachelor Degree of Science (Chemistry) from Ubonratchathani University in 2000. In 2000, she was accepted as a Ph.D. student in the Program of Petrochemistry, Faculty of Science, Chulalongkorn University and complete the program in 2006.